

New Geochemistry and Geochronology data from the Prøven Igneous Complex, North-West Greenland

Thomas Find Kokfelt, Diogo Rosa,
John Grocott & Erik Vest Sørensen



New Geochemistry and Geochronology data from the Prøven Igneous Complex, North-West Greenland

Thomas Find Kokfelt, Diogo Rosa, John Grocott & Erik Vest Sørensen

Contents

1.	Preamble	6
2.	Executive summary	8
3.	Introduction	9
4.	Previous work	14
5.	Geological background	15
5.1	Archaean basement rocks	15
5.2	Karrat Group.....	16
5.3	Prøven Igneous Complex (PIC).....	16
5.3.1	The 'massive PIC' unit.....	17
5.3.2	The 'layered PIC' unit.....	17
5.3.3	Mafic enclaves.....	18
5.3.4	Ultramafic rocks.....	18
5.4	Structural architecture and deformation history of the PIC.....	22
6.	Analytical methods	24
6.1	Optical microscopy.....	24
6.2	Whole rock geochemistry.....	24
6.3	U/Pb dating by LA-ICPMS	25
7.	Results	27
7.1	Petrography.....	27
7.1.1	PIC granites.....	27
7.1.2	Mafic enclaves within the 'layered PIC' unit.....	28
7.1.3	(Garnet) leucogranite dykes.....	29
7.1.4	Nukåvsak Formation paleosome and neosome rocks.....	29
7.2	Whole rock geochemistry.....	33
7.2.1	Effects of alteration.....	33
7.2.2	Major elements characteristics.....	33
7.2.3	Trace elements characteristics	39
7.2.4	Summary of major and trace element variations	46
7.3	Geochronology.....	47
7.3.1	PIC charnockites	47
7.3.2	Norites	59
7.3.3	Leucogranite.....	63
7.3.4	Migmatitic rocks of the Nûkavsak Formation	66
7.4	Summary of geochronology.....	68

7.4.1	Magmatic ages	71
7.4.2	Metamorphic ages	78
7.4.3	Inherited ages	79
8.	Conclusions	81
9.	References	83

1. Preamble

The Upernavik Mapping project at GEUS (2018-2023) began as an offspring to the overarching Karrat Zinc and Karrat Map projects (2015-2020) with the aim to carry out limited reconnaissance field work to produce two new map sheets at the scale 1:100 000 covering the Prøven Igneous Complex (PIC) in NW Greenland (72-73° N), namely:

- Kokfelt, Thomas F.; Sørensen, Erik V.; Grocott, John; Sleath, Phoebe. R.; McCaffrey, Kenneth. W.; Rosa, Diogo, in prep., "Geological map of Greenland 1:100 000, **Prøven 72 V. 1 Syd**"
- Kokfelt, Thomas F.; Sørensen, Erik V.; Sleath, Phoebe. R.; Grocott, John; McCaffrey, Kenneth. W.; Rosa, Diogo, in prep., "Geological map of Greenland 1:100 000, **Upernavik 72 V. 1 Nord**"

This report summarises the main analytical results obtained in the Upernavik Mapping project, including new whole rock geochemistry and geochronology data covering a large part of the PIC, based on the recently collected samples as well as samples retrieved from the GEUS archives. The first mapping of the PIC was undertaken by GGU first by Chris Pulvertaft in the late 1960's and continued by Jan Escher and Ole Stecher in the late 1970's, who together produced detailed field maps in scale 1:40,000 that have provided the basis for the new maps. Seventy-one of the analysed archived samples were collected by Ole Stecher and Jan Escher during their 1979 boat-based fieldwork to the Upernavik and Prøven area. We also include five previously published results on samples collected in the western part of the area by Kristine Thrane and Adam Garde, in 2002. Subsequent reconnaissance fieldwork by the current authors in 2018 resulted in 57 new rock samples, of which 43 were analysed, along with over 10000 oblique photos for photogrammetric mapping.

Therefore, the total dataset covered by this report includes 119 rock samples (= 71 + 5 + 43) analysed for major and trace elements, most of which have been studied petrographically and of which 28 samples were selected for zircon U-Pb dating at GEUS. This dataset forms an unparalleled high-density sample set of Greenland's largest intrusive complex and represents an important basis for understanding the PIC within the framework of the Rinkian Orogen. Several research papers are planned with co-workers at Universities in Durham, Aberdeen and Bochum, aiming to address the structural architecture of the PIC, as well as its magmatic and metamorphic evolution based on the new data.

We would like to thank to the following contributors to the project:

- MMR (Ministry of Mineral Resources) for co-financial support of the project
- Logistic support during the 2018 fieldwork in Greenland by pilot Tore Sievertsen (HeliGreenland A/S).
- Tony B. Thomsen, Benjamin Heredia, Mojagan Alaei and Høgni Vesturklett for invaluable analytical help at the GEUS laboratories, including the LA-ICPMS and SEM-laboratories.

Hours of fruitful discussions with co-workers Kenneth McCaffrey, Phoebe Sleath (Durham University), Annika Dziggel and Laura Bramm (Ruhr-Universität Bochum), and GEUS colleagues, Pierpaolo Guarnieri, Kristine Thrane and Stefan Bernstein.

2. Executive summary

The Paleoproterozoic Prøven Intrusive Complex in North-West Greenland is the largest magmatic intrusion in Greenland. It is dominated by orthopyroxene-bearing granitic to granodioritic rocks, collectively known as charnockites, with subordinate mafic and ultramafic components. Detailed mapping of the complex was undertaken by GGU in the 1960 and 1970's but was only much later followed by modern geochemical and isotopic investigations that established a Paleoproterozoic emplacement age. Despite the recognised significance of the PIC to understanding the Rinkian Orogen, a precise geo-tectonic association has remained enigmatic. The PIC was variably ascribed to anorogenic, rift-related, or syn-collisional settings. To finally address this uncertainty, we report a comprehensive geochemical and geochronological dataset based on old and newly collected samples. In tandem with this, a structural analysis of the PIC was conducted based on interpretation of archive maps and supported by new reconnaissance fieldwork and mapping. This has showed that the PIC was emplaced as sheet-like bodies into metasedimentary strata of the Karrat Group near the contact to the underlying Archean basement, and that it later underwent a prolonged phase of ductile deformation and partial migmatisation. The 1:100 000 scale mapping has identified two main charnockitic units: (1) a massive upper part constituted by massive coarse-grained granitic charnockite dominated by magmatic state fabrics with a weak to moderate overprinting, and (2) a heterogeneous, pervasively migmatised charnockite unit that represents the floor of the complex and that contains mafic enclaves and inclusions of wall rock lithologies and intrusive leucogranite sheets. The ductile deformation led to flattening and transposition of the inclusions and enclaves along the basal contact, supplying unique guidance for the mapping. The roof of the complex is not preserved. Geochemically the PIC forms a calc-alkalic series with metaluminous to mildly peraluminous compositions encompassing both magnesian and ferroan granitoid types. The magnesian group has a typical I-type geochemical signature, while the ferroan group has some similarities to A2-type (post-orogenic) granites. The new geochronology data expands the recorded time span for PIC magmatism and shows three intrusive phases: an early phase at ca. 1900 Ma (largely obliterated), a main phase at ca. 1875 Ma, and a late phase at ca. 1850 Ma. The two older phases are exclusively magnesian and dominate the central and southern part of the complex. The youngest phase mostly includes ferroan granitoid types and occurs mainly in the northern part. The regional peak metamorphism reached granulite facies during the collisional stage of the Rinkian orogen at ca 1830 Ma which caused widespread migmatisation as witnessed by injection of leucogranite sheets of this age. The new geochemical and geochronological data indicate that the PIC was

emplaced in a subduction setting over a 50 Myr period leading up to the Rinkian orogen, in a generally NW-ward retreating arc system.

Key words: Paleoproterozoic, subduction magmatism, I-type granite, charnockite, Rinkian Orogen

3. Introduction

The Paleoproterozoic Prøven Igneous Complex (PIC), situated between 72°15'N and 73°10'N in North-West Greenland, is the largest intrusive complex in Greenland, with an exposed surface area of at least ca. 6000 km² (Figure 1). The rocks are mainly orthopyroxene-bearing granitoids (monzogranite, granite and granodiorite), locally containing minor mafic components in the form of gabbroic enclaves. The PIC is temporally and spatially related to the Rinkian orogen of West Greenland which is considered part of the Trans-Hudson orogen of North America (Escher & Pulvertaft 1976; Henderson & Pulvertaft 1987; Grocott, & Pulvertaft 1990; Thrane et al. 2005; St-Onge et al. 2009; Corrigan et al. 2009; Wodicka et al. 2014; Grocott & MacCaffrey 2017; Guarnieri et al. 2023) (Figure 1). The Rinkian orogen was recently interpreted as a back-arc fold and thrust system, resulting from the east-ward collision between a magmatic arc and the Karrat basin (Guarnieri et al. 2023). Despite its pivotal role for understanding the Paleoproterozoic tectono-stratigraphic development of the region, there has been a distinct lack of detailed studies of the PIC, and a firm identification of its geochemical affinity remains unsettled. Based on current literature data, the PIC was emplaced over a ca. 30 Myr period from ca. 1900 to 1870 Ma (Thrane et al. 2005; Sanborn-Barrie 2017) into a crustal sequence of Palaeoproterozoic metasedimentary rocks of the Karrat Group, which were contact metamorphosed by the intrusion (Thrane et al. 2005). According to Grocott et al. (1987), however, the emplacement proceeded shortly after sediment deposition in association with ductile thrusting in the Karrat Fjord thrust system during the closing stage of the Rinkian orogen. The PIC has by some authors been correlated to the much larger ca. 1860-1845 Ma Cumberland Batholith (CB) in Baffin Island (Whalen et al. 2010; Grocott & MacCaffrey 2017), but such a correlation has been disputed by others based on arguments of distinct chemistries and emplacement ages (Thrane et al. 2005; Sanborn-Barrie et al. 2017). Whalen et al. (2010) classified the Cumberland Batholith as I-type (following the classification scheme by Chappell & White (1974)), resulting from continental arc-related intrusions placed above a north-dipping subducting plate. In contrast, Thrane et al. (2005) argued for an A-type chemical signature of the PIC and proposed an anorogenic continental marginal rift-related setting for the complex. The published geochronology data also

seem to indicate a discrepancy in emplacement ages, with the PIC seemingly (1900-1870 Ma) predating the CB (1865-1845 Ma).

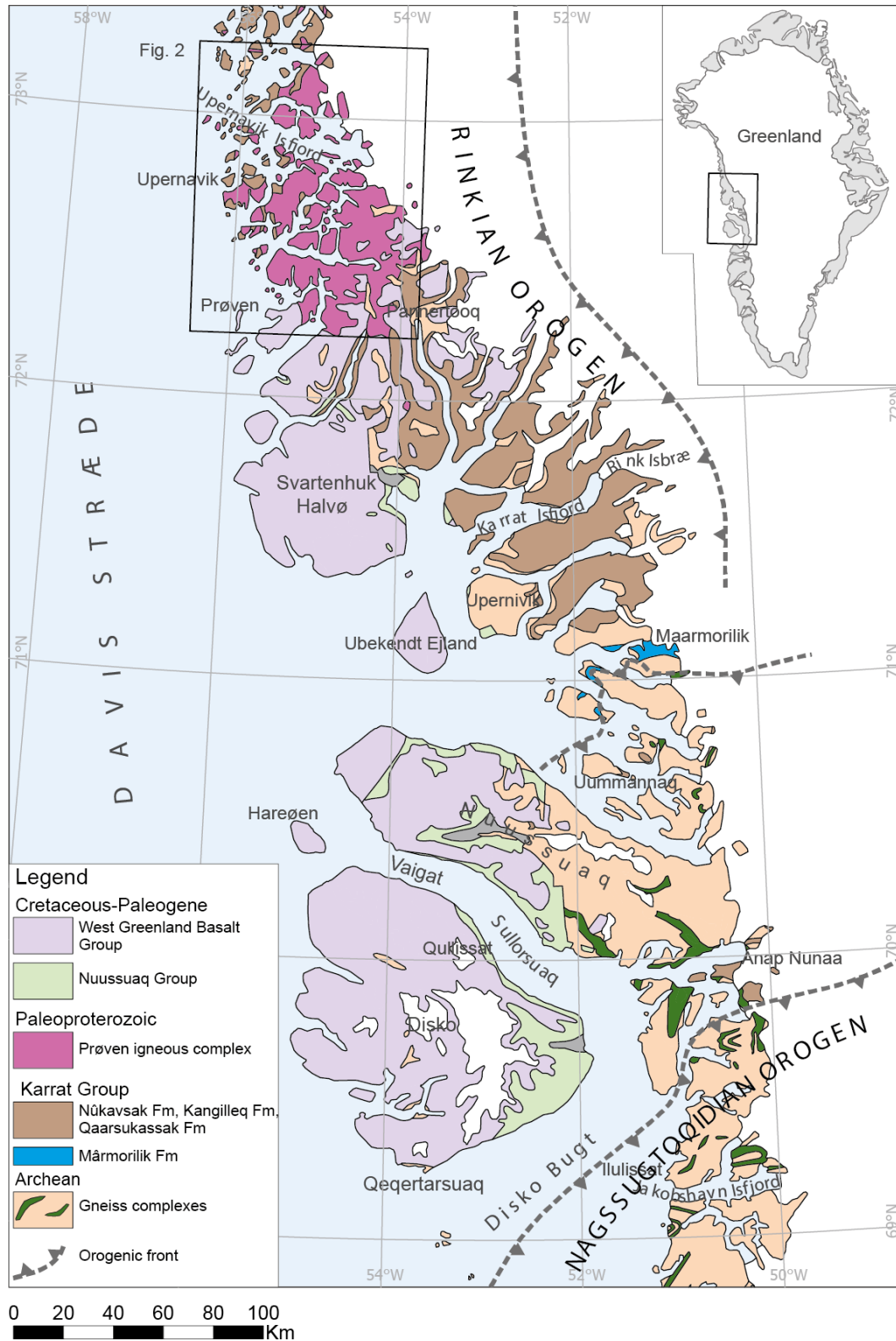
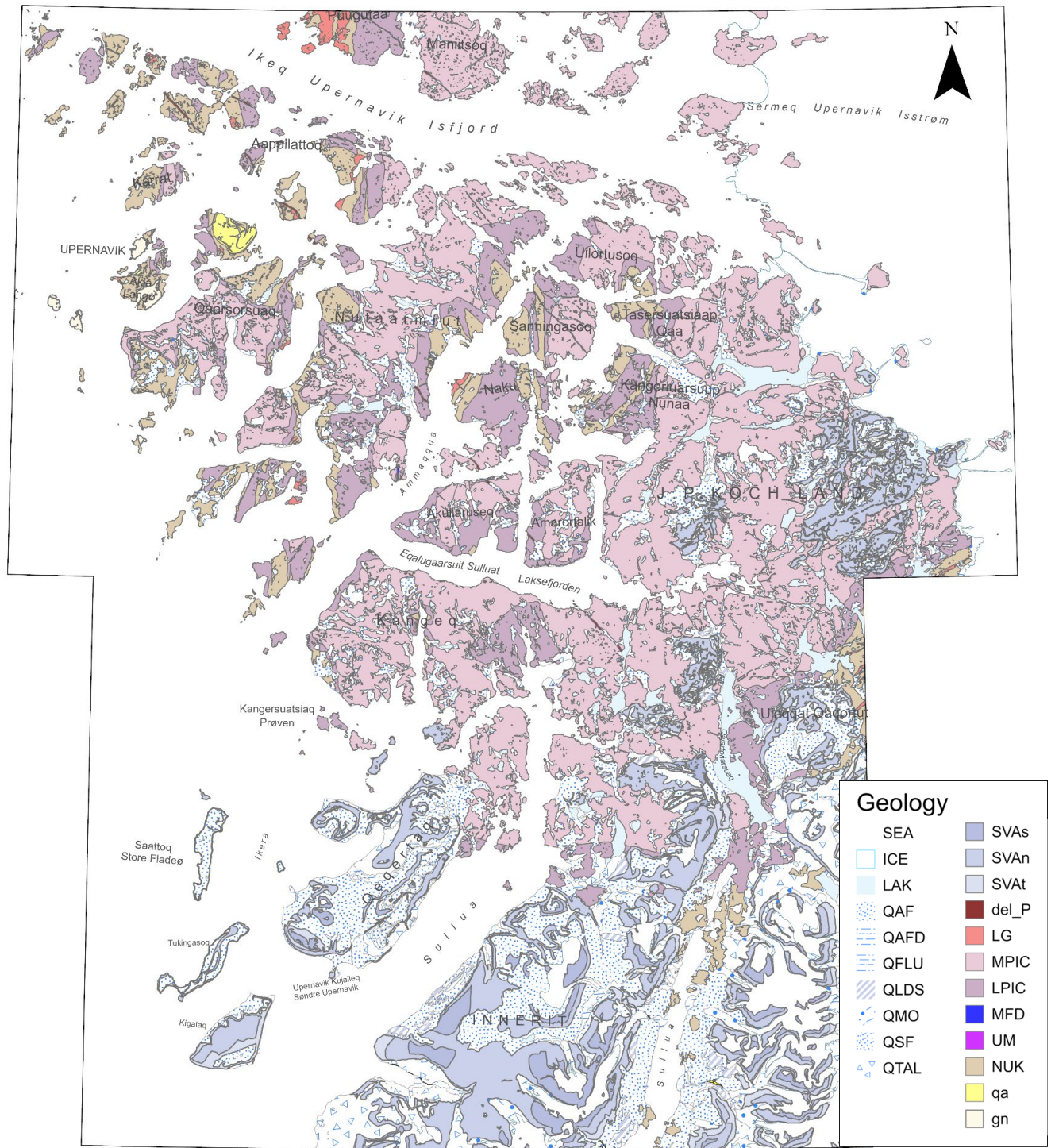


Figure 1. Regional geological map of central West Greenland after Guarnieri et al (2023) showing the relationship between the Prøven Igneous Complex (PIC) to the Rinkian Orogen to the east and the Nagsugtoqidian Orogen to the south.

However, as new geochemistry and geochronology data were produced along with better maps, the gap in composition and age appeared to vanish (as demonstrated in this work). Furthermore, recent mapping in Baffin Island has revealed the existence of older discrete intrusive components within the CB manifested by the ca. 1900-1880 Ma Qikiqtarjuaq plutonic suite (QPS), which includes similar range of granitoid rock types and ages to those found in the PIC (Whalen et al. 2010; Hamilton 2016; Sanborn-Barrie et al. 2017). With the present dataset we demonstrate that the duration of PIC magmatism is extended to ca. 1850 Ma, effectively closing the time gap between the PIC and the Canadian counterparts, the CB and QPS, and thus reinforcing a plausible genetic relationship across the Davis Strait.

The new PIC dataset gives an unprecedented, comprehensive coverage of the complex with 119 samples analysed for whole rock geochemistry and 33 samples for zircon U/Pb dating (Figure 2). The reported samples are derived from GGU/GEUS field operations set about 40 years apart in time. The new data and geological maps give a unique framework for interpreting the petrological and structural evolution of the complex. We use geochemical discrimination plots as a basis for discussing geochemical affinities and relevant tectonic settings which, combined with the new age information, is used to develop a petrogenetic model.



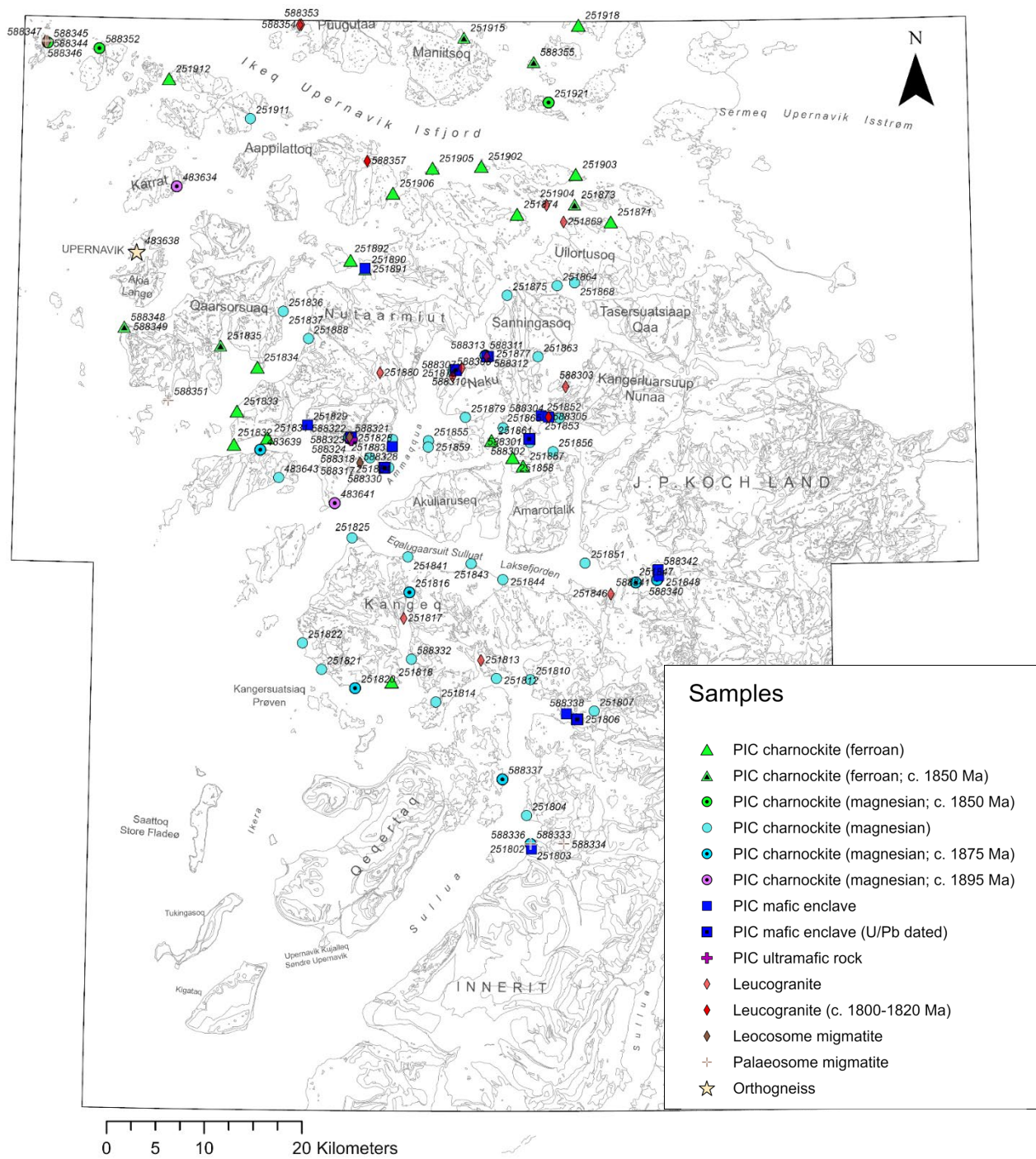


Figure 2. (a) Geological map of the PIC after Kokfelt et al. (2024). Key for geological units: SVA = Svartenhuk Formation: s = Skalø Member, n = Nuiit Member, t = Tunuarsuk Member; del_P = Paleoproterozoic mafic dyke; LG = Leucogranite; MPIC = massive Prøven granite; LPIC = layered Prøven granite; MFD = Mafic feeder dyke (norite); UM = Ultramafic rock (mainly glimmerite); NUK = Nùkavsak Formation; qa = Qaarsukassak Formation (quartz arenite); gn = Archaean orthogneiss. (b) Sample location map.

4. Previous work

The PIC was originally referred to as the Prøven Granite by Escher & Pulvertaft (1968), later renamed to the Prøven Charnockite as it was realised that it had orthopyroxene (hypersthene) (Escher & Stecher 1978). Later, Thrane et al. (2005) introduced the term 'Prøven Igneous Complex', because the sheer size of it indicates that it is a complex rather than a single intrusion.

Over two hundred rock samples were collected in association with the early GGU mapping campaigns, unfortunately a large part of which was discarded in the early 2000's. Nonetheless, well over hundred samples survived thanks to Ole Stecher's resilience, and many of which have been included in this study. A large fraction of these early samples was analysed in house by X-ray fluorescence (XRF) for major and some trace elements, but the data remained unpublished.

In 2002 and 2003 ship-based expeditions to the Upernavik region funded by grants from the NERC (UK Research Council) and the Carlsberg Fonds were carried out under the auspices of GEUS. Participants were Ken McCaffrey, John Grocott, Adam Garde, Jim Connelly, Martin Hand and Kristine Thrane. Results of these expeditions were reported in Thrane et al. (2005), Sanborn-Barrie et al. (2017), Grocott & McCaffrey (2017) and Grocott et al. (2023). To assure consistency between the current dataset and previously published data, we reanalysed five previously reported samples for major and trace elements and a single sample by zircon U/Pb dating.

An overarching goal of the 2018 reconnaissance field work was to collect enough new data to support the compilation of two new 1:100 000 scale geological maps of the PIC. The main tasks included: (1) acquisition of oblique stereo images for later analysis in the photogrammetry laboratory at GEUS, (2) ground stops to clarify and calibrate information embedded in the old GGU archive maps, and (3) recording field data and collecting samples for laboratory work including petrography, geochemistry and geochronology. Key fieldwork aims were to evaluate and change, as necessary, lithostratigraphic mapping units used in the historical field mapping and update the terminology used with modern descriptive terms.

A long-established view was that the PIC was emplaced at ca. 1830 Ma about the same time as structural and metamorphic events in the Rinkian orogen, including emplacement of a suite of leucogranite intrusions spatially associated with the PIC (Grocott & Pulvertaft 1990).

This view changed as Thrane et al. (2005) presented a zircon U/Pb (SIMS) age of 1869 ± 9 Ma, which they interpreted as the crystallisation age of the PIC, as well as the timing of widespread contact metamorphism. The crystallisation age was later confirmed and expanded to a 30 Myr period from ca. 1900 to 1870 Ma (Sanborn-Barrie et al. 2017). Thrane et al. (2005) argued for pronounced contact metamorphism within a ca. 15 km wide contact aureole, and thus linked the emplacement of the PIC to the migmatisation of the Nûkavsak Formation metasediments at ca. 1870 Ma. Evidence for this were the so-called 'PIC dykes' intruding the host rocks that show granulite facies mineral assemblages. The suggestion of high-grade metamorphism at 1870 Ma was however contradicted by the authors own Lu-Hf and Sm-Nd data that indicated isochron ages of ca. 1830 Ma based on peak metamorphic mineral assemblages. To explain this apparent contradiction Thrane et al. (2005) simply argued for open system behaviour of the Lu-Hf and Sm-Nd isochrons, dismissing these isotope systems as inadequate to date granulite facies events. Sm-Nd isotope data from four whole-rock samples showed crustally-influenced $\epsilon\text{Nd}_{1870\text{Ma}}$ values of -5.2 to -4.3, corresponding to TDM ages of 2660-2500 Ma (Thrane et al. 2005). The same authors also presented whole rock data from four PIC samples and categorised them as A-type, describing them with high Fe^*/Mg ratios and high HFSE+REE contents. Based on the chemistry and the lack of juvenile input they proposed a model where the PIC was generated in a continental margin (rift) setting from melting of Archean lower crust, with variably contamination by sedimentary rocks of the Karrat Group. The heat source for magmatism was envisaged to be upwelling mantle in response to delamination of the lithospheric keel.

5. Geological background

5.1 Archean basement rocks

The study area is underlain by Archean basement belonging to the Rae Craton, making up mainly trondhjemite-tonalite-granodiorite (TTG) type orthogneiss of Mesoproterozoic to Neoproterozoic age (Thrane 2021), as well as quartzites, micaschists and amphibolites of the Qeqertarsuaq Formation, now assigned to the Archean (Guarnieri et al. 2023; and below). The Rae Craton, which extends across from north-eastern Canada formed in the late Neoproterozoic part of the supercontinent Nunavutia (Pesonen et al. 2003; Pehrsson et al. 2013). Following the break-up of Nunavutia at ca. 2050 Ma (Hoffmann 1988) a new configuration of the Archean cratons involving Rae Craton, North Atlantic Craton, Superior Craton and Meta Incognita, eventually amalgamated into the Nuna-Columbia supercontinent during the Trans-

Hudson Orogeny between 1950 to 1750 Ma (St-Onge et al. 2009). In the study area, Archean TTG rocks are only observed and mapped out in a few places on some of the islands and islets in the westernmost part (Figure 2). They occur typically in tectonic windows, i.e., through the eroded cores of antiforms of deformed PIC rocks, and with few exceptions, in contact to Karrat Group metasediments, rather than the PIC itself.

5.2 Karrat Group

The Paleoproterozoic Karrat Group unconformably overlies the Archean basement (Henderson & Pulvertaft 1967, 1987). This is an approximately 5-7 km thick metasedimentary sequence, extending along more than 400 km of the west coast of Greenland, broadly from latitude 71°N to 75°N. The Karrat Group was originally defined as including the carbonate dominated Marmorilik Formation, present in the south, the lower, mainly siliciclastic, Qeqertarsuaq Formation, and the upper, extensive, turbiditic, Nûkavsak Formation (Henderson & Pulvertaft 1987). However, based on the revised stratigraphy of the Karrat area, the Qeqertarsuaq Formation is now separated from the Karrat Group and considered together with the gneiss complex as part of the southern margin of the Rae craton (Guarnieri et al. 2023). Instead, some carbonate-siliciclastic sequences belonging to the Karrat Group are now assigned to the recently defined Qaarsukassak Formation (Guarnieri et al. 2016). In the study area, despite the intensity of the migmatization, both the Nûkavsak and the Qaarsukassak formations of the Karrat Group have been recognised and mapped. The Karrat Group metasediments are exposed in tectonic windows through the complex (Figure 2). The rocks are paragneiss migmatites consisting of garnet- and orthopyroxene-bearing rocks that show widespread evidence for in situ partial melting with paleosome, melanosome and leucosome components (Figure 3m-n; Sawyer 2008).

5.3 Prøven Igneous Complex (PIC)

The PIC is situated in NW Greenland, east of the town of Upernavik where the landscape is dominated by numerous islands and islets as well as more coherent landmasses further inland. Overall, the PIC outcrops over ca 110 km north-to-south, from south of the village of Prøven to north of Upernavik Isfjord, and ca 70 km west-to-east, from the western part of Qaarsorsuaq island to the Inland Ice (Figure 2). To the south and east the PIC is covered by Eocene lavas belonging to the West Greenland Basalt Group (Larsen & Larsen 2022) and to the east the PIC disappears underneath the Ice Sheet. Thus, the actual extent of the complex is unknown and it could continue well beyond the currently exposed limits. The central part the complex is well exposed, and dissected by the deeply incised fjords, which makes the

area very well suited for photogrammetry work. Recent photogrammetry-based mapping has shown that the PIC has an overall sheet-like (rather than plug-like) geometry. It was emplaced along the contact zone between the Archean gneiss basement and the overlying sedimentary cover represented by the Karrat Group (Sleath 2021). After the emplacement, the complex underwent ductile deformation during prolonged phases of folding and thrusting that produced complex interference folding patterns. The current erosional level exposes the base of the intrusion over a wide area, while the roof is nowhere exposed.

The PIC is dominated by orthopyroxene-bearing granite (charnockite), monzogranite or granodiorite (charno-enderbite; see also Le Maitre et al. 2005) with subordinate amounts of mafic and ultramafic lithologies, including orthopyroxene-bearing gabbroic rocks (mainly norites) and rare glimmerites. On the two 1:100 000 scale geological maps (Kokfelt et al. in prep. 2024a, b), the complex presents two discernible lithostratigraphic charnockitic units: a stratigraphically lower unit referred to as 'the layered PIC' that is the base of the intrusion, and a stratigraphically overlying thicker unit named 'the massive PIC' (Sleath 2021). The boundary between these two granite units is usually transitional over 50-100 m and represents a unique marker for mapping out the structures towards the base of the complex.

5.3.1 The 'massive PIC' unit

The 'massive PIC' unit is a discernible map unit of the Prøven granite that is particularly dominant in the eastern and southern parts of the complex, where it outcrops as distinct rounded massifs showing regular jointing patterns and characteristic orange-brown weathering colours (Figure 3a). It is placed stratigraphically above the 'layered PIC' unit and tends to constitute topographic highs. The unit constitutes coarse-grained granitoids (charnockite), usually porphyritic with cm-sized (≤ 10 cm) alkali feldspar megacrysts. The rocks typically show a weak but distinct crystal-plastic fabric that reflects minor overprinting. Where least affected by deformation, the rock preserves primary magmatic-state fabrics, including feldspar-porphyritic texture (Figure 3b) and even rare examples of rhythmic magmatic layering (Figure 3c). The contact to the underlying 'layered PIC' unit is characterised as a gradual shift over 50-100 m, where enclaves and inclusions first appear, and rock textures become increasingly overprinted by deformation (see below).

5.3.2 The 'layered PIC' unit

The 'layered PIC' unit represents the lower, metamorphic part of the complex and is prevalently exposed towards the north-western area (Figure 2). The unit usually displays a

characteristic layering that can be observed from a distance and therefore used as mapping criteria (Figure 3d-f). The main granite of the 'layered PIC' unit is an alkali feldspar megacrystic charnockite with a clear crystal-plastic planar fabric (Figure 3g). The unit contains abundant inclusions and enclaves that are broadly aligned parallel to the intrusive contact with the Nûkavsak Formation below. Inclusions are mainly xenoliths of metasedimentary rocks of the Nûkavsak Formation, while enclaves represent flattened mafic bodies. The structural and lithological layering is locally emphasised by dense swarms of pale (garnet) leucogranite sheets, including different generations (Figure 3e,f). Locally, on the NW coast of Qaarsorsuaq (Figure 2), the 'layered PIC' granite is migmatized and transformed into diatexite (Figure 3h).

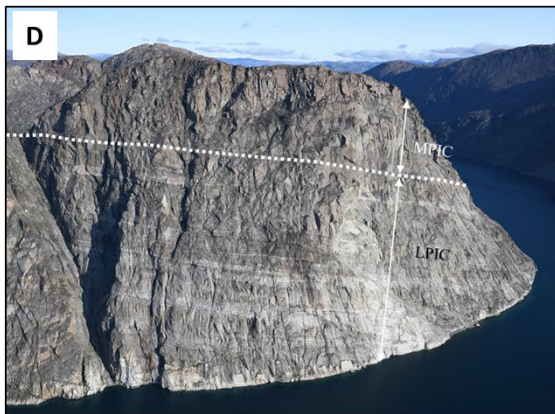
5.3.3 Mafic enclaves

The mafic enclaves hosted within the 'layered PIC' unit occur as flattened, rounded bodies, usually measuring a few meters across and rarely traceable for more than a few tens of metres. The enclaves comprise plagioclase-dominated, orthopyroxene- (\pm clinopyroxene) bearing gabbroic rocks (norites and gabbronorites) that are distinctly biotite-rich (Figure 3i). They are fine to medium-grained with granular equilibrated textures and without evidence of partial melting. The contact to the host granite is usually sharp, but without any clear intrusive relationship (Figure 3j). The enclaves generally do not constitute a discernible map unit on the 1:100 000 scale geological map. However, on the southeast coast of Nutaarmiut island, a discordant dyke measuring up to ca 250 m at its widest point, cuts into both the 'layered PIC' and 'massive PIC' units (labelled as 'possible feeder' on the old GGU archive maps; Figure 2). The dyke constitutes similar mafic rock type, a biotite-rich norite (sample 588330) as found as enclaves in the 'layered PIC' elsewhere. This observation, supported by new age dating (see below), is consistent with the mafic enclaves being fed from a common source near the base of the complex representing an integral part of the PIC magmatism.

5.3.4 Ultramafic rocks

On the archive field maps small outcrops of ultramafic rocks are shown in a few places within the complex. One such example was visited in 2018 at Tasiusaq on the southern part of Nutaarmiut island (Figure 2), where migmatites outcrop along a stretch of coast (Figure 3m,n). The migmatites are cut by a 10-20 cm wide glimmerite vein that is surrounded by a reaction zone of unconstrained thickness. The reactive host rock zone includes coarse-grained plagioclase-quartz-garnet rocks, with very large (≤ 8 cm) porphyroblastic garnets. The association of glimmerite veins and migmatitic rocks points to a late metasomatic origin of

the glimmerites, rather than them representing a magmatic component of the PIC. We envisage that glimmerites formed from fluids that were liberated from the breakdown of mica-rich sediments during migmatization. Glimmerites have also been noted on the archive maps elsewhere (e.g. NW-most island to the S of Upernavik Isfjord) and appear to make up the only ultramafic rocks in the complex.



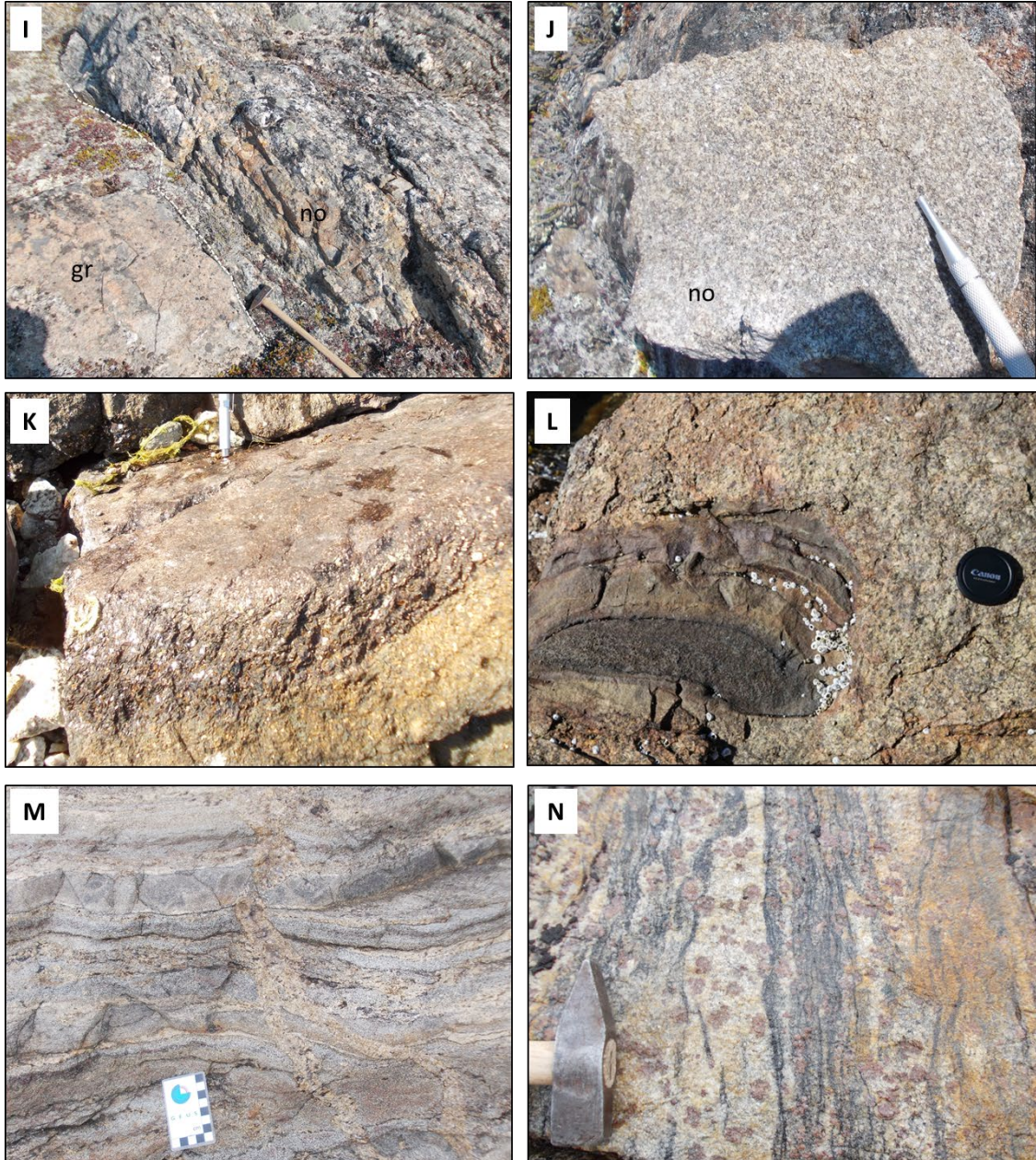


Figure 3. (A) Coastal cliff exposure of dark grey-brown homogeneous charnockite of the 'massive PIC' unit, Timmiitsoq (photograph: E.V. Sørensen); (B) Coarse-grained feldspar-phyric charnockite with weakly overprinted magmatic state fabric (sample 588340), Qeqertasuaq Kangilleq (photograph: T.F. Kokfelt); (C) Rare example of magmatic modal layering showing rhythmic 5-8 cm thick curving layers, Kangerlussuaq (photograph: T.F. Kokfelt); (D) Coastal cliff exposing a transitional contact between 'layered PIC' (below) and 'massive PIC' unit (above), SE Akuliaruseq (photograph: E.V. Sørensen); (E) Coastal cliff exposure of 'layered PIC' charnockite showing an antiformal structure highlighted by intrusive white leucogranite dykes, SW Qaarsorsuaq (photograph: E.V. Sørensen); (F) Layered PIC charnockite with intrusive 40-50 cm wide leucogranite dyke with 'wavy' contacts (intruded at a 'ductile' state), Nutaarmiut, Tasiusaq (photograph: T.F. Kokfelt); (G) Strongly foliated coarse-grained 'layered PIC' charnockite showing characteristic brownish-orange weathering colour (sample 588337, Sullua, Qaarusulik (photograph: T.F. Kokfelt); (H) Diatexite migmatite of the 'layered PIC' (sample 588348), NW Qaarsorsuaq (photograph: T.F. Kokfelt); (I) Mafic enclave (no) in 'layered PIC' unit, Nutaarmiut, Tasiusaq (photograph: T.F. Kokfelt); (J) Fine- to medium-grained biotite-rich norite (sample 588322), Nutaarmiut, Tasiusaq (photograph: T.F. Kokfelt); (K) Glimmerite vein (bronze coloured upper unit) in metasomatic zone (sample 588325), Nutaarmiut, Tasiusaq (photograph: T.F. Kokfelt); (L) Meta-sandstone enclave (paleosome migmatite) in coarse hypersthene granite, Aappilattoq (photograph: J. Grocott); (M) Inclusion of meta-sandstone (paleosome migmatite) in 'layered PIC' granite, Sullua, Illorullit (photograph: T.F. Kokfelt); (N) Deformed migmatitic metasediment with leucosome and melanosome layers and large garnets, N. Assaqtuaq (photograph: T.F. Kokfelt).

5.4 Structural architecture and deformation history of the PIC

A structural analysis from rule-based cross-sections suggests that the PIC is underlain by a series of flat-lying WNW-verging thrust systems along which the PIC has been transported at the order of 100 km horizontally to the west without any significant vertical transport component (Grocott et al. 2023; Grocott et al. in prep). The reconstruction also shows that the PIC, prior to deformation, probably had a maximum thickness of about 3-5 km (Sleath 2021). Preliminary P-T estimates based on Thermocalc modelling shows emplacement depths of around 3.5-5 kb (12-18 km) (Bramm 2021; Dziggel et al. in prep.).

At least two distinct phases of deformation produced small- to large-scale folds and related deformation fabrics observed in the migmatized orthogneiss and paragneiss units, as well as in the LPIC unit.

- i) Tight- to isoclinal, originally flat-lying folds with an intense axial planar fabric which has transposed bedding in the fold limbs which has transposed bedding in the fold limbs to give a composite, regional planar fabric (S1+S2+S3) associated, in detail, with three phases of isoclinal folding (F1+F2+F3) (Sleath, 2021; Grocott et al. 2023). Lithological layering and mineral shape fabrics are parallel at most localities except in the hinge zones of the folds.
- ii) Upright to steeply inclined large-scale folds highlighted by the shape of the base PIC horizon (F4).

The phases of folding have produced a large-scale fold interference pattern expressed most clearly at the base Palaeoproterozoic horizon on Akia (Figure 2). Elsewhere, structural patterns are dominated by F4 upright- to steeply inclined folds is best expressed by the shape of the base PIC horizon. All phases post-date the emplacement of the PIC but only the later phase of folding appears to have deformed the MPIC.

High fabric intensity deformation associated with F1 + F2 + F3 in the northern and western part of the PIC and its host rocks formed during (thrust) transport to the NW. A strong planar fabric which has transposed bedding everywhere except in fold hinge zones is parallel to the base PIC horizon. The metatexite and diatexite migmatite in the paragneiss (PG) and the syn-tectonic garnet leucogranite intrusions – all horizons below the base PIC – were deformed by strongly disharmonic, upright, large-scale folds (F4). Traced upwards along the axial traces, F4 above the base PIC and the MPIC are much more harmonic (consistent wavelength and amplitude) at higher levels in the PIC.

There is a regional-scale bend in the trend of F4 folds in the PIC. To the northwest of a line between Kuungut and the narrow ice shelf where Upernavik Isstrøm (Sermeq) enters the sea (Figure 2), the trend of lithological contacts, planar fabrics and the traces of fold axial surface in the PIC is NNW to NNE. To the south of this line lithological contacts and planar features trend E to ENE. This defines a 100 km-scale bend in the trend of the Rinkian orogen. The change in trend is associated with an NNE-trending fold axial surface trace and a rounded fold hinge exposed on the islands Paaq, Sanningasoq and adjacent peninsulas of eastern Naku and Kangerluarsuup Nunaa (Figure 2).

To the southeast of this line:

- i) high grade metamorphism and anatexis in metasedimentary rocks below the PIC took place in a narrower (and thinner?) zone;
- ii) deformation (folding and boudinage) of leucocratic garnet granite veins, sheets and dykes emplaced below or in the lower part of the PIC is of lower intensity;
- iii) folding of the PIC is more open.

Our preliminary conclusion is that the bend in the orogen represents a strain gradient with deformation increasing to the NW leaving the intrusion in the east and south relatively undeformed, although thrust to the south at its southern margin (Grocott et al. 2023).

6. Analytical methods

6.1 Optical microscopy

Examination was done at GEUS using a Zeiss Axioskop 40 equipped with an AxioCam MRc5 for photo documentation.

6.2 Whole rock geochemistry

Out of the 57 samples collected in the field during the 2018 fieldwork 43 were analysed for their whole rock composition at Acme Laboratories in Vancouver, Canada. To ensure that only the freshest possible rock material was selected for analyses the samples had all weathered surfaces removed at GEUS using a diamond saw prior to further processing in Canada. For the crushing and milling preparation code 'PRP90-250' was applied by which 1 kg of rock material was processed so that 90% passed under 10 mesh grain size (c. 2 mm), followed by a pulverisation stage where 250 g was milled so that 85% passed under a 200-mesh grain size (c. 75 μm). Approximately 5 g of rock powder was dissolved by lithium borate fusion method producing a glass bead for further analysis. The chemical analysis included the 'LF600' package, which involves determination of major elements by X-ray fluorescence (code XF700), volatile contents by weight loss upon ignition to 1000 C (code TC-000) and trace elements by ICP-MS (inductively coupled plasma mass spectrometry) (code LF100-EXT, including 45 elements).

Of the 80 GGU/GEUS archive samples included 65 were originally (in 1979-80) analysed by XRF at former GGU following the procedures described by Kystol & Larsen (1999), determining concentrations of the major elements and some trace elements (the latter omitted here as new trace element data by ICPMS were acquired). The remaining 15 archive samples were analysed for major and trace elements by XRF and ICPMS, respectively, at Acme Laboratories. All trace elements were analysed by Quadrupole ICPMS at GEUS in 2021, following two separate protocols for the sample digestion. The standard protocol involved acid ($\text{HF}+\text{HNO}_3+\text{HCl}$) digestion, followed by determination of 41 trace elements (list elements). To ensure a reliable determination of the most refractory elements, Zr and Hf (restitic in zircon) an added batch of 54 samples was prepared involving digestion by Lithium borate flux fusion. In view of the combined nature of the dataset we assess for consistency of the

trace elements by comparing analyses of the 15 samples analysed at Acme Laboratories and GEUS (Appendix). As can be seen from Figure A1 the duplicated samples agree generally within a range of ± 2 in z-score value, thus confirming consistency between the data of the two laboratories. The data are reported as Appendix tables (Table A2-A7).

6.3 U/Pb dating by LA-ICPMS

U-Pb age dates were obtained in selected samples by LA-ICPMS at the laboratory at GEUS following the standard procedures outlined in Gerdes & Frei (2009) with adjustments described in Dziggel et al. (2014). Zircon analyses were conducted at the Department of Petrology and Economic Geology, Geological Survey of Denmark and Greenland (GEUS). Chips from the rock samples were crushed directly in a tungsten carbide disc mill. The crushed material was sieved and the fraction 250-1000 μm was poured onto a Wilfley[®] shaking table for heavy mineral grain separation. The heavy mineral fraction was transferred to disposable plastic Petri dishes using ethanol, and magnetic minerals were removed using a hand magnet. Zircon grains were then hand-picked from the final heavy mineral concentrate in the Petri dish. The handpicked zircon grains were cast into epoxy and polished to expose a central cross-section of each grain. Approximately 150 grains were picked if possible. The mount was documented prior to ablation using backscattered electron imaging in a scanning electron microscope. The mount was later cleaned in an ultrasonic bath with propanol, and then loaded into the sample cell of the laser ablation system for age dating.

Zircon U-Pb geochronology was carried out on mineral separates embedded in the epoxy mounts by LA-ICPMS. A NWR213 frequency-quintupled solid-state Nd:YAG laser system from Elemental Scientific Lasers, mounted with a TV2 ablation cell was coupled to an ELEMENT2 double-focusing single-collector magnetic sector-field ICPMS from Thermo-Fisher Scientific. To ensure stable laser output energy, a laser warm-up time of at least ~ 15 min was applied before operation, supplying stable laser power and flat ablation craters. The mass spectrometer was run for at least 1h before analysis to stabilise the background signal. Prior to loading, samples and standards were carefully cleaned with ethanol to remove surface contamination. After insertion, the ablation cell was flushed with helium to minimise gas blank level. The ablated material was swept by the helium carrier gas and mixed with argon 0.5 min before introduction into the plasma of the mass spectrometer. Just prior to analysis, the ICPMS was optimised for dry plasma conditions through continuous linear ablation of the GJ-1 zircon standard. The signal-to-noise ratios for the heavy mass range of interest (i.e., from ^{202}Hg to ^{238}U) were maximised, while concurrently opting for low element-oxide

production levels by minimising the $^{254}\text{UO}_2/^{238}\text{U}$ ratio. To minimise instrumental drift, a standard-sample-standard analysis protocol was followed, bracketing 8 sample analyses by three measurements of the standard zircon GJ-1 (Jackson et al. 2004) and one each of Harvard 91500 (Wiedenbeck et al. 1995; 2004) and Plesôvice (Sláma et al. 2008) zircons for quality control of the standard analyses, yielding average age accuracies and precisions of <3%. Data were acquired from single spot analysis of 30 μm , using nominal laser fluence of $\sim 10 \text{ J/cm}^2$ and a pulse rate of 10 Hz. Total acquisition time for single analysis was max. 1.5 min, including 30 s gas blank measurement followed by laser ablation for 30 s and wash out for 20 s. Factory-supplied software was used for the acquisition of the transient data, obtained through automated running mode of pre-set analytical locations. Data reduction was performed off-line through the software *lolyte* (Paton et al. 2011), using the *lolyte-integral Visual-Age DRS* (data reduction scheme) routine (Petrus & Kamber 2012). This DRS includes a correction routine for down-hole isotopic fractionation and provides routines for data that require correction for common Pb (cPb).

The results include mainly non-corrected data. However, in some cases where only data with cPb existed a correction was applied. Individual analyses with high analytical errors (>10%) were filtered out and not considered. The Concordia diagrams were produced in the *IsoplotR* software (Vermeesch 2018). Unless otherwise stated, all reported ages are $^{207}\text{Pb}/^{206}\text{Pb}$ ages, and the reported errors are internal errors at the 2σ level or 95% confidence interval.

Thirty-two samples of the various rock units of the PIC and host rocks were selected for age determination, ensuring a geographical spread in the analysed samples. Four samples returned too poor data due to either massive cPb or metamictisation and were rejected, leaving a total of 28 samples. Zircons were documented prior to LA-ICPMS analysis by back-scattered electron (BSE) imaging at the SEM-instrument at GEUS and representative zircons for each sample are shown in Figure 14 - Figure 17.

7. Results

7.1 Petrography

7.1.1 PIC granites

The granitic rocks of both the 'massive PIC' and the 'layered PIC' units are medium to coarse-grained, two feldspar granites with alkali feldspar, plagioclase and quartz constituting 80-90 % combined. Alkali feldspar occurs as megacrysts that can be tabular or more rounded in shape, and measuring typically 3-4 cm, but can be up to 10 cm long. The mafic phases constitute 10-20 % of the rocks, and include orthopyroxene and biotite, sometimes associated with amphibole, clinopyroxene \pm garnet. The granites of the 'layered PIC' unit tend to be more leucocratic and contain occasional garnet. Accessory phases include magnetite, ilmenite, apatite, zircon, occasionally pyrite and chalcopyrite.

The rock textures show a transition going from the 'massive PIC' to the 'layered PIC' unit, with progressively stronger metamorphic overprinting in the latter. In general, the 'massive PIC' granites show magmatic state fabrics, with relatively minor overprinting, whereas the granites from the 'layered PIC' unit have strongly transposed fabrics and include almost ubiquitous evidence of migmatization (see below). The 'massive PIC' granites have hypidiomorphic granular textures, typically with a weak magmatic foliation expressed by a preferred orientation of feldspar megacrysts. Towards the 'layered PIC' unit, the rocks have increasing crystal plastic fabrics, often with characteristic granoblastic textures.

Under the microscope the least overprinted rocks show an intergranular texture, with feldspars forming the textural network, the interstitial spaces occupied by mafic minerals that constitute clusters (Figure 4). The porphyritic variants show alkali feldspar megacrysts, typically with Carlsbad twinning (Figure 4a, f). Plagioclase is often subhedral, tabular with characteristic polysynthetic albite twinning. Feldspars are variably turbid reflecting some effects of deuteric alteration (saussuritisation in plagioclase). Quartz occurs interstitially, either as larger anhedral grains with distinct undulating extinction (Figure 4a), or as fine sub-grained domains in more intensely deformed rocks (Figure 4h), or as myrmekitic intergrowth with

feldspars along grain boundaries (Figure 4d, f). Myrmekite growth may reflect a late magmatic or metasomatic reaction process under volatile-rich conditions.

Mafic minerals constitute 10-20 vol.% and are mainly orthopyroxene (≤ 10 vol.%) that shows a pale greenish beige pleochroism, low birefringence and parallel extinction (Figure 4b, e). Orthopyroxene is sometimes partially replaced by secondary amphibole in patchy domains or along borders (Figure 4c). Primary amphibole occurs along with orthopyroxene in some rocks; in which case amphibole crystals are closer to idiomorphic (Figure 4h). In incipiently altered rocks, orthopyroxene is variably replaced by yellowish brown fibrous minerals (smectite-chlorite?) (Figure 4h). Biotite (≤ 5 vol.%) occurs interstitially as late foliation-parallel trains superimposed on the primary magmatic fabric or as coronas around opaque Fe-Ti oxide minerals (Figure 4f, h). It is typically strongly pleochroic from dark reddish brown to pale light beige and has characteristic parallel extinction and high abnormal interference colours. Garnet is sometimes present in granites of the LPIC unit, where it occurs as small (< 0.5 mm) rounded grains (porphyroblasts) with inclusions plagioclase and quartz.

Accessory mineral phases are magnetite, ilmenite, zircon and apatite. The two geochemical groups of PIC granites (magnesian and ferroan groups; see below) are petrographically quite similar, except for the fact that ferroan granites generally have more magnetite relative to ilmenite, compared to the magnesian granites.

Late structural features, such as brittle deformation is present in some samples as cracks, as development of kink bands inside larger grains of feldspar and quartz, and bending of twinned crystals, e.g., plagioclase crystals with polysynthetic albite twins.

7.1.2 Mafic enclaves within the 'layered PIC' unit

The mafic enclave rocks are fine- to medium-grained norites with plagioclase, alkali feldspar and minor quartz with up to 25 vol.% mafic phases represented by orthopyroxene, biotite, \pm amphibole and clinopyroxene, and with opaque phases constituted by ilmenite or magnetite. The texture is equigranular, hypidiomorphic, intergranular with small clusters of mafic mineral phases occupying the interstices of the feldspar network (Figure 4i-j). Often the rocks display a semi-granoblastic texture with near 120° angles at triple junction boundaries (Figure 4i).

Orthopyroxene shows sharp contacts to adjacent mafic minerals, including amphibole grains (Figure 4j). Amphibole, identified by its distinct cleavage (56 and 124°), strong pleochroism from pale to creamy yellow and high birefringence, occur as separate subhedral grains (Figure 4j,l), or replaces orthopyroxene at grain boundaries (Figure 4k). Biotite shows strong

pleochroism from nearly colourless to foxy red and has high anomalous interference colours and characteristic parallel extinction (Figure 4j). Some biotite grains with irregular outlines are strongly zoned with foxy red (Fe-rich) rims and pale (Fe-poorer) cores (Figure 4j). Biotite typically defines a weak foliation in the rocks due to a preferential growth direction (Figure 4l).

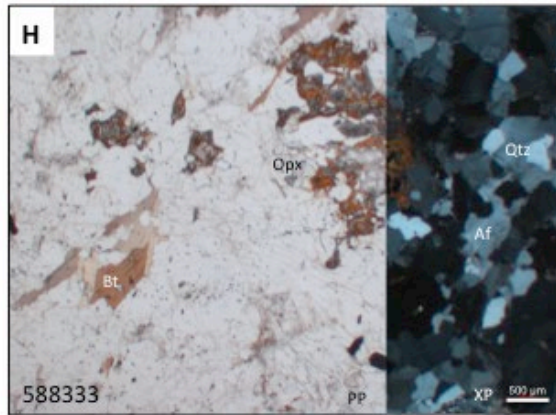
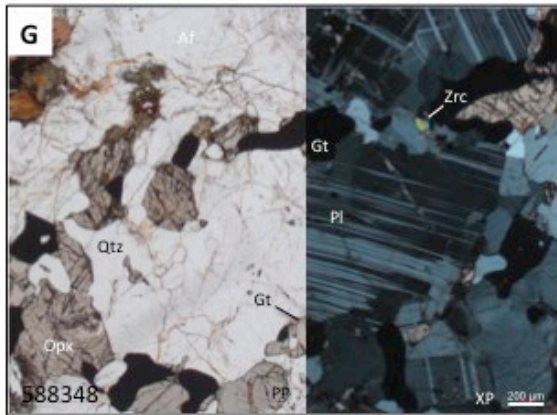
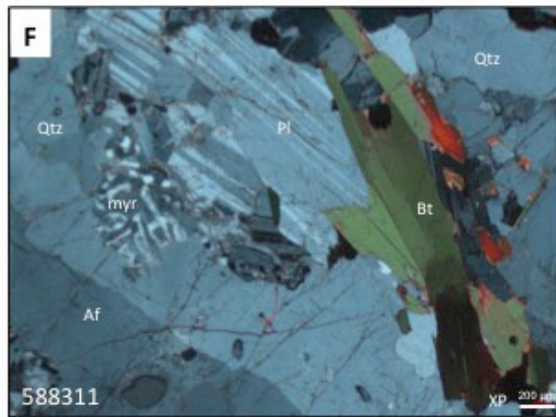
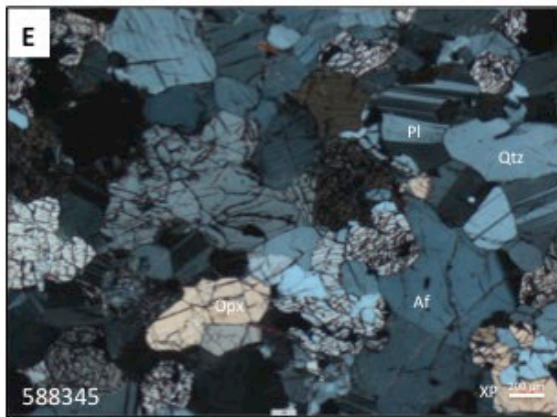
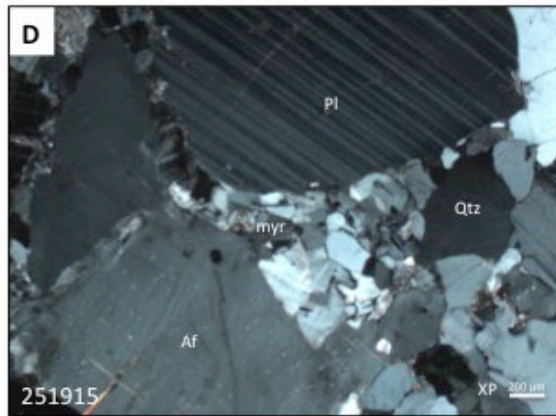
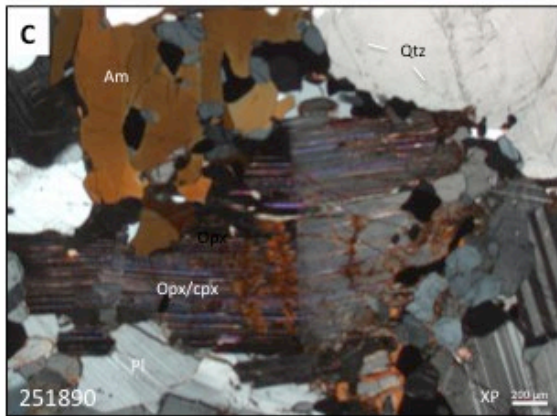
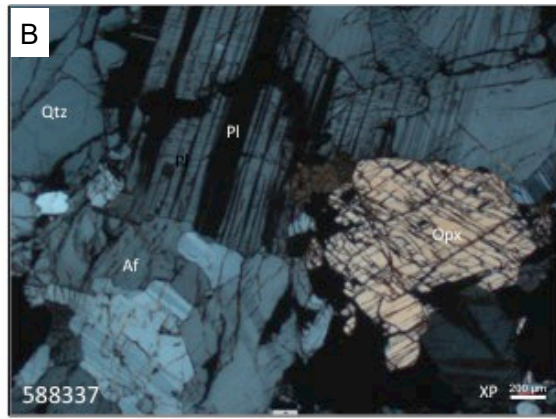
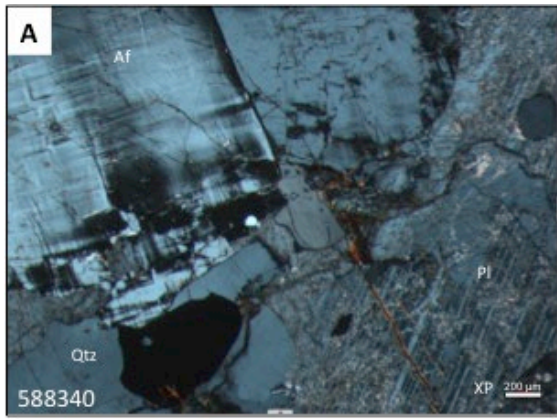
Plagioclase occurs as network-forming anhedral grains, typically showing polysynthetic albite twinning. Some twinned grains are noticeably bended, showing plastic (rather than brittle) deformation. Alkali feldspar and quartz generally occur interstitially to plagioclase. Most samples are fresh, but in some cases incipient alteration is seen as turbidity or saussuritisation of plagioclase, chloritisation of biotite or pyroxenes, and occasionally also late epidotisation of feldspars along brittle fractures (Figure 4l).

7.1.3 (Garnet) leucogranite dykes

The rocks are coarse-grained and highly leucocratic constituting alkali feldspar, plagioclase, and quartz, with up to 5 vol.% mafic minerals constituted by amphibole, biotite ± garnet (Figure 4n). Garnet occurs as large (often several mm, up to cm-sizes) spherical porphyroblasts, often with abundant inclusions of quartz and plagioclase (Figure 4m). Alkali feldspar is often turbid, and amphibole is often partly broken down to chlorite, suggesting common deuteric alteration effects in these late granitic dykes (Figure 4n).

7.1.4 Nukâvsak Formation paleosome and neosome rocks

To characterise the host rocks to the PIC, migmatitic samples (paleosome and neosome parts) the Nukâvsak Formation were collected at three different places across the PIC: from the westernmost island in Upernavik Isfjord, at SW Qaarsorsuaq, and at E Sullua. A paleosome metasandstone from Sullua shows remnant layering on a macroscopic scale (Figure 3m), which on a microscopic scale is seen to reflect alternating fine and coarser quartzofeldspathic layers, with the finer layers having additional biotite and garnet (Figure 4p). A melanosome part of the same outcrop at Sullua is a biotite-rich garnet rock with alkali feldspar and quartz (Figure 4o). Overall, these metasedimentary enclaves are garnet- and orthopyroxene-bearing migmatites. They have a similar mineral assemblage as to the paragneiss and are attributed to the Nûkavsak Formation.



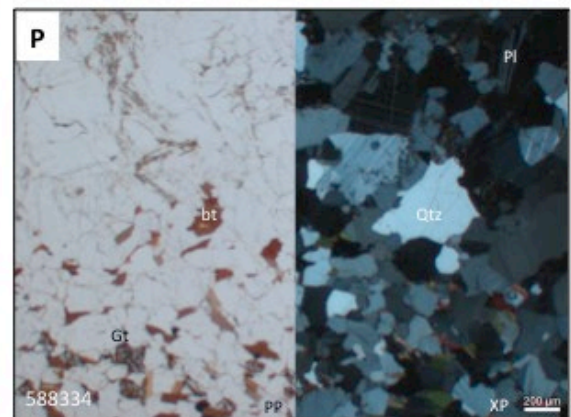
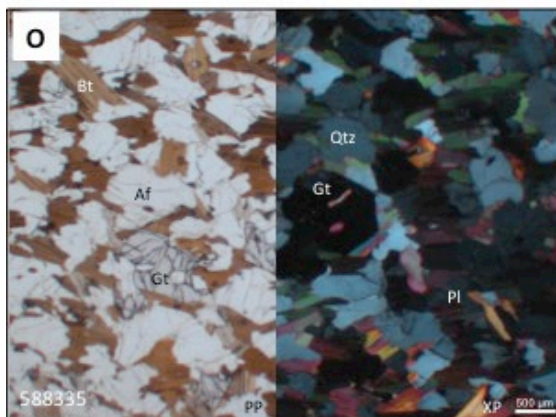
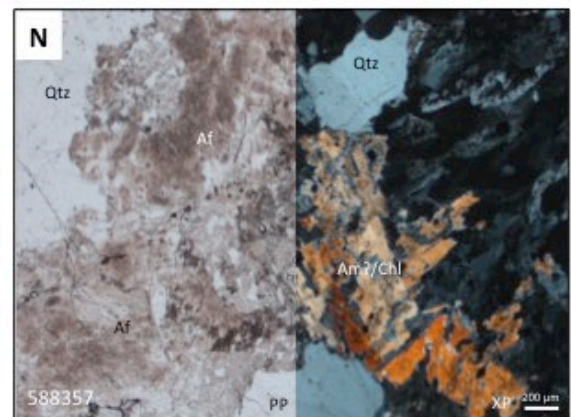
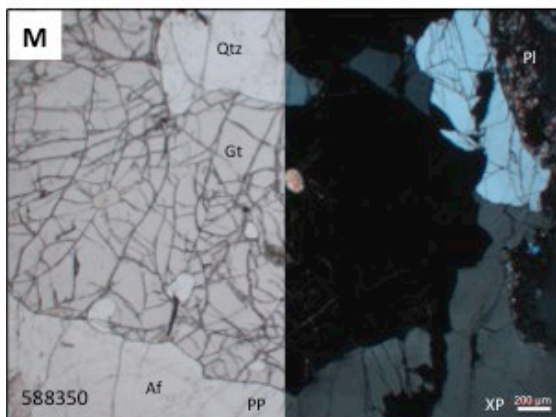
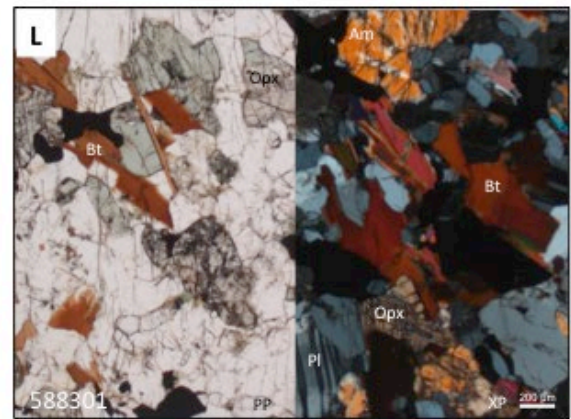
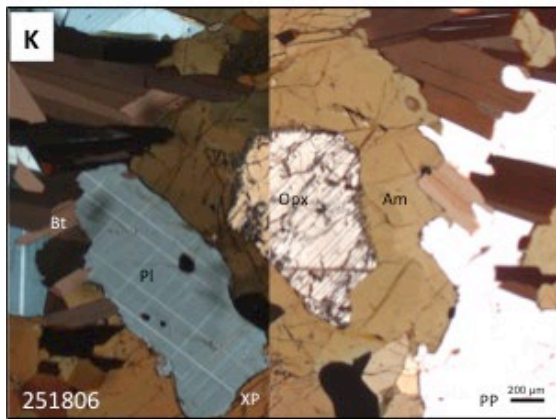
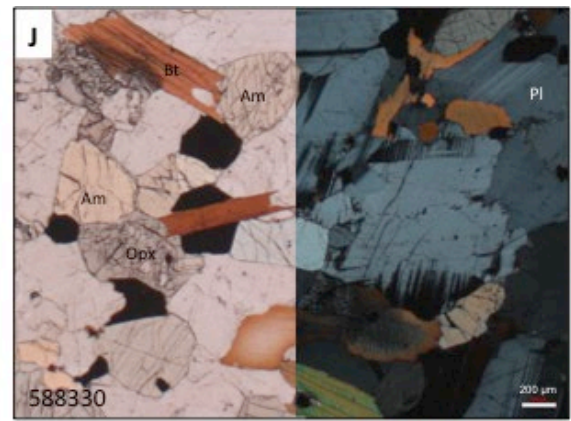
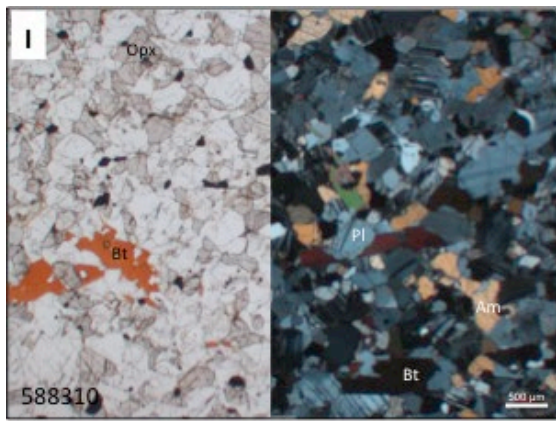


Figure 4 (previous pages). *Representative petrographic images for the PIC rocks shown in plane polarised (PP) and cross polarised XP) views. A) 588340 'massive PIC': B) 588337 'massive PIC': Fresh sample with plagioclase, alkali feldspar and quartz and subhedral opx. C) 251890, 'massive PIC': Opx with exsolution lamellas (pigeonite?) and partial overgrowth of amphibole; D) 251915, 'massive PIC': Interstitial myrmekitic texture between coarse plagioclase and alkali feldspar crystals, indicative of the presence of an intergranular melt. E) 588345, 'layered PIC': Medium- to coarse-grained granite (charnockite) with opx, alkali feldspar, plagioclase and quartz; semi-granoblastic texture. F) 588311, 'layered PIC': Myrmekite texture developed in contact between plag Kfsp and Qtz seen as worm-like intergrowth of quartz and plagioclase. G) 588348, 'layered PIC': Diatexitic granite with semi-granoblastic texture and intergranular clusters of opx and garnet. H) 588333, 'massive PIC': crystalloblastic fabric, late growth of biotite, breakdown of opx. I) 588310 Fine-grained norite, equigranular, granoblastic texture. J) 588330 Fine-grained norite, equigranular. K) 251806: Fine-grained norite, showing resorbed orthopyroxene partially replaced by amphibole and overgrown by biotite. L) 588301: Fine-grained norite, equigranular, partially altered. M) 588350: Garnet leucogranite. N) 588357: Leucogranite (altered). O) 588335: Neosome migmatite (Nûkavsak Fm). P) 588334: Paleosome (Nûkavsak Fm).*

7.2 Whole rock geochemistry

7.2.1 Effects of alteration

The studied rocks generally contain pristine igneous mineral assemblages and only sparse signs of alteration. Incipient alteration features are however not uncommon and are exemplified by turbidity of feldspar, replacement of orthopyroxene with amphibole, chloritisation of biotite and pyroxene, and local epidotisation along late brittle fractures (see section 7.1). Such effects are not indicative of major hydrothermal alteration that would cause a chemical change in the element budget and can best be ascribed to auto-metasomatism processes, which is a common phenomenon in cooling plutons. Loss on ignition in the PIC rocks is typically around 1 wt. % or below, supporting the notion of the rocks being unaltered. When plotting the PIC rocks in the ternary MFW-diagram of Ohta & Arai (2007) (not shown), the samples show only a minor displacement towards the W (weathering index) apex, suggesting relatively minor weathering effects on the chemistry of the rocks. Thus, we conclude that the chemical variations in all essence record igneous processes.

7.2.2 Major elements characteristics

In the total-alkali–silica (TAS) diagram modified by Middleton (1991) for plutonic rocks (Figure 5a), the PIC rocks (blue, green and turquoise symbols; note filled symbols indicate dated samples) form a broad range in SiO₂ from 44 to 78 wt.%, encompassing a smaller group of gabbroic and noritic rocks, some intermediate diorites, and a large group of granodiorites, quartz monzonites and granites.

Despite some scatter, particularly for the gabbroic rocks, most PIC rocks form a positive array that projects close to division line of Miyashiro (1978), but below this, and thus classify the PIC rocks as subalkaline. Overall, there is a marked bimodal distribution skewed towards higher SiO₂ with a paucity of rocks in the 53-62 wt.% interval. Most of the leucogranites (red symbols) classify as proper granites (69.0-78.3 wt.% SiO₂), while a subgroup of four samples with elevated alkali contents straddles the quartz monzonite field. The paragneiss migmatites (four leucosome, three paleosome migmatites) form a relatively tight cluster at high SiO₂ (70.8-74.9 wt.%) and relatively low Na₂O + K₂O (2.5-5.2 wt.%) and fall below the main PIC array.

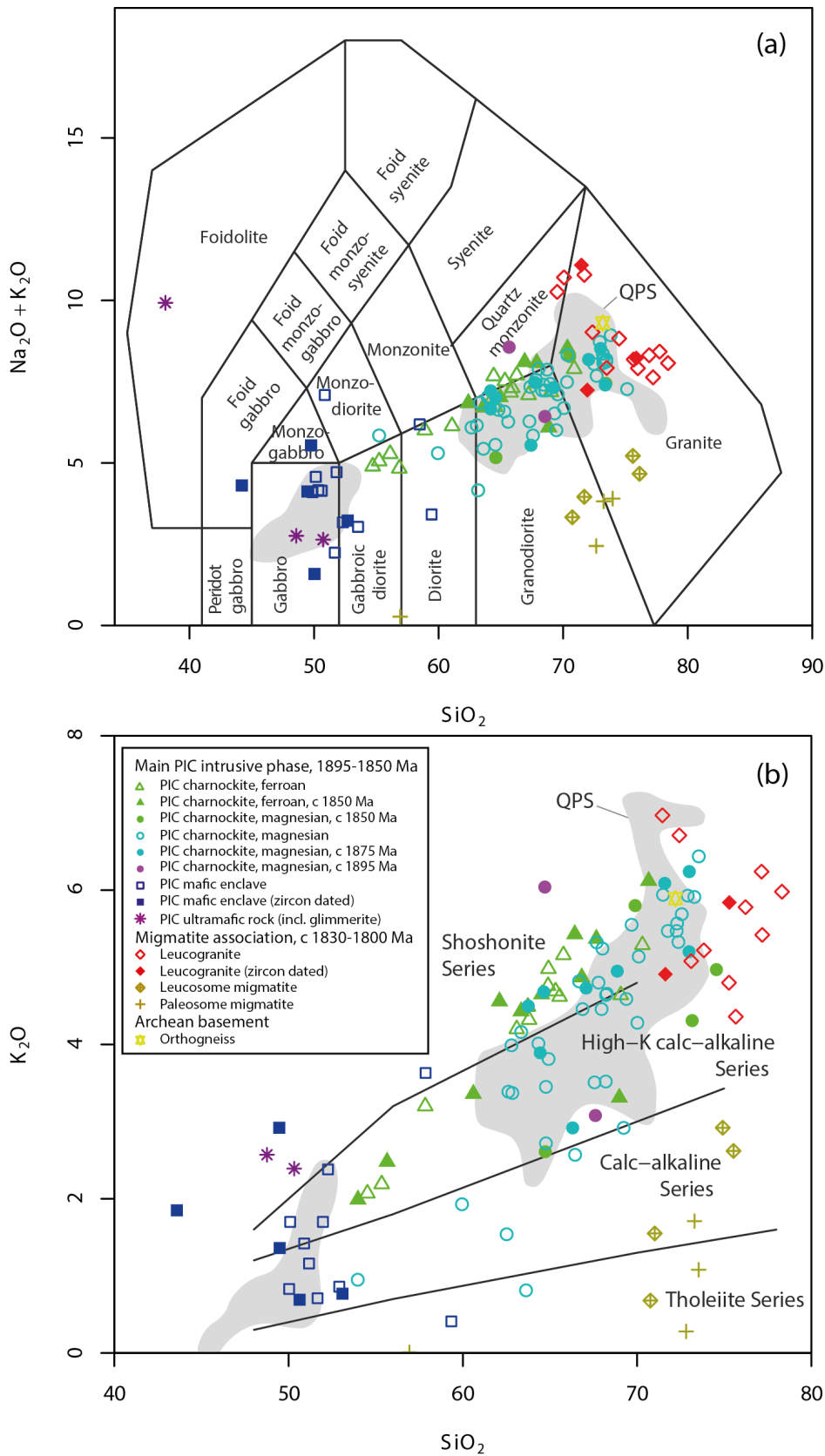


Figure 5. Chemical classification of the PIC rocks. (A) Total alkali vs. silica diagram (Middlemost, 1991); (B) K_2O vs. SiO_2 (Peccherillo and Taylor 1976; Lemaître 1989). Grey field: Qikiqtarjuaq plutonic suite from Baffin Island (data source: Whalen et al. 2012).

In the K_2O vs. SiO_2 diagram (Figure 5b), despite some scatter, the PIC rocks show high-K to shoshonitic affinity. Although alteration and weathering effects are generally believed to be insignificant, two of PIC samples (588304 and 588323) have anomalously low K_2O , which could reflect loss of potassium, possibly in tandem with mobility of other fluid mobile (LIL) elements. As a result, these samples will not be considered further in terms of their mobile element geochemistry. The leucogranites have comparable K_2O contents to the PIC granites, while the metasediments have distinctly lower K_2O , and they fall well below the general PIC array.

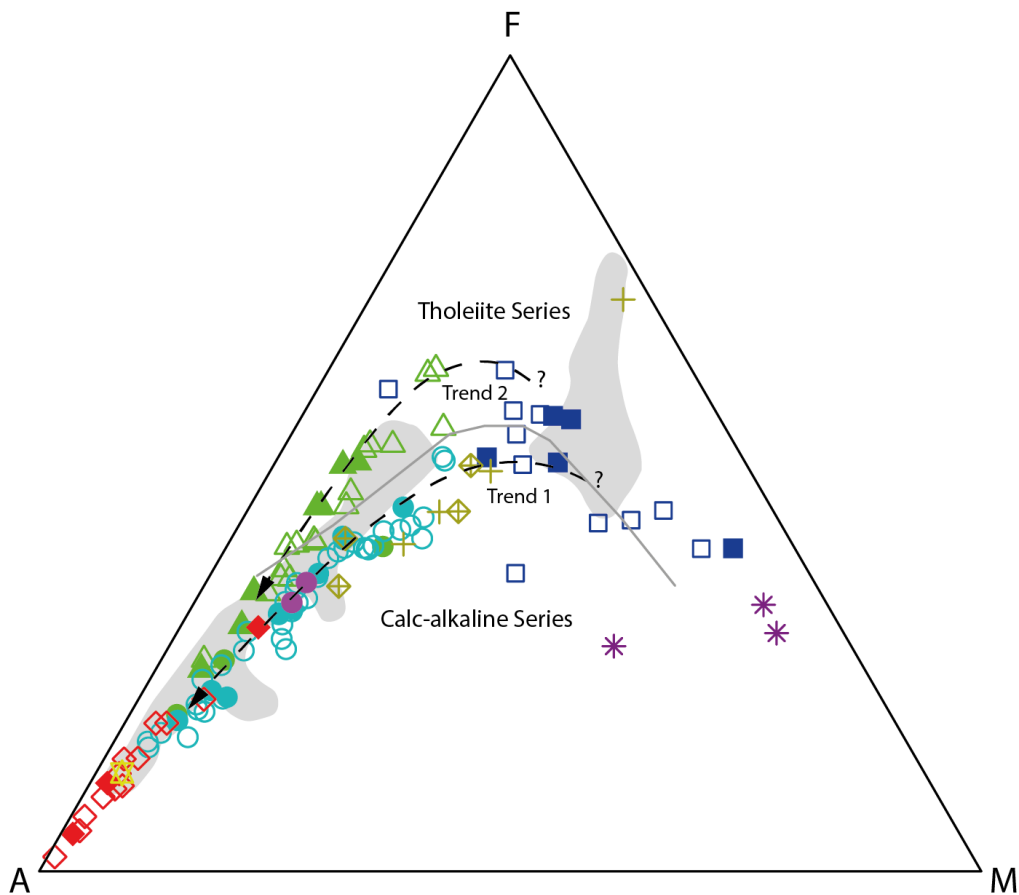


Figure 6. IC rocks plotted in the A ($Na_2O + K_2O$) F (FeO_t) M (MgO) diagram (Irvine and Barager, 1971). Two distinct PIC trends (1 and 2) with different FeO^*/MgO ratios are identified. Grey field: Qikiqtarjuaq plutonic suite (data source: Whalen et al. 2012). Symbols as in Figure 5.

In the AFM-diagram the PIC granites define two distinct trends ('Trend 1' and 'Trend 2') with slightly different Fe/Mg ratios that both project across the diagram towards the $Na_2O + K_2O$ apex (Figure 6). While 'Trend 1' is a typical calc-alkaline trend with low Fe/Mg ratios, 'Trend 2' plots above the division line between calc-alkaline and tholeiitic rock series with slightly higher Fe/Mg ratios. In the following the two trends are referred to as 'magnesian' vs. 'ferroan', respectively (see also Figure 7a and below). The major element characteristics of the

magnesian PIC granites (Figure 5 & Figure 6) closely resemble those of the QPS (shown by grey fields). The mafic enclave samples (norites) project back towards the MgO apex on the extension of the two PIC trends and could as such be petrogenetically related to the PIC granites, albeit display a great deal of scatter. The leucogranites overlap partly with the most evolved PIC charnockites, however extending to even more SiO₂-rich compositions.

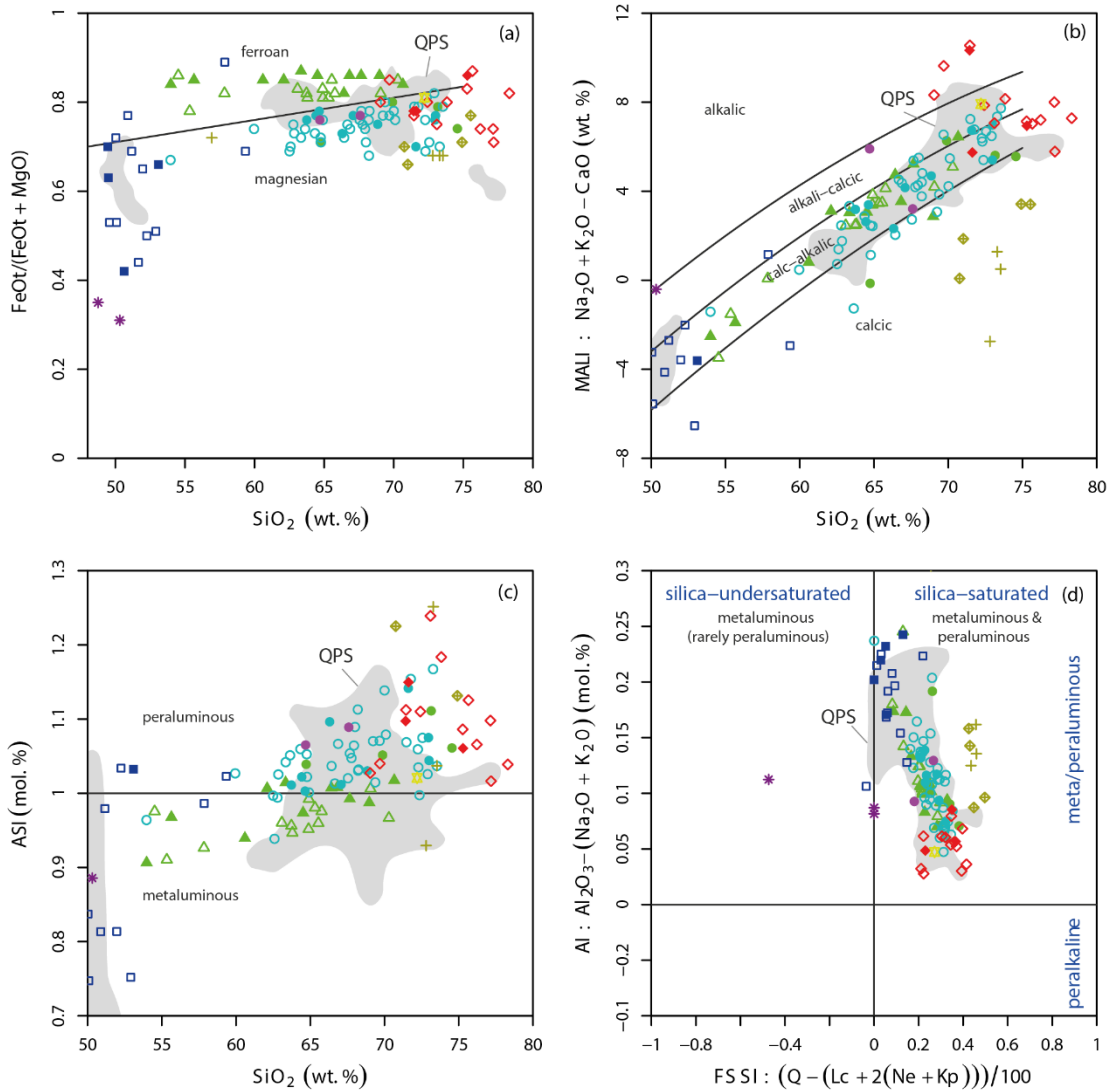


Figure 7. Classification of the PIC rocks following the classification scheme of Frost et al. (2001) and refined by Frost & Frost (2008). (a) FeOt/(FeOt+MgO) vs. SiO₂; (b) Na₂O+K₂O-CaO (MALI) vs. SiO₂; (c) Al/(Ca+Na+K) (ASI) vs. SiO₂; (d) Al₂O₃ - (Na₂O + K₂O) (Al) vs. (Q - (Lc + 2(Ne + Kp)))/100 (FSSI). Grey field: Qikiqtarjuaq plutonic suite (data source: Whalen et al. 2012). Symbols as in Figure 5.

Further classification of the PIC granites employs the scheme of Frost and Frost (2008) (Figure 7), which is based on Frost et al. (2001). In the FeO_t/(FeO_t + MgO) vs. SiO₂ diagram (Figure 7a) the PIC rocks form two distinct groups, which closely corresponds to the identified

'Trends' in the AFM-diagram (Figure 6): a magnesian group (= 'Trend 1') and a ferroan group (= 'Trend 2'). The magnesian and ferroan groups generally overlap in terms of their SiO₂ contents, however, the ferroan group includes more samples with SiO₂ <60 wt.%. Again, both groups form broad trends that project back towards the mafic enclave samples that show variable FeO_t/(FeO_t + MgO). The QPS granites generally overlap with the magnesian PIC granites ('Trend 1'), but also include some ferroan types. The leucogranites and migmatitic rocks are mostly magnesian and form a high-SiO₂ cluster at the extension of 'Trend 1'.

In the modified alkali-lime index (MALI) vs. SiO₂ diagram (Figure 7b) both the magnesian and the ferroan PIC groups follow the same sub-parallel trend of calc-alkalic affinity, while the most evolved compositions partly transgress into the alkali-calcic field. Again, the mafic enclave samples show a consistent calc-alkalic affinity and lie on the same trend as the other PIC rocks. The leucogranites range from alkalic to calc-alkalic affinities. In contrast the migmatitic rocks are distinctly calcic.

Plotting the aluminium saturation index (ASI = molar ratio of Al/(Ca + Na + K)) vs. SiO₂ (Figure 7c) produces two sub-parallel, positive arrays with increasing ASI for increasing SiO₂, and with a clear separation between the ferroan and magnesian groups. The ferroan group is generally displaced towards lower ASI (0.90-1.10), compared to the magnesian group (0.95-1.15) for similar SiO₂ contents. The mafic enclave samples are generally metaluminous (three are slightly peraluminous), and generally lie at the low-SiO₂ end of the two trends. In contrast, the leucogranites as well as the migmatitic rocks, are distinctly peraluminous with ASI > 1 and up to 1.25.

Figure 7d shows that all PIC samples are silica-saturated and either metaluminous or peraluminous and form a broad negative trend of increasing silica-saturation with falling alumina index (AI). Noteworthy, the magnesian PIC granites are displaced towards higher silica-saturation values (for the same alumina index) and plot closer to the migmatitic rocks that are all highly silica-saturated.

In Figure 8 selected major elements (TiO₂, Al₂O₃, FeO_t, MgO, CaO, P₂O₅) are plotted vs. SiO₂. In several of these diagrams the ferroan and magnesian groups form distinct trends: For a given SiO₂ contents the magnesian group ('Trend 1') has lower TiO₂ and P₂O₅, and higher Al₂O₃ and MgO, but similar FeO_t and CaO, compared to the ferroan group ('Trend 2'). In most cases the leucogranites plot on the extension of the two PIC trends but do have comparatively higher Al₂O₃ and lower TiO₂. In contrast, the migmatitic rocks tend to have higher FeO_t, MgO and CaO, and lower Al₂O₃ relative to the PIC granites.

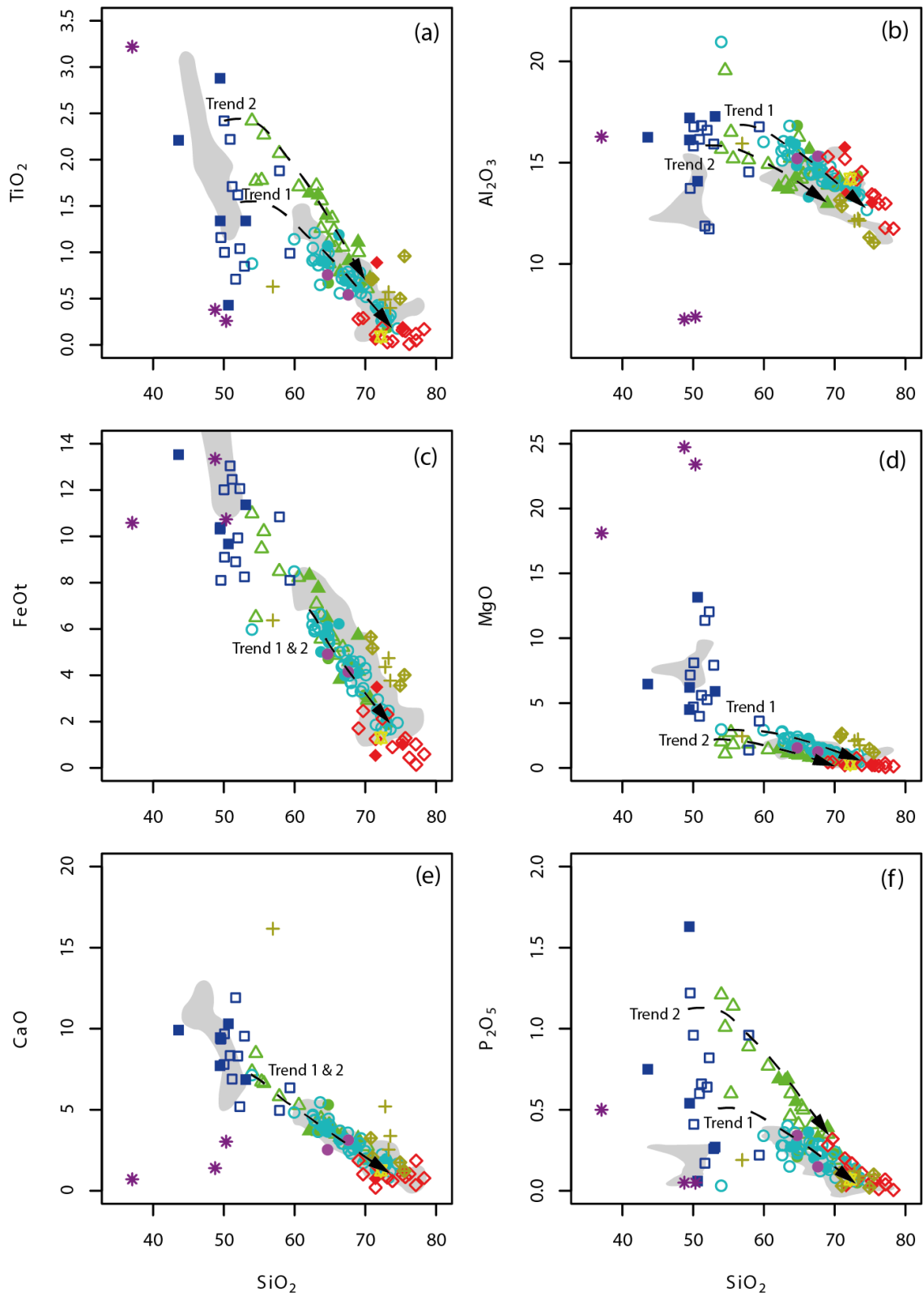


Figure 8. Selected major elements plotted in Harker-diagrams: (a) TiO_2 , (b) Al_2O_3 , (c) FeO^t , (d) MgO , (e) CaO , (f) P_2O_5 vs. SiO_2 . Grey field: Qikiqtarjuaq plutonic suite (data source: Whalen et al. 2012). Symbols as in Figure 5.

7.2.3 Trace elements characteristics

Trace element compositions of the PIC and related rocks show substantial variation, as illustrated in Figure 9 & Figure 10.

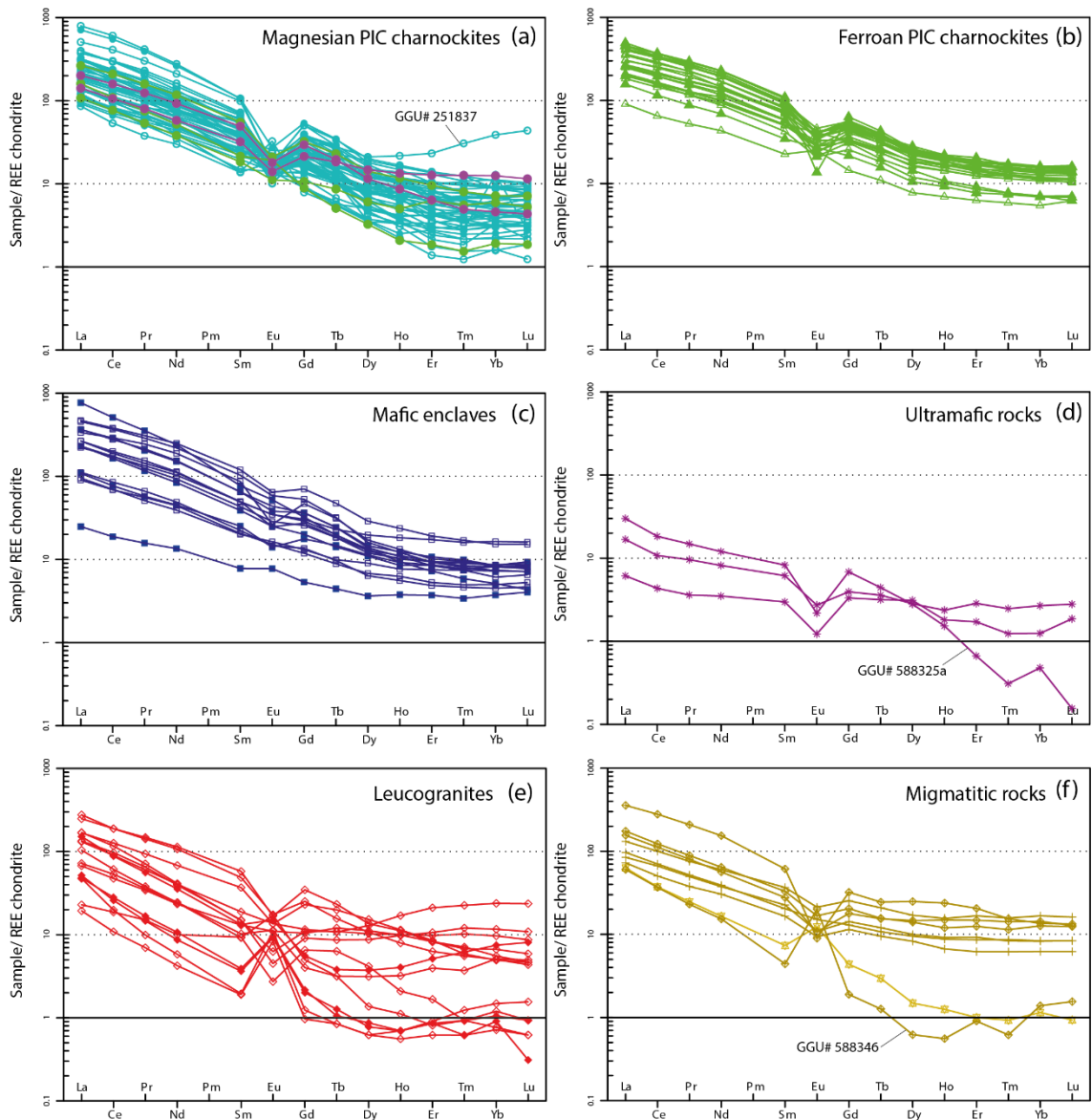


Figure 9. (a)-(f) Chondrite-normalised rare earth element diagrams for PIC samples. Symbols as in Figure 5.

In the chondrite-normalised rare earth elements (REE) the two groups of PIC granites display rather similar patterns characterised by enrichment in the light rare earth elements (LREE) relative to the middle (MREE) and heavy rare earth elements (HREE), generally with negative Eu-anomalies (average $\text{Eu}/\text{Eu}^* \sim 0.64$, $(\text{Eu}/\text{Eu}^* = 2 \cdot \text{Eu}_{\text{ch}} / (\text{Sm}_{\text{ch}} + \text{Gd}_{\text{ch}}))$) (Figure 9a,b). In

detail the ferroan group show a tighter range with slightly higher average LREE and HREE contents and less fractionated (LREE, MREE)/HREE ($La_{ch} = 401 \pm 146$, $Yb_{ch} = 16.1 \pm 4.0$, $La_{ch}/Yb_{ch} = 24.9 \pm 6.8$, $Dy_{ch}/Yb_{ch} = 1.66 \pm 0.17$; 1 std. dev., subscript 'ch' denotes chondrite-normalisation), compared to the magnesian group ($La_{ch} = 298 \pm 185$, $Yb_{ch} = 8.0 \pm 7.0$, $La_{ch}/Yb_{ch} = 53.3 \pm 44.7$, $Dy_{ch}/Yb_{ch} = 1.92 \pm 0.85$). One magnesian granite sample (251837) has anomalously high HREE ($Yb_{ch} = 50.4$) and low MREE/HREE ($Dy_{ch}/Yb_{ch} = 0.55$). The norites show a great deal of scatter in terms of REE contents, broadly matching the range of the PIC granites ($La_{ch} = 360 \pm 244$, $Yb_{ch} = 10.4 \pm 4.5$) (Figure 9c). Like the granites the norites are characterised by (LREE, MREE)/HREE enriched patterns ($La_{ch}/Yb_{ch} = 37.7 \pm 34.2$, $Dy_{ch}/Yb_{ch} = 1.66 \pm 0.45$), albeit they have smaller or missing Eu-anomalies (average $Eu/Eu^* = 0.81 \pm 0.18$). Overall, Eu/Eu^* values in the PIC rocks correlate positively with Sr/Nd (not shown), suggesting a control by plagioclase fractionation. The ultramafic samples (Figure 9d) form a scattered group with low REE concentrations, LREE-enriched patterns and negative Eu-anomalies ($La_{ch} = 23 \pm 16$, $Yb_{ch} = 1.9 \pm 1.5$, $La_{ch}/Yb_{ch} = 24.8 \pm 33.2$, $Eu/Eu^* = 0.40 \pm 0.13$). The glimmerite sample 588325a has particularly low HREE contents. The leucogranite and migmatitic paragneiss samples (Figure 9e,f) show consistent LREE-enriched patterns with variable MREE-HREE variations patterns, including variable Eu-anomalies. Two types of patterns can be distinguished: one type with relatively low HREE-MREE contents and a depression in MREE (i.e., $Dy_{ch}/Yb_{ch} < 1$) coupled with positive Eu-anomaly ($Eu/Eu^* > 1$), and another type with higher MREE-HREE contents showing the opposite characteristics (i.e., $Dy_{ch}/Yb_{ch} > 1$ and $Eu/Eu^* < 1$). These different patterns could signify a coupled effect of amphibole (\pm garnet) versus plagioclase crystallisation. In contrast, the paleosome migmatite samples (quartzites) show highly consistent patterns with flat MREE-HREE and only weak negative, or absent Eu-anomalies.

In the primitive mantle (PM)-normalised multi-element, or 'spiderdiagram' (Figure 10a-c), the PIC granites show the same overall patterns with relative enrichment of the (traditionally) most incompatible elements, such as Rb (~ 210 x PM) and K (~ 150 x), relative to the less incompatible elements, such as Sr (~ 15 x) and Y (~ 6 x). The ferroan granites show higher enrichments in Ba (~ 228 x PM), Nb (~ 48 x), Ta (~ 54 x), Zr (~ 44 x), Hf (~ 40 x), Ti (~ 6.9 x), Y (~ 34 x), and lower enrichment in Th (~ 50 x) and U (~ 44 x) relative to the magnesian granites that have Ba (~ 148 x PM), Nb (~ 23 x), Ta (~ 29 x), Zr (~ 23 x), Hf (~ 22 x), Ti (~ 3.3 x), Y (~ 16 x), Th (~ 296 x) and U (~ 89 x). Particularly for the magnesian granites, Th and U show a very large range (Th: 9-2200 x PM, U: 9-611 x) with an almost bimodal distribution of these elements. A common feature of all PIC granites is variably pronounced negative anomalies for Nb, Sr, P and Ti. The size of the anomalies increases with increasing silica contents (not shown). The Nb anomaly expressed as $Nb/Nb^* (= 2 \times Nb_{PM}/(Th_{PM} + K_{PM}))$, subscript-PM denotes primitive mantle-normalisation), where values below unity equals negative anomaly,

and vice versa. The Nb/Nb* is systematically lower in the magnesian (0.19 ± 0.19) compared to the ferroan granites (0.55 ± 0.29). In contrast, the Sr anomaly, expressed as Sr/Sr^* ($= 2 \times Sr_{PM}/(Pr_{PM} + Nd_{PM})$), is higher in the magnesian (0.33 ± 0.27) than the ferroan granites (0.22 ± 0.13). The P anomaly, expressed as P/P^* ($= 2 \times P_{PM}/(Pr_{PM} + Nd_{PM})$), is higher in the magnesian (0.33 ± 0.27) than the ferroan granites (0.22 ± 0.13). In contrast, the Ti anomaly, expressed as Ti/Ti^* ($= 2 \times Ti_{PM}/(Sm_{PM} + Y_{PM})$), is similar in two granite types (0.33 ± 0.20 and 0.34 ± 0.13). Most of these anomalies are likely mineralogically controlled, e.g., through fractional crystallisation of major rock forming phases such as plagioclase (Sr), apatite (P) and Fe-Ti oxides (Ti). In case of the incompatible element niobium, the size of the anomaly most likely records an inherent source characteristic.

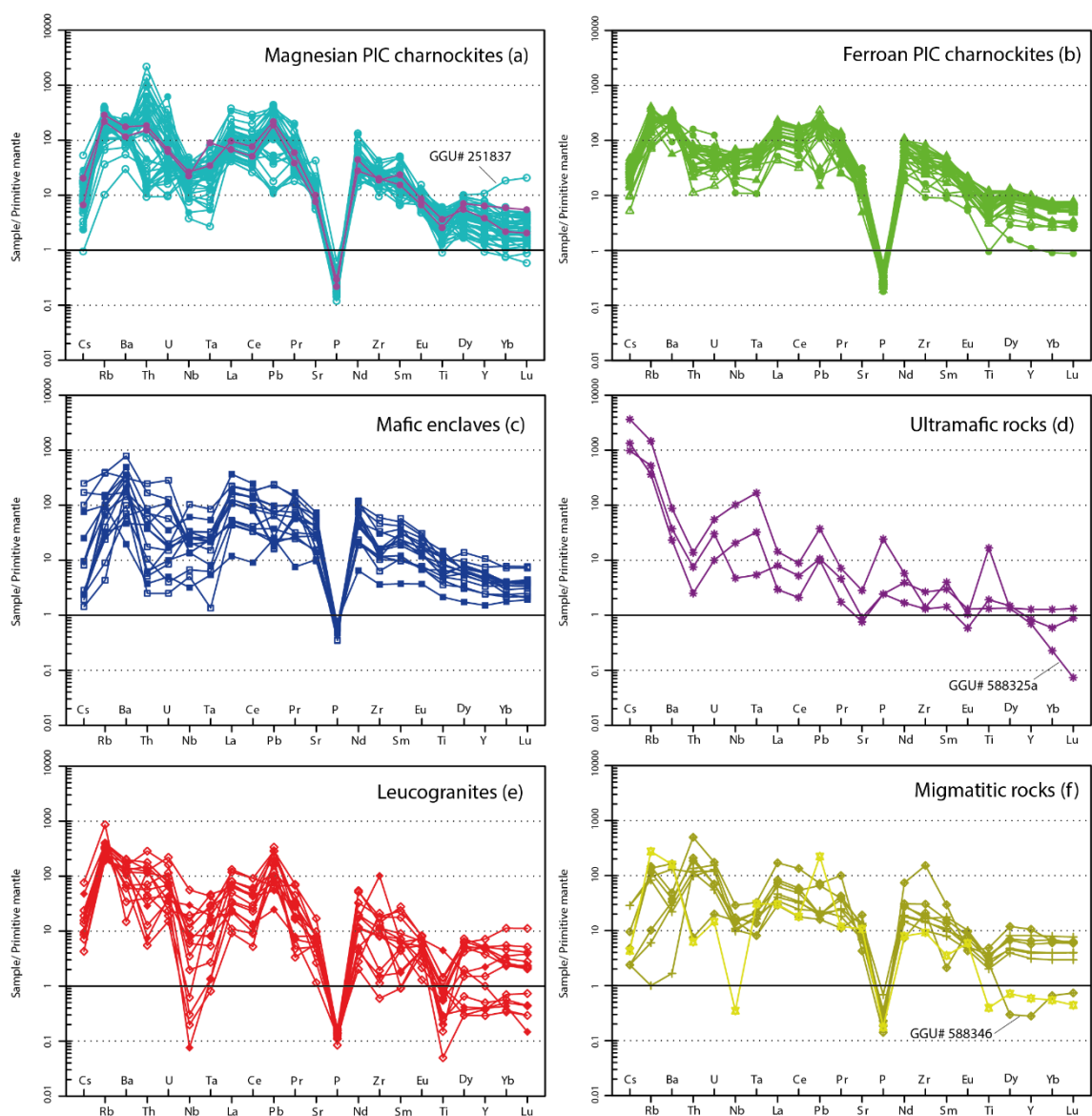


Figure 10. Multi-element variation diagrams (spider-plots) (a)-(f). Normalised to Primitive Mantle (McDonough & Sun, 1995). Symbols as in Figure 5.

The main differences between ferroan and magnesian granites in terms of incompatible trace elements can be illustrated by the following ratios: Nb/U (41 vs. 20, in ferroan and magnesian granites, respectively), Nb/Th (9.8 vs. 4.5) and Ba/Th (514 vs. 292). These ratios likely reflect primary source features, supporting evidence for different protolith sources for the ferroan and magnesian granites. Noteworthy, the PIC samples presented by Thrane et al. (2005) fall within the group of magnesian granites in terms of the REE and incompatible trace element characteristics (not shown).

The norite enclaves (Figure 10c) show broadly similar patterns to the PIC granites, particularly the magnesian granites, but also show a wide scatter in concentration levels, especially the most incompatible ones from Cs to Ta.

The ultramafic rocks (glimmerites, Figure 10d) are characterised by 'spiked' patterns with generally low concentrations of most trace elements, and positive anomalies for Cs, Rb and to some extent also Ba and Ti. These elements are major constituents in phlogopite and reflect the modal composition of these samples.

In Figure 10e and f the leucogranites and migmatitic metasediments show highly varied, multi-spiked patterns with pronounced troughs for Nb, Sr, P and Ti. Particularly the leucogranites show extreme negative anomalies for Nb and Ti ($Nb/Nb^* = 0.08$, $Ti/Ti^* = 0.02$) and several samples also have variable Zr-Hf troughs suggesting fractionation of zircon; in some cases, positive Zr anomalies (i.e., high Zr/Sm ratios) indicate likely zircon accumulation in these specific samples.

Figure 11 shows selected discrimination plots by Whalen et al. (1987) to distinguish A-type granites from I- and S-types (*cf.* Chappell & White, 1974) plotting the contents of incompatible high field strength elements ($Zr+Nb+Ce+Y$) and Ga/Al ratio vs. selected major and trace element parameters ($FeOt/MgO$, Na_2O+K_2O , K_2O/MgO and Zr). In the $FeOt/MgO$ vs. $Zr+Nb+Ce+Y$ diagram (Figure 11a) the magnesian granites have generally lower $\Sigma(Zr+Nb+Ce+Y)$ and $FeOt/MgO$ and mainly plot as I/S/M-type, whereas the ferroan granites have the opposite characteristics and plot as A-type. In Figure 11b-d the ferroan charnockite samples generally have elevated $10^4 * Ga/Al$ (> 2.6), again classifying them as A-type granites in these diagrams. The magnesian PIC charnockites generally plot as I/S//M-types with lower Ga/Al, although some samples transgress across the boundary to $10^4 * Ga/Al > 2.6$. Noteworthy, there is a complete overlap in the range of Na_2O+K_2O and K_2O/Mg for the two granite groups, and despite the slightly elevated alkali contents, none are alkaline (see also Figure 4a). The magnesian granites are mainly peraluminous and are increasingly so with

increasing SiO_2 (Figure 7c). From Figure 11 The argument can be made that the magnesian granites represent S-type, which in a few cases may be supported by some of the samples containing garnet (Section 7.1). However, in general the mineralogy of the magnesian granites is not consistent with that of typical S-type granites (orthopyroxene and biotite are normally the only mafic mineral phases, and muscovite or cordierite are not observed). It is therefore more conceivable that the magnesian granites may be regarded as I-type granites that may have seen various degrees of crustal contamination (see also below). The four published samples by Thrane et al. (2005), include one with A-type character (sample 493639), the remaining have I- or S-type character. The PIC granites overlap closely with the variation of the Qikiqtarjuaq plutonic suite (QPS) in all diagrams.

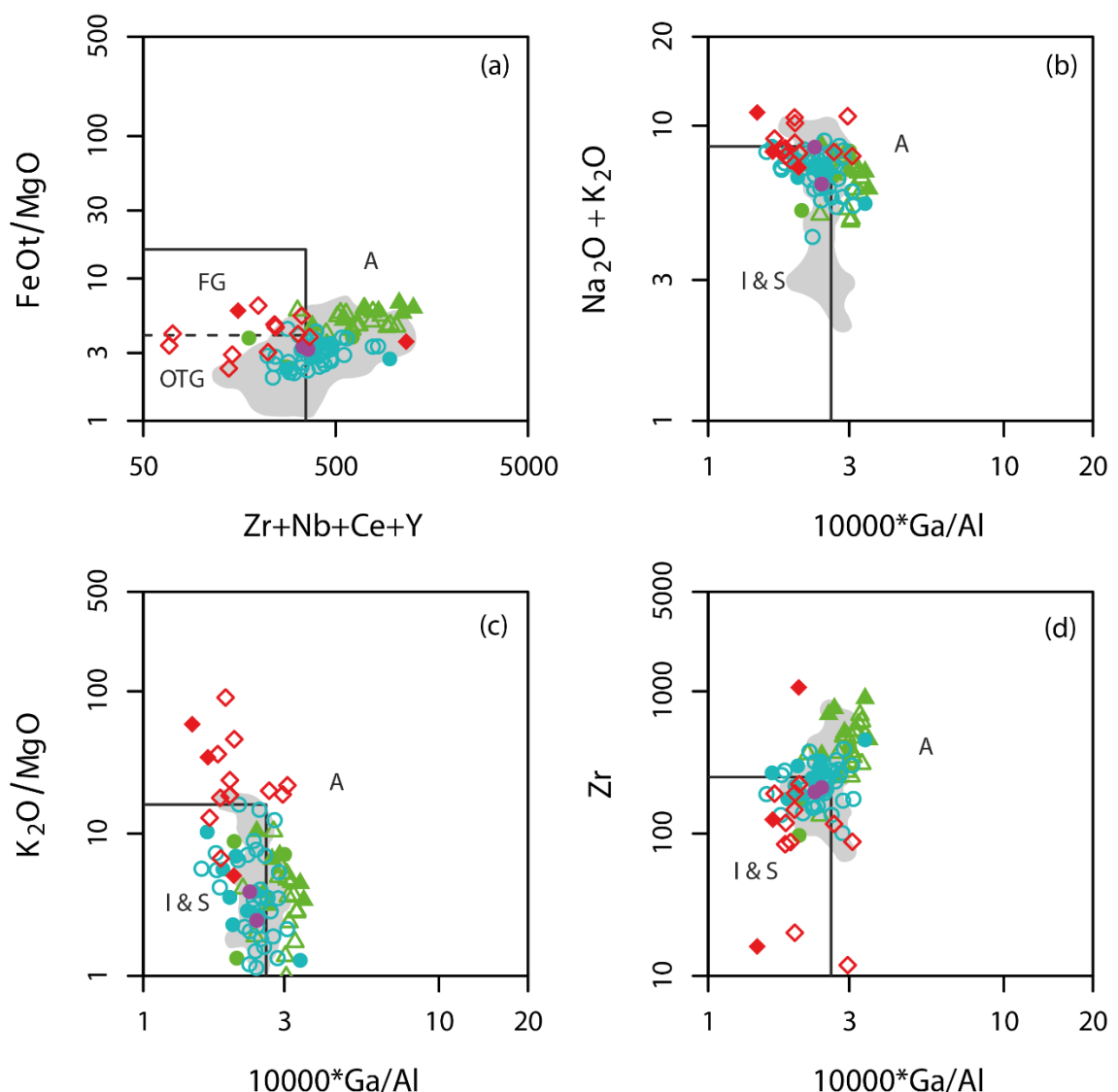


Figure 11. Discriminating S- / I-type from A-type granites plotting (a) FeO^t/MgO vs. $\text{Zr}+\text{Nb}+\text{Ce}+\text{Y}$, (b) $\text{Na}_2\text{O}+\text{K}_2\text{O}$ vs. $10^4 \times \text{Ga}/\text{Al}$, (c) Zr vs. $10^4 \times \text{Ga}/\text{Al}$, (d) Nb vs. $10^4 \times \text{Ga}/\text{Al}$. After Whalen et al. (1987). Grey field: Qikiqtarjuaq plutonic suite (data source: Whalen et al. 2012). Symbols as in Figure 5.

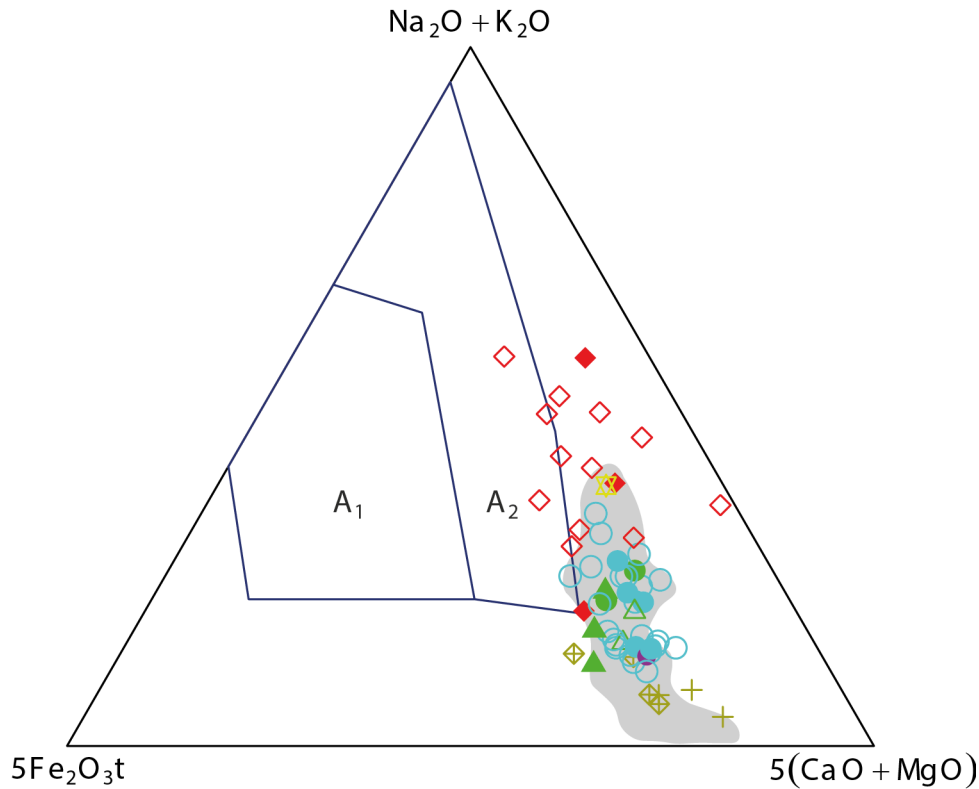


Figure 12. Discriminating different A-type granites ($\text{SiO}_2 > 67 \text{ wt\%}$). After Grebennikov (2014). Grey field: Qikiqtarjuaq plutonic suite (data source: Whalen et al. 2012). Symbols as in Figure 5.

Figure 12 shows the PIC rocks in the ternary discrimination scheme for A-type granites by Grebennikov et al. (2014) plotting $5 \times \text{Fe}_2\text{O}_3^{\text{T}}$, $\text{CaO} + \text{MgO}$, and $\text{Na}_2\text{O} + \text{K}_2\text{O}$. This diagram considers granites with $\text{SiO}_2 > 67 \text{ wt\%}$ and distinguishes A_1 and A_2 -type granites vs. other types (I & S). The PIC charnockites plot outside the A_1 and A_2 fields. The PIC granites tend to straddle the A_2 field, which denotes alkaline granites formed in postorogenic extensional settings. There is no distinct difference in this plot between the magnesian and ferroan granites. Again, there is a close overlap with the granitoids of the QPS. The highly evolved leucogranites have higher relative alkali contents and generally straddle the A_2 field, two samples plotting inside the field.

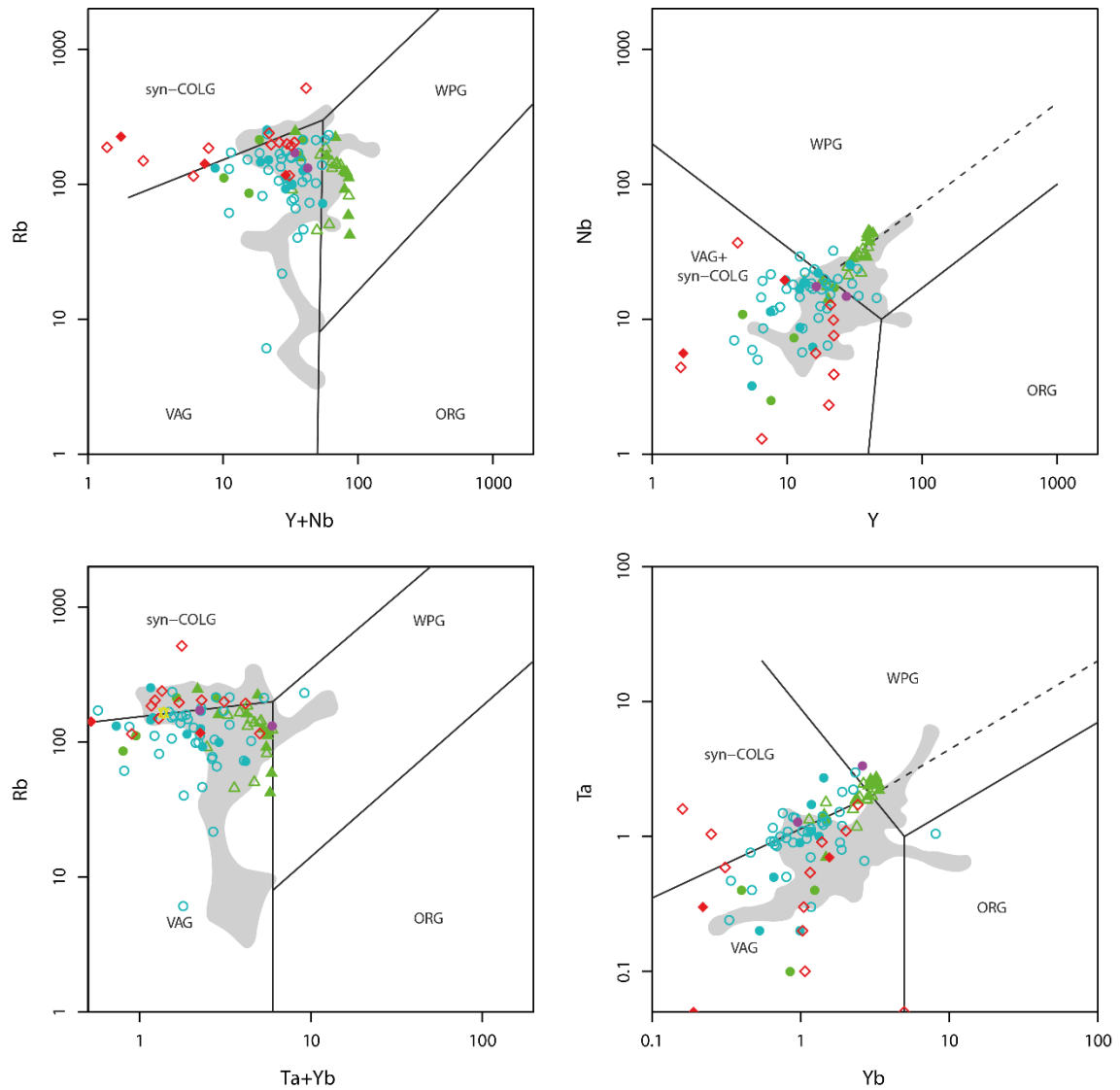


Figure 13. Tectonic discrimination diagrams (Pearce et al. 1984; Pearce 1996). (a) Rb vs. Y+Nb; (b) Nb vs. Y; (c) Rb vs. Ta+Yb; (d) Ta vs. Yb. Syn-COLG: Syn-collisional granite; WPG: Within Plate Granite; VAG: Volcanic Arc Granite; ORG: Orogenic Granite. Grey field: Qikiqtarjuaq plutonic suite (data source: Whalen et al. 2012). Symbols as in Figure 5.

Figure 13 presents tectonic discrimination plots based on incompatible trace elements after Pearce et al. (1984). The magnesian and ferroan PIC granites are well separated in these plots. The majority of ferroan granites have elevated concentrations of high-field strength elements (Nb, Ta, Yb, Y) and plot as 'within-plate granites, or close to this, inside the fields for volcanic arc granites or syn-collisional granites. The magnesian PIC granites plot as volcanic arc granites or syn-collisional granites. The leucogranites plot mostly as syn-collisional granites.

7.2.4 Summary of major and trace element variations

In summary, the major and trace element variations demonstrate the existence of two distinct geochemical groups of PIC granites:

- A magnesian group of granites (i.e., with relatively low $\text{FeOt}/(\text{FeOt}+\text{MgO})$) have relatively low TiO_2 and P_2O_5 , are metaluminous to mildly peraluminous ($\text{ASI} = 0.95\text{--}1.15$), show moderate REE-enrichment with high LREE/HREE ratios, and have moderately low HFSE (Nb, Ta, Y) contents.
- A ferroan group of granites (i.e., with relatively high $\text{FeOt}/(\text{FeOt}+\text{MgO})$) have relatively high TiO_2 and P_2O_5 , are metaluminous to mildly peraluminous ($\text{ASI} = 0.9\text{--}1.1$), are enriched in HFSE and REE, with lower LREE/HREE ratios.
- Both major elements and trace elements point to an I-type character for both the magnesian and ferroan groups, and not as previously proposed an A-type character (Thrane et al. 2005).
- The magnesian granites show a very close chemical correspondence to the c. 1900–1880 Ma Qikiqtarjuaq Plutonic Suite in Baffin Island.
- The mafic enclaves (norites) have similar trace elemental geochemical characteristics as the magnesian granites, albeit show a wider scatter in elemental contents.
- The leucogranites that are younger than the PIC granites (see below) are all peraluminous, show LREE-enriched patterns with variable MREE-HREE fractionations and variable Eu-anomalies.

7.3 Geochronology

Individual rock samples analysed are described in the following section. The U/Pb data are presented in Wetherill Concordia diagrams or density distribution plots, along with representative zircon images in Figure 14 to Figure 17.

7.3.1 PIC charnockites

251816 ('layered PIC' unit): Most of the grains show oscillatory zoning in cores and thin metamorphic rims. A total of 151 grains were analysed of which 18 returned poor data, 25 had significant common Pb (cPb) and were not considered further. Of the 108 acceptable analyses a main population of magmatic zircon from interior domains with high Th/U (0.06-0.73) give an intrusion/crystallisation age of **1870.7 ± 3.0 Ma** (MSWD = 2.9, n/N = 67/68). A smaller group metamorphic zircon with intermediate Th/U (0.04-0.36) yields an age of **1855.0 ± 3.4 Ma** (MSWD = 2.3, n/N = 8/12). In addition, a population of inherited magmatic grains yield an age of **1896.7 ± 1.4 Ma** (MSWD = 3.7, n/N = 22/25).

251820 ('massive PIC' unit): Most grains are subhedral showing oscillatory zoning in cores and thin metamorphic rims. A total of 120 grains were analysed of which 17 returned poor data, 10 had significant cPb and were not considered further. Of the remaining 93 good analyses a main population with high Th/U (0.16-1.29) from interior domains gives an intrusion/crystallisation age of **1875.6 ± 3.0 Ma** (MSWD = 3.3, n = 47). A group of grains with lower Th/U (0.09-0.52) yield a metamorphic $^{207}\text{Pb}/^{206}\text{Pb}$ age of **1848.8 ± 3.1 Ma** (MSWD = 5.3, n/N = 16/18). Sixteen inherited grains give ages from ca. 1890 to 2600 Ma; of which a sub-group gives a well-defined age of **1894.6 ± 3.6 Ma** (MSWD = 0.16, n = 9).

251835 ('massive PIC' unit): Most of the grains are subhedral with distinct oscillatory zoning in cores, sometimes with homogenous metamorphic rim domains. A total of 95 grains were analysed of which only four were discarded due to cPb. A large population of interior domains showing oscillatory zoning and average Th/U = 0.63 (0.15-0.94) give an intrusion/crystallisation age of **1849.2 ± 3.0 Ma** (MSWD = 1.7, n/N = 55/56). A heterogeneous group of overprinted cores and rim domains with average Th/U = 0.51 (0.20-0.86) yield a metamorphic age of **1835.7 ± 3.1 Ma** (MSWD = 2.0, n/N = 25/28). A small group of inherited magmatic grains give an age of **1873.0 ± 4.3 Ma** (MSWD = 0.8, n = 5), with a single grain at ca. 1900 Ma.

251847 ('layered PIC' unit): Most grains are subhedral showing oscillatory zoning in cores, sometimes with thin metamorphic rims. A total of 78 grains were analysed of which 19 returned poor data, 11 had significant cPb and were not considered further. Of the 48 acceptable analyses a group of interior domains showing magmatic zoning and high Th/U (0.11-0.98) give an intrusion/crystallisation age of **1877.7 ± 2.2 Ma** (MSWD = 1.2, n = 41). A group with variably overprinted interior domains gives a metamorphic age of **1853.4 ± 3.4 Ma** (MSWD = 0.5, n/N = 7/9). A group of 14 inherited grains give ages from ca. 1900 to 2600 Ma, of which a sub-group of magmatic grains yields an age of **1897.0 ± 3.5 Ma** (MSWD = 1.7, n = 7).

251873 ('massive PIC' unit): Most of the grains show oscillatory zoning in cores and thin metamorphic rims. A total of 105 grains were analysed of which eight returned poor data, 14 had significant cPb and were not considered further. A main group of magmatic, variably zoned core domains with average Th/U = 0.63 (0.35-1.04) give an intrusion/crystallisation age of **1851.4 ± 3.0 Ma** (MSWD = 0.8, n/N = 48/50). Another group of mostly homogenous cores and more clearly metamorphic domains give an age of **1837.5 ± 3.1 Ma** (MSWD = 2.3, n = 20). Thirteen inherited grains of magmatic origin yield a consistent $^{207}\text{Pb}/^{206}\text{Pb}$ age of **1865.8 ± 3.3 Ma** (MSWD = 1.7, n = 13).

251890 ('massive PIC' unit): Most of the grains show oscillatory zoning in cores and thin metamorphic rims. A total of 104 grains were analysed of which 11 returned poor data, seven had significant cPb and were not considered further. Of the 86 acceptable analyses 65 spots with high Th/U (0.4-2.5) of interior domains give an intrusion/crystallisation age of **1850.1 ± 3.1 Ma** (MSWD = 0.63, n/N = 64/65) based on average Pb/Pb. A similar age is derived from an upper intercept. A small group of homogeneous rim domains give a metamorphic age of **1839 ± 10 Ma** (MSWD = 0.75, n/N = 7/8). A group of variably zoned cores yields an inheritance age of **1872 ± 10 Ma** (MSWD = 0.51, n = 13).

251915 ('massive PIC' unit): Most grains are subhedral and show oscillatory zoning in cores occasional overgrown by homogeneous metamorphic rims. A total of 128 grains were analysed of which 30 returned poor data, 13 had significant cPb and were not considered further. Of the 85 acceptable analyses 65 spots with high Th/U (0.33-1.23) of interior mainly oscillatory zoned domains give an intrusion/crystallisation age of **1853.6 ± 3.0 Ma** (MSWD = 2.64, n/N = 62/65) based on average Pb/Pb. A group of mottled core and homogeneous rims give a metamorphic age of **1832.2 ± 3.3 Ma** (MSWD = 3.61, n = 11). A smaller group of inherited grains yield a well-defined $^{207}\text{Pb}/^{206}\text{Pb}$ age of **1873.9 ± 3.5 Ma** (MSWD = 0.60, n = 7).

251921 ('massive PIC' unit): Most of the grains show oscillatory or diffuse zoning in cores, some have homogeneous metamorphic rims. A total of 141 grains were analysed of which 39 returned poor data, 23 had significant cPb and were not considered further. Of the 79 acceptable analyses 39 spots with high Th/U (0.37-1.27) of interior mainly oscillatory zoned domains give an intrusion/crystallisation age of **1850.1 ± 3.1 Ma** (MSWD = 0.96, n = 39) based on an upper Concordia intercept. A group of homogeneous grains from rim or mantle domains give a metamorphic $^{207}\text{Pb}/^{206}\text{Pb}$ age of **1838.6 ± 3.5 Ma** (MSWD = 0.77, n = 26/27). A small group of inherited grains give a $^{207}\text{Pb}/^{206}\text{Pb}$ age of **1872.5 ± 7.8 Ma** (MSWD = 0.34, n = 6).

483634 ('layered PIC' unit): Most grains are subhedral or anhedral, show oscillatory zoning in cores, sometimes with metamorphic rims. A total of 105 grains were analysed of which eight returned poor data, 14 had significant cPb and were not considered further. A main group of magmatic, variably zoned core domains with average Th/U = 0.35 (0.13-0.51) give an intrusion/crystallisation age of **1894.8 ± 3.1 Ma** (MSWD = 2.1, n = 29). A smaller group of metamorphic grains give a poorly constrained upper intercept age of **1864.3 ± 1.6 Ma** (MSWD = 4.5, n = 13). Four inherited grains have ages at 1925-1980 Ma, with one grain at ca. 2200 Ma. This sample was previously analysed by Sanborn-Barrie al. (2017) and was reanalysed in order to confirm the existence of the rare c. 1900 Ma age they reported. The new age determination agrees within error with the published age.

588311 ('layered PIC' unit): The zircon grains are usually 100-150 µm long, with aspect ratios of 1:2 – 1:3 and have rounded, subhedral crystal shapes. Many grains show faint zoning with BSE-dark (U-poor) cores and BSE-brighter (U-rich) mantles, sometimes overgrown by thin rims (<10µm). Some grains have BSE-bright cores with high U (up to 3500 ppm) and are surrounded by cracked (metamict) mantle domains. A total of 127 grains were analysed of which 56 returned poor data, 39 had significant cPb and were not considered further. Of the remaining 32 grains a sub-group of 12 concordant (97-106%) analyses of magmatic cores with high Th/U (> 0.1) and low U (<2000 ppm) gives a $^{207}\text{Pb}/^{206}\text{Pb}$ age of **1870.6 ± 3.5 Ma** (MSWD = 1.5), which we interpret as the crystallisation age of the granite. Five concordant grains arguably form a separate inherited population yielding an age of 1891.0 ± 5.2 Ma (MSWD = 1.1). Grains with high U (>2000 ppm) and low Th/U (<0.1) give lower ages, suggesting a partial metamorphic resetting or Pb-loss due to metamictisation in these grains. Four inherited grains occur at ca. 1931, 1950, 2085 and 2505 Ma.

588321 ('layered PIC' unit): The zircon grains are subhedral, elongate rounded, usually 100-150 µm long (up to 300µm) with aspect ratios of 1:2 – 1:3, occasionally higher. Most grains show faint zoning with BSE-dark (U-poor) cores and BSE-brighter (U-rich) mantles,

sometimes overgrown by thin rims (<10µm). Some grains are metamict. In total 144 grains were analysed, of which 46 returned acceptable data, the remaining being significant cPb contaminated or being bad analyses. A group of 14 analyses with Th/U > 0.1 gives a $^{207}\text{Pb}/^{206}\text{Pb}$ age of **1867.3 ± 4.4 Ma** (MSWD = 2.0), interpreted as the crystallisation age. A group of metamorphic grains with low Th/U (<0.1) extend down to 1806 Ma but do not define a discernible age peak. Three inherited grains occur at ca. 1926, 2417 and 2484 Ma.

588333 ('massive PIC' unit): Most zircon grains are about 100 µm, (up to 200 µm), subhedral crystal habits with aspect ratios of 1:2 – 1:3. Many grains show diffuse oscillatory zoning in BSE-dark cores that often are cracked and surrounded by BSE-brighter metamorphic rims (<20 µm). Some grains are distinctly anhedral, BSE-bright and texturally homogenous, likely metamorphic in origin. In total 112 grains were analysed of which 70 gave acceptable results, 27 were variously cPb contaminated and 15 returned bad data. Uranium concentration correlates negatively with $^{207}\text{Pb}/^{206}\text{Pb}$ age. Based on 38 oscillatory zoned core analyses with U < 2000 ppm and Th/U > 0.1 an age of **1875.1 ± 3.0 Ma** (MSWD = 3.7) is calculated, which we interpret as the crystallisation age. Zircons with U = 2000-5500 ppm form two broad age groups at ca. 1850 Ma and ca. 1800 Ma, both of which are likely to reflect a metamorphic recrystallisation. Two inherited Archean grains occur at ca. 2550 and 2650 Ma.

588337 ('massive PIC' unit): Most zircon grains are subhedral or anhedral and vary in size from about 100-150 µm with aspect ratios of 1:2 – 1:3. Grains often show diffuse oscillatory zoning in cores that are variably overgrown by relatively homogenous rims. A total of 106 grains were analysed, 78 returned good data, nine showed cPb contamination, and 19 returned bad/unacceptable data. Most grains are concordant, some analyses are slightly reversely discordant. Th/U is broadly correlated with $^{207}\text{Pb}/^{206}\text{Pb}$ age; a group of 42 zircon grains with Th/U > 0.2 gives a crystallisation age of **1865.5 ± 2.4 Ma** (MSWD = 2.9). Four inherited grains with variable Th/U give ages at ca. 1950 and 2070 Ma. In one case an inherited large grain is overgrown by a rim that gives the PIC crystallisation age.

588339 ('massive PIC' unit): The zircon grains are subhedral, elongate partly rounded, usually 100-150 µm long (up to 300µm) with aspect ratios of 1:2 – 1:3, occasionally higher. Most grains show faint zoning with BSE-dark (U-poor) cores and BSE-brighter (U-rich) mantles, occasionally overgrown by thin rims. In total 144 grains were analysed, of which 100 returned acceptable data, the remaining being significant cPb-contaminated or being bad analyses. Uranium concentration correlates negatively with $^{207}\text{Pb}/^{206}\text{Pb}$ age. Out of a group of 29 analyses with low U (<1500 ppm) and high Th/U (>0.15) a sub-group defines an age at **1875 ± 4 Ma** (97.8 % conf.), which is interpreted as the crystallisation age. Two inherited grains occur in 1910 and 2360 Ma.

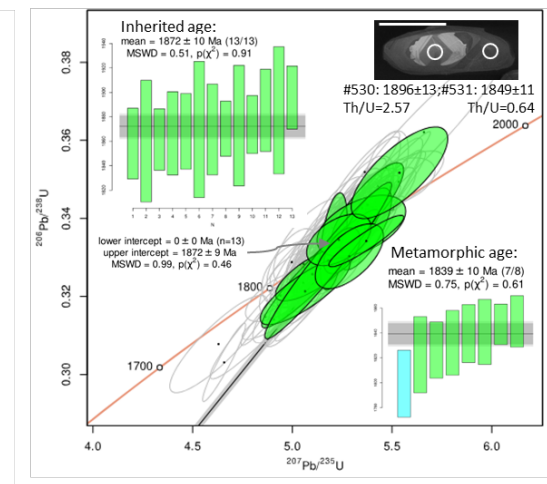
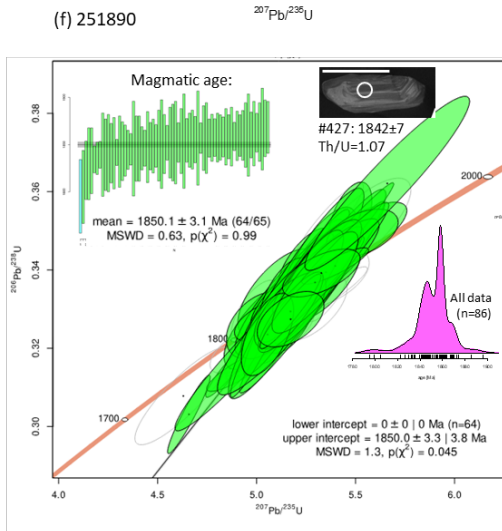
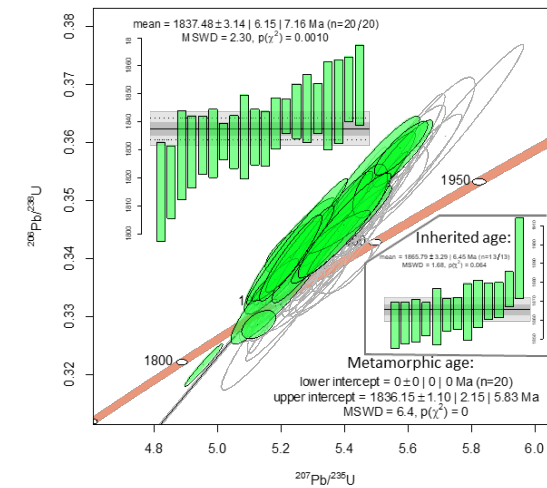
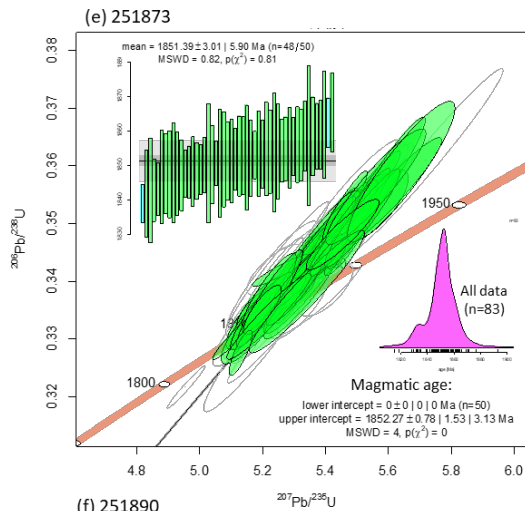
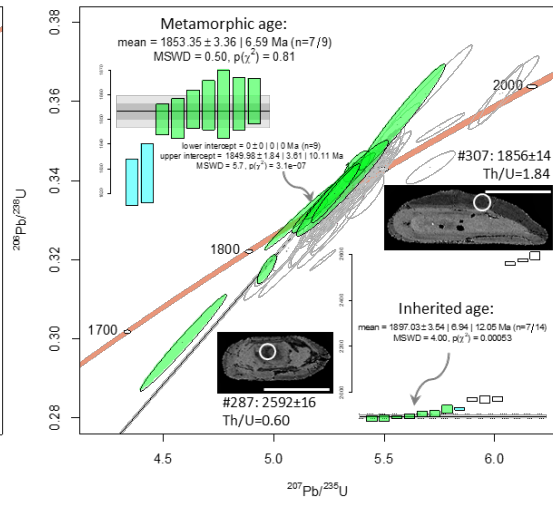
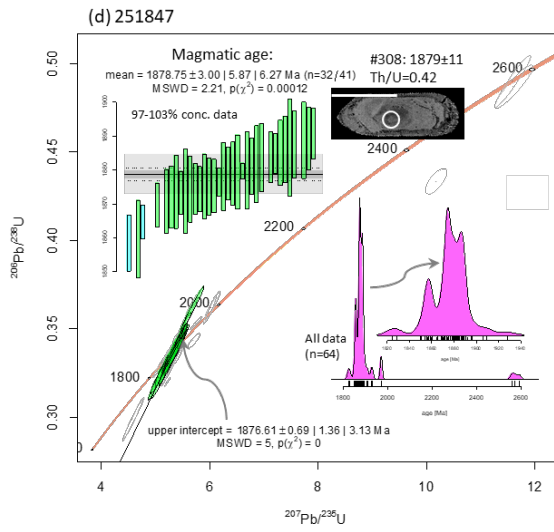
588340 ('massive PIC'): Most zircon grains are subhedral and typically box-shaped, large from about 100-200 μm long with aspect ratios of about 1:2 – 1:3. Many grains show oscillatory zoning in cores and homogenous outer domains often capped by a thin rim (too narrow to target). Some grains have BSE-bright cracked (metamict?) cores surrounded by BSE-dim outer homogenous domains. A total of 158 grains were analysed, 71 returned good data, the remaining either having significant cPb or being poor. Most grains are concordant, a few being slightly reversely discordant. A subgroup of 32 analyses with Th/U > 0.1 and U < 2000 ppm defines a plateau age of **1870.6 \pm 2.0 Ma** (MSWD = 0.61) interpreted as the timing of crystallisation. A group of 21 grains from metamorphic overgrowth domains yield an age of **1852.5 \pm 2.4 Ma** (MSWD = 1.2). Four inherited grains between 1887 and 1920 Ma.

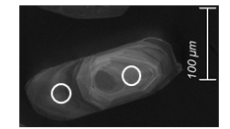
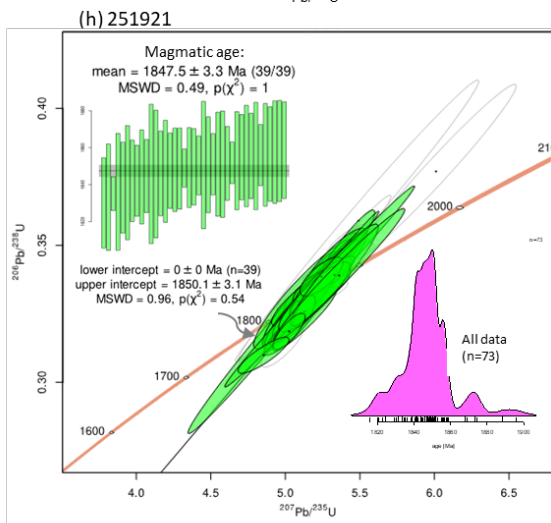
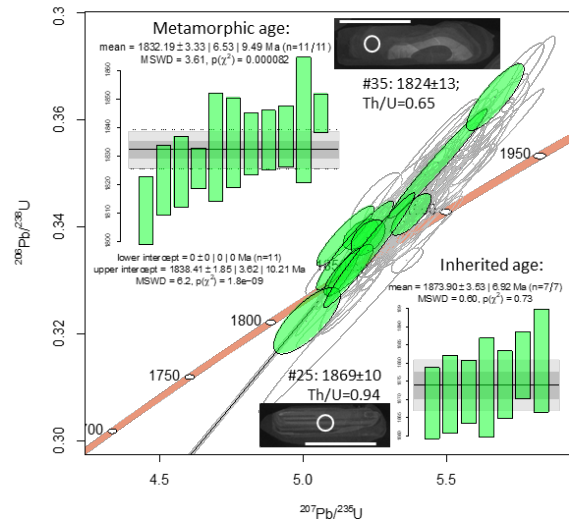
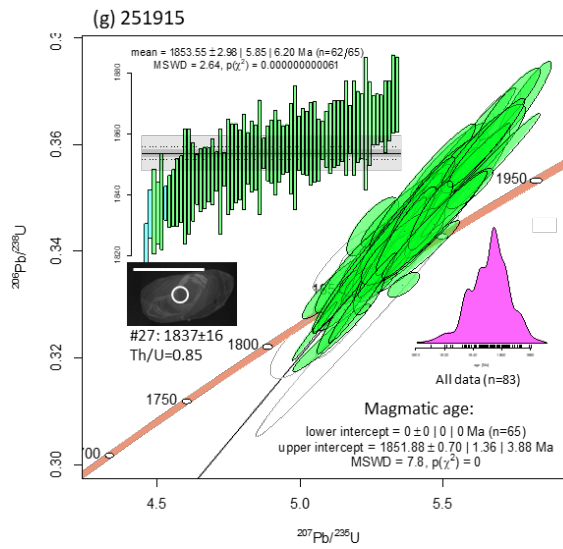
588345 ('layered PIC' unit): Zircon grains are typically subhedral, variably rounded, usually 100-200 μm long with aspect ratios of about 1:2 – 1:4. Many grains have cores with relict diffuse oscillatory zoning that are variably overprinted by homogenous rims that often present radiating cracks. Inclusions of lighter silicate minerals are common. Out of 168 grains analysed 123 returned acceptable concordant data, 17 showed cPb contamination, and 28 were bad. Uranium contents range widely (950-4270 ppm) and are broadly correlated (negative) with $^{207}\text{Pb}/^{206}\text{Pb}$ age. Thorium/U ratio is generally low (<0.1). Two age groups can be defined: (1) a low-U (<2000 ppm) group of magmatic textured grains at **1854.7 \pm 3.6 Ma** (MSWD = 1.8, n = 18); (2) a group of texturally homogenous grains with high U (2000-3000 ppm) and Th/U < 0.05 at **1823.2 \pm 2.9 Ma** (MSWD = 2.6, n = 30). The two age groups are interpreted as crystallisation and metamorphic overprinting, respectively. Besides, a very high-U (>3000 ppm) group of partly metamictised grains scatter at around 1800 Ma, likely to reflect partial Pb-loss. Three older inherited grains occur at 2118, 2171 and 2718 Ma.

588349 ('layered PIC' unit): Zircon grains are typically subhedral, sometimes anhedral, usually 100-150 μm long with aspect ratios of about 1:3. Many grains show relict oscillatory zoning in cores that are variably overprinted by diffuse homogenous, usually somewhat BSE-brighter (U-rich), mantles and rims. In total 144 spots were analysed of which 74 presented acceptable data, the remaining representing cPb-contaminated or poor analyses. All the filtered data have relatively low U (124-510 ppm) and high Th/U (>0.25) and mainly represent a magmatic textural association. A coherent zircon population of 26 concordant analyses yields a weighted average $^{207}\text{Pb}/^{206}\text{Pb}$ age of **1851.3 \pm 3.3 Ma** (MSWD = 0.49), interpreted as the formation age of the granite. Two additional populations are suggested at **1830.7 \pm 2.7 Ma** (MSWD = 0.7, n/N = 28/73) and **1868.0 \pm 4.0 Ma** (MSWD = 0.52, n/N = 16/73), interpreted as metamorphic overprinting and inherited populations, respectively. A single inherited grain occurs at 1955 Ma.

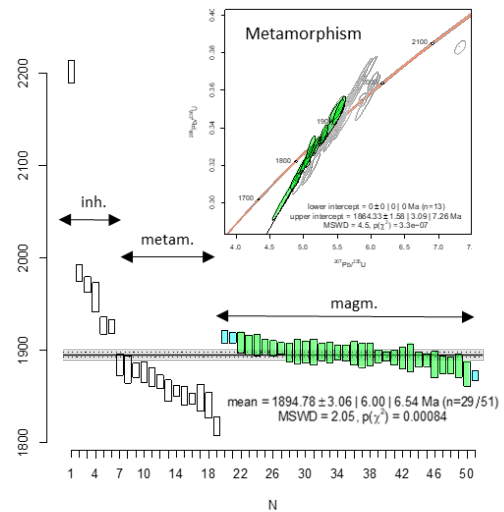
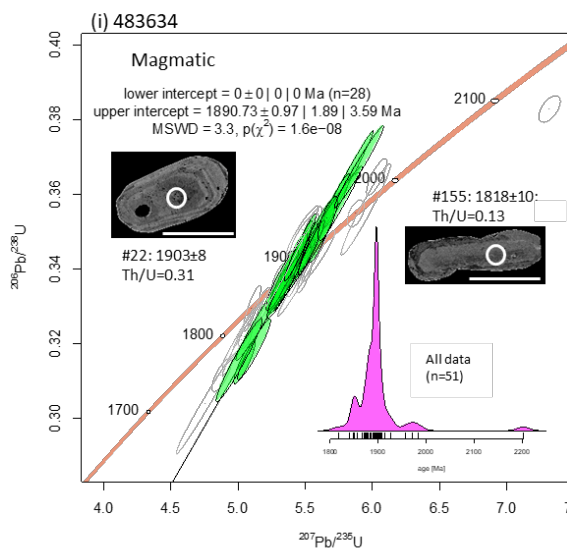
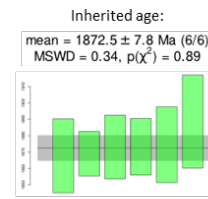
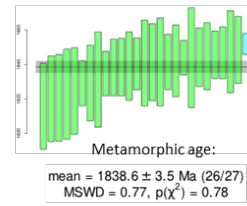
588352 ('layered PIC' unit): Zircon grains are typically subhedral, elongate with aspect ratios of 1:3 – 1:4, rarely up to 1:6. Most grains have variably diffuse oscillatory-zoned cores that are variably overgrown by homogenous rims that often present radial cracks. Inclusions of lighter silicate minerals are common. Of a total of 170 spots analysed only 20 were cPb-free and of these seven grains from zoned cores with Th/U = 0.07-0.19 domains give an age of **1856.0 ± 3.4 Ma** (MSWD = 1.9), interpreted as the timing of crystallisation. Ten inherited grains occur at ca. 1875, 1910-1940, 2300-2320, 2460 and 2660 Ma.

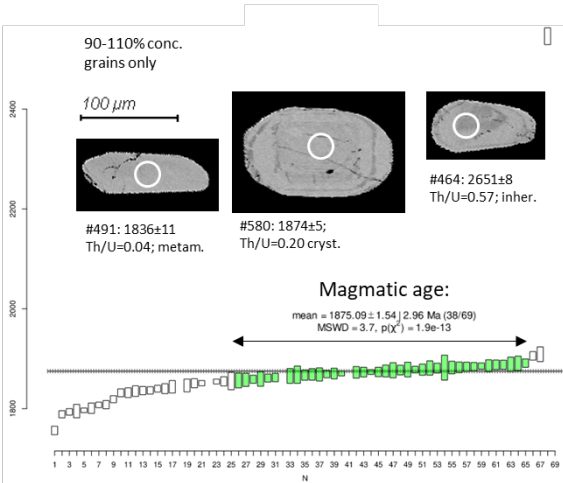
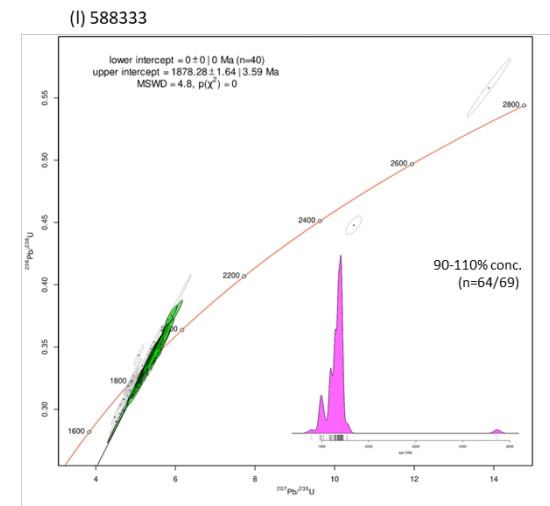
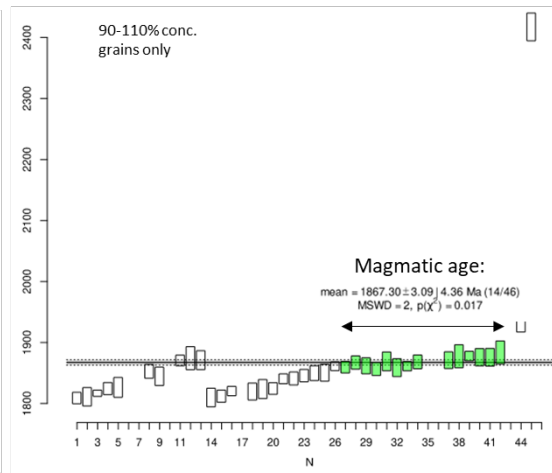
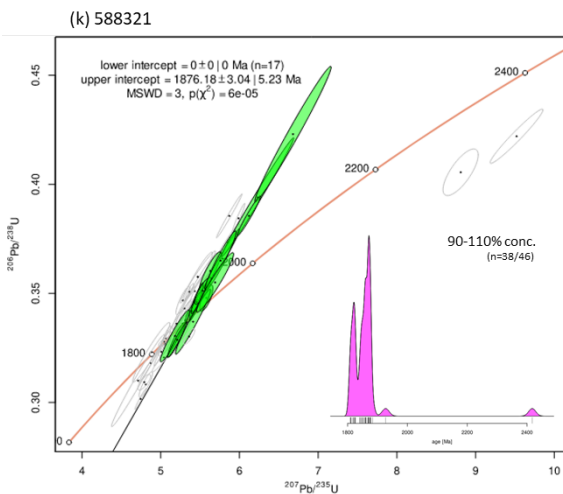
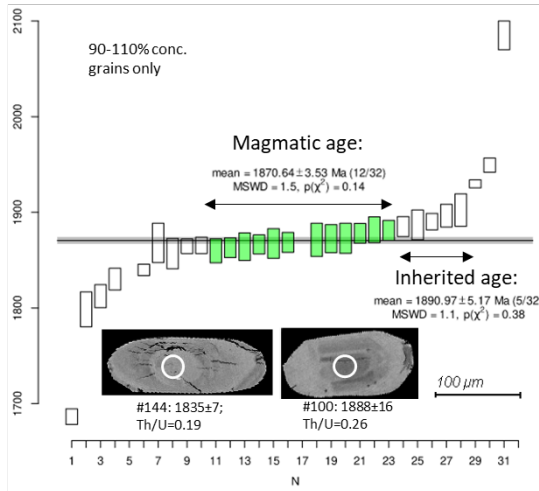
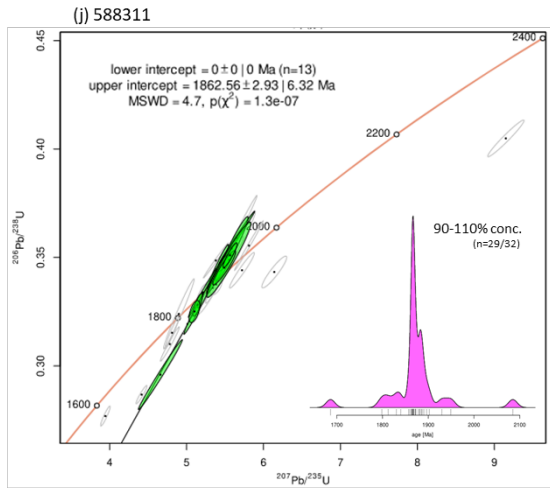
588355 ('massive PIC' unit): Zircon grains are typically subhedral, elongate, up to 300 µm in longest direction with typical aspect ratio of about 1:3 – 1:4. Grains often show relict oscillatory zoning in cores that are variably overprinted by diffuse homogenous metamorphic domains and rims that are commonly cracked. Inclusions of silicate minerals are common. Some grains are distinctly metamictised. In total 128 spots were analysed of which 64 presented acceptable data, 40 were cPb-contaminated and 24 represented poor analyses. The data is dominated by a peak of metamorphic zircon with intermediate U (750–2000 ppm) at **1829.8 ± 2.3 Ma** (n/N = 17/37, MSWD = 1.3), a smaller population of magmatic grains with low U (< 750 ppm) at **1845.7 ± 3.3 Ma** (n/N = 12/37, MSWD = 1.3) and a lower age tail towards ca 1800 Ma consisting of grains with high U (> 2000 ppm).



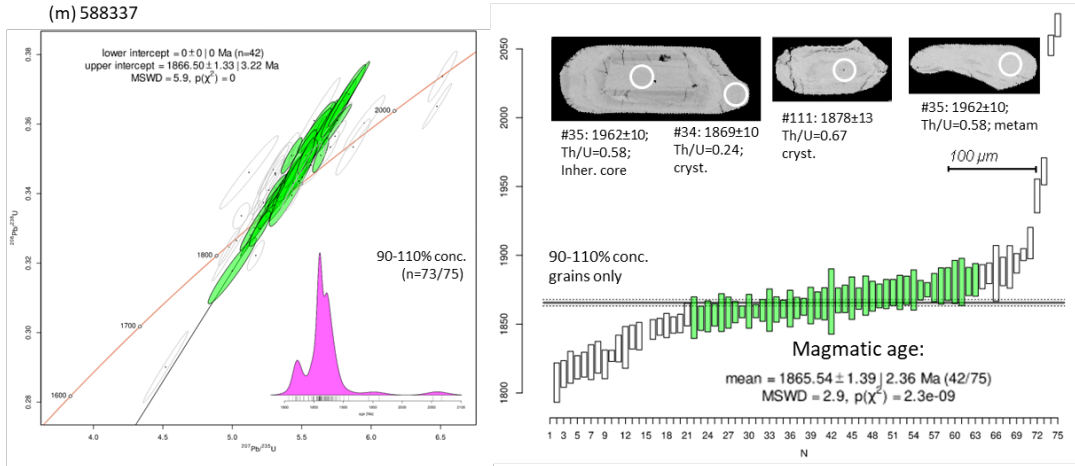


#348: 1845±10; #347: 1838±13;
Th/U=0.52 Th/U=0.87

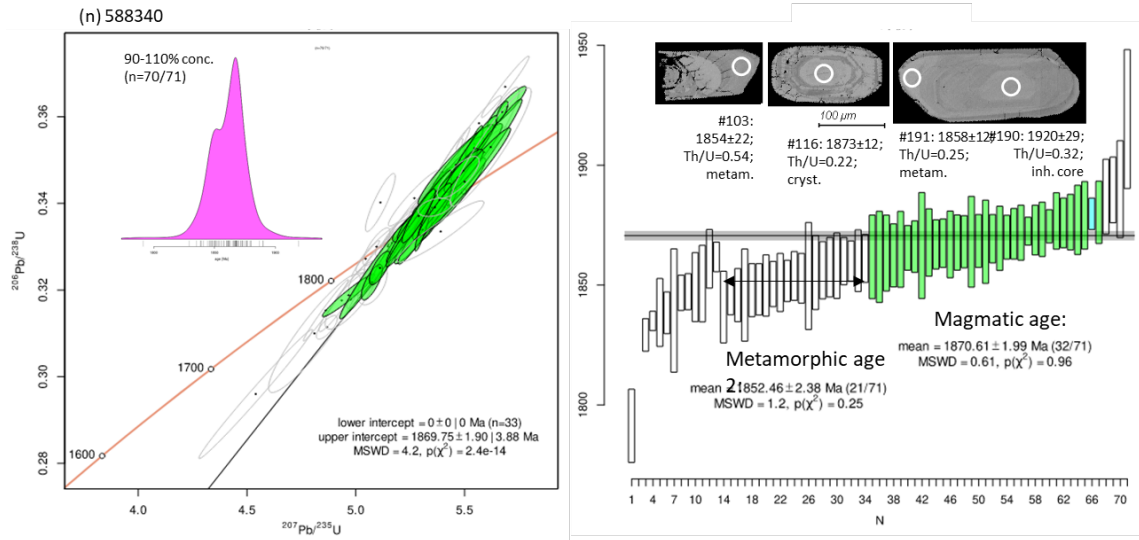




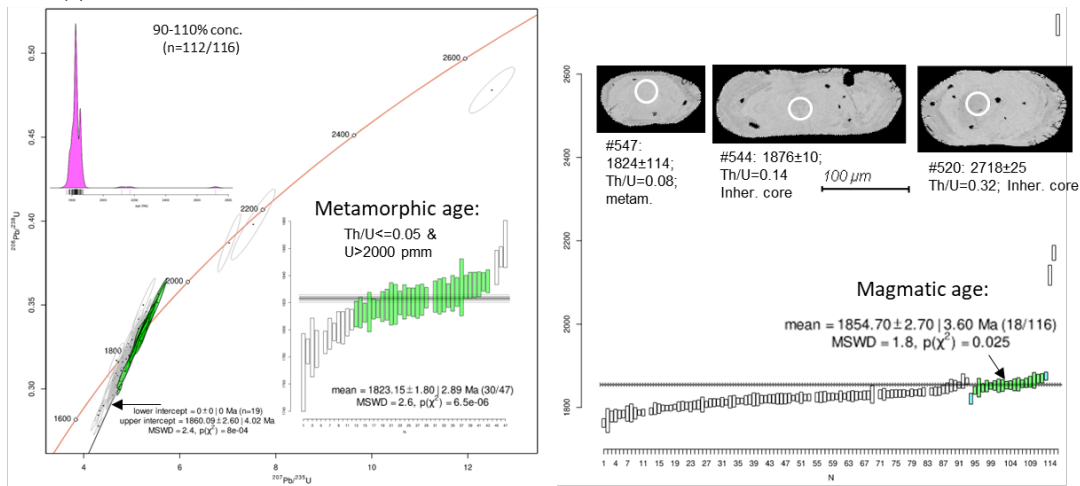
(m) 588337



(n) 588340



(o) 588345



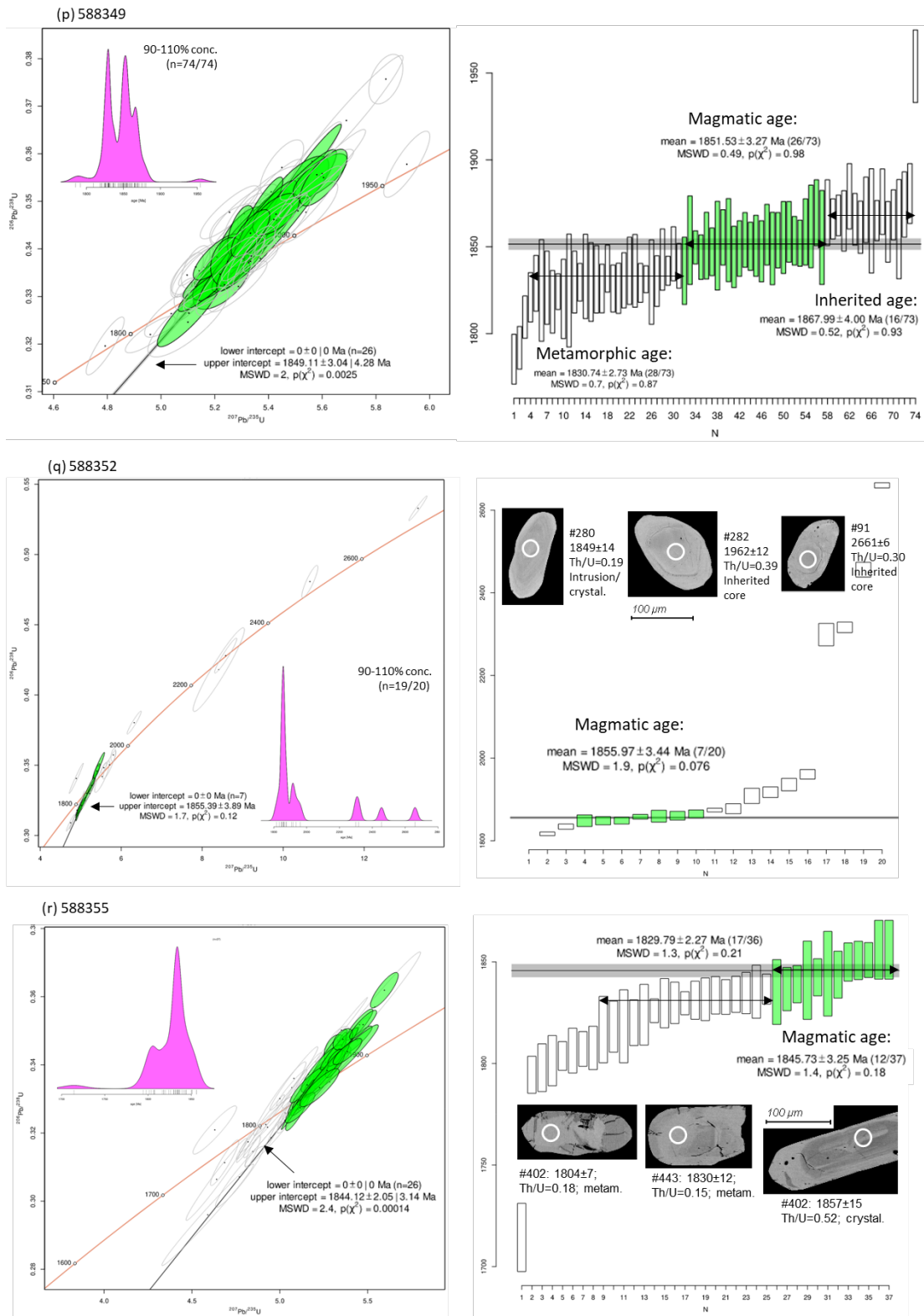


Figure 14. U-Pb data for PIC charnockites represented in Wetherill Concordia diagrams, calculated weighted average ^{207}Pb - ^{206}Pb ages and in Kernel Density Estimation (KDE) plots.

In summary, many PIC charnockites from a wide range of localities have crystallisation ages of 1875-1870 Ma, an age that agrees well with previous published age data (Thrane et al. 2005; Sanborn-Barrie et al. 2017). Yet, Sanborn-Barrie et al. (2017) also reported PIC charnockites with crystallisation ages a ca 1900 Ma, an age which is apparently rare in our larger data set, although seen in sub-populations among inherited grains. In order to eliminate any doubt there might be about the significance of the 1900 Ma age we decided to reanalyse the same sample (483634) to possibly reproduce this age, notably with a different analytical technique (LA-ICPMS instead of SIMS). The result of this test shows an overall consistency as we obtain the same age within error. It should be mentioned that the sample did not produce the best data due to a high number of disturbed zircon grains. As something completely new we find a significant group of PIC samples that have consistent intrusive ages of ca 1850 Ma; these include mostly charnockite samples with ferroan chemistry coming mainly from the northern part of the complex (see below). Zircon with age profiles overlapping that of the Nukâvsak Formation rocks (see below) commonly constitutes up to several percent of the zircon populations in the PIC granites, implying variable degrees of crustal reworking/contamination associated with granite formation and emplacement.

7.3.2 Norites

251806 ('layered PIC' unit): Large rounded anhedral grains, up to 300 µm, showing core-rim relations with irregular oscillatory zoned cores overgrown by metamorphic mantles and rims. A total of 80 grains were analysed of which three returned poor data, four had significant cPb and were not considered further. A large group of variously zoned, magmatic grains with high Th/U (0.41-3.50) yields an age of **1874.0 ± 3.0 Ma** (MSWD = 3.0, n = 53), interpreted as the crystallisation age. A smaller group of more homogeneous core and mantle domains give a metamorphic age of **1837.2 ± 3.5 Ma** (MSWD = 2.2, n/N = 14/15). A small group of variably discordant inherited grains give an age of **1899.3 ± 5.4 Ma** (MSWD = 1.7, n = 4).

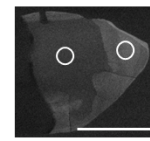
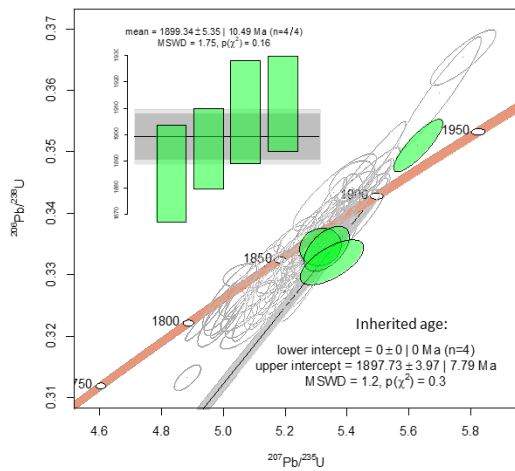
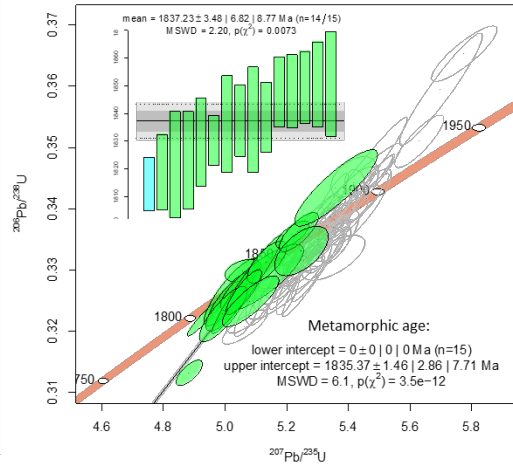
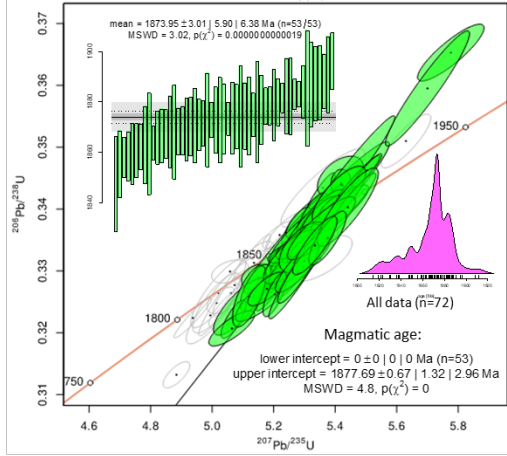
588301 ('layered PIC' unit): Most grains are often distinctly anhedral with irregular lobate outlines. Most grains are 100-200 µm long with aspect ratios of about 1:1 – 1:3, but a few grains are significantly larger. Many grains show relatively homogenous cores, occasionally as more patchy domains, of recrystallised BSE-bright zircon, often surrounded by BSE-dark cracked mantle domains. In total 71 spots were analysed of which 24 presented acceptable data, 37 held cPb and 10 represented poor analyses. Eleven analyses from BSE-bright domains with Th/U < 0.2 and U > 1000 ppm define a $^{207}\text{Pb}/^{206}\text{Pb}$ age of **1851.4 ± 3.3 Ma** (MSWD = 0.75), interpreted as the timing of metamorphism. Three grains with Th/U > 0.5 give a very

rough age at ca. 1876 ± 6 Ma, likely to reflect the crystallisation age of the noritic enclave, alternatively inheritance from the host PIC charnockite.

588310 ('layered PIC' unit): Grains are generally subhedral and between 50 and 150 μm long with aspect ratios of 1:2 – 1:3. Many grains present relict oscillatory zoning in cores that are variably overprinted by diffuse recrystallised mantle domains or rims. Several grains are severely cracked, and some have metamict cores. A group of homogenous grains are distinctly BSE-bright and tend to be small and anhedral. In total 95 spots were analysed of which 34 presented acceptable data, 32 had cPb and 27 represented poor analyses. The data are generally concordant, with a few very high-U grains being clearly discordant. $^{207}\text{Pb}/^{206}\text{Pb}$ ages vary from ca. 1870 to 1800 Ma and correlate inversely with U concentration (less so with Th/U). A group of grains with low U (<1600 ppm) yield an age of **1866.4 ± 5.6 Ma** (MSWD = 4.4, n/N = 13/34), interpreted as the likely crystallisation age. A smaller group at **1848.3 ± 4.8 Ma** (MSWD = 2.3, n/N = 8/34) is interpreted as metamorphic. A single inherited grain occurs at ca. 2430 Ma.

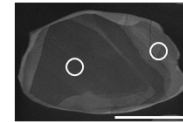
588322 ('layered PIC' unit): Grains are generally subhedral and mostly between 100 and 150 μm long (up to 200 μm) with aspect ratios around 1:3 (spanning 1:2 – 1:4). Many grains present relict oscillatory zoning in cores that are variably overprinted by diffuse recrystallised domains. Several grains have intensely cracked rim domains, and some have clearly metamict cores. Some homogenous grains are distinctly BSE-bright and resemble metamorphic zircon. In total 124 spots were analysed of which 71 presented acceptable data, 17 held cPb and 36 represented poor analyses. There are broad correlations of Pb/Pb age with U contents (negative) and with Th/U (positive). A coherent group of 38 magmatic grains give an age of **1872.3 ± 2.0 Ma** (MSWD = 0.76). Two metamorphic groups can be defined at 1852.0 ± 2.6 Ma (MSWD = 1.1, n/N = 15/71) and 1836.7 ± 3.3 Ma (MSWD = 0.88, n/N = 9/12). The sample includes five inherited grains, four of Paleoproterozoic age (1940 – 2180 Ma) and one Paleoproterozoic (3480 Ma).

(a) 251806



#38: 1836±18;
Th/U=1.1

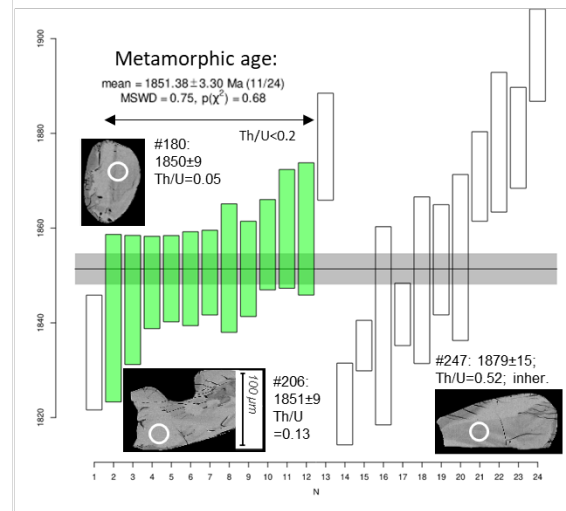
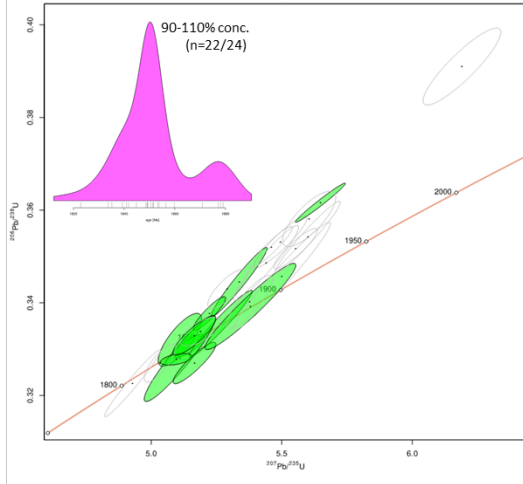
#37: 1867±10;
Th/U=2.6



#60: 1829±17
Th/U=1.1

#59: 1855±13
Th/U=1.7

(b) 588301



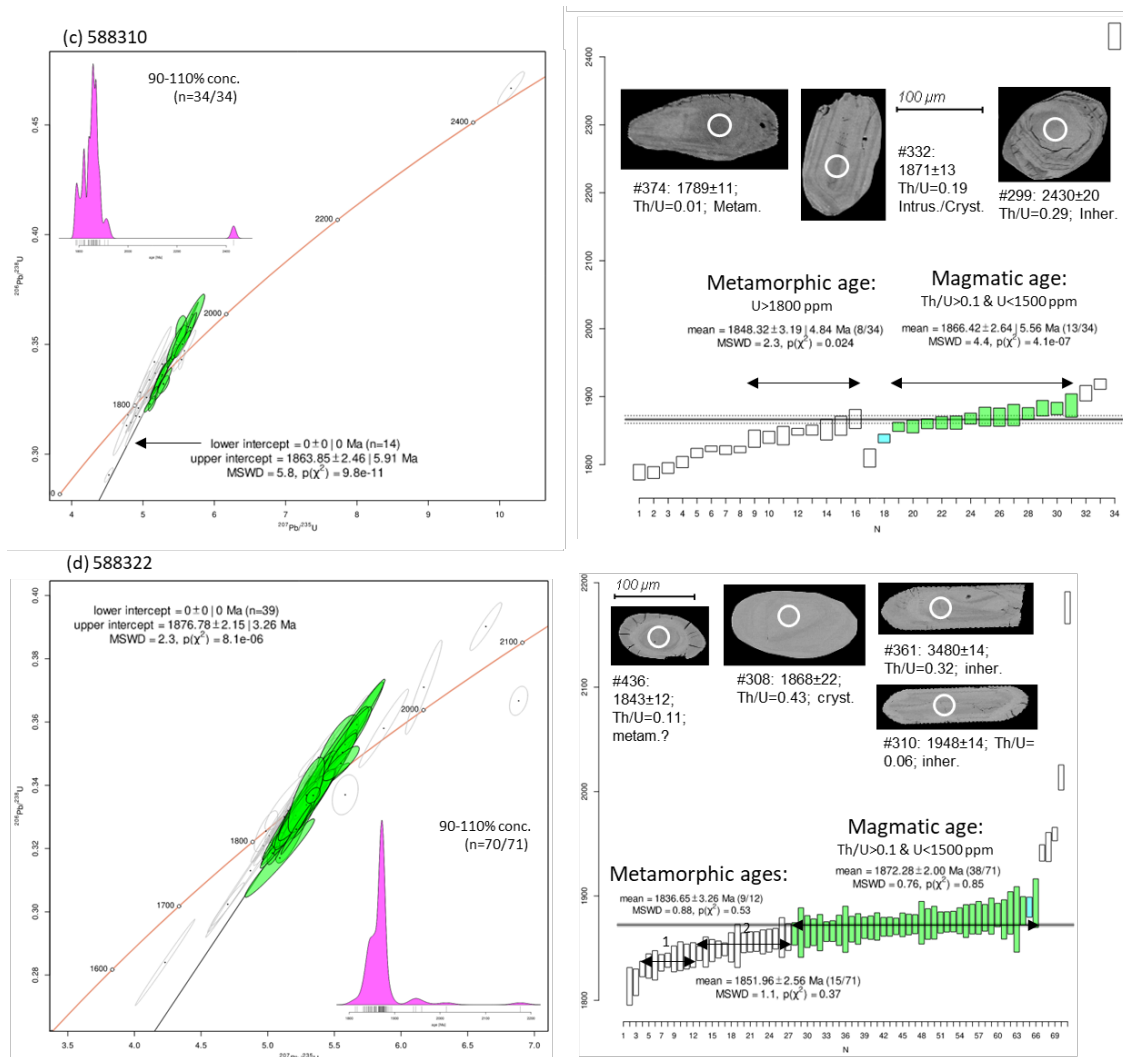


Figure 15. U-Pb data for PIC norites represented in Wetherill Concordia diagrams, calculated weighted average ^{207}Pb - ^{206}Pb ages and in Kernel Density Estimation (KDE) plots.

In summary, the norite zircon data reveal a complex history of intense overprinting, zircon disequilibria textures and metamorphism in what appears to be two distinct episodes, at first ca. 1850 Ma and later at ca. 1830 Ma. There are remnant magmatic textures in some samples (clearest in 588322), that show magmatic crystallisation of zircon at ca. 1870 Ma, i.e., corresponding to the main emplacement time of PIC granites.

7.3.3 Leucogranite

588317: Zircon grains are subhedral, elongate and partially rounded, mostly between 100 and 150 μm long (up to 200 μm) with aspect ratios around 1:3 (ranging 1:2 – 1:4). Most grains have BSE-bright cores surrounded by BSE-dark usually cracked mantles and rims. A few grains show relict magmatic zoning in cores. In total 85 spots were analysed of which 23 presented acceptable data with only minor cPb, the remaining having either massive cPb or being poor analyses. Using the uncorrected $^{207}\text{Pb}/^{206}\text{Pb}$ data three textural groups are defined: (1) BSE-bright, U-rich (1300-3000 ppm) cores yield an age of **1813 \pm 8 Ma** (n = 5), (2) BSE-dark, U-poor (320-450 ppm) outer domains give an age of **1829 \pm 4 Ma**, (n = 4), and (3) a group of relict oscillatory zoned core analyses give ages from 1850 to 1870 Ma. The former two groups are both metamorphic while the third is inherited grains, presumably from the PIC granites. In addition, two older ages occur at ca. 2475 and 2500 Ma, reflecting inheritance from the gneiss basement.

588350: Zircon grains are distinctly anhedral, rounded, typically about 100-150 μm long (up to 200 μm) with low aspect ratios of around 1:1 – 1:2. Most grains have homogenous BSE-bright core and mantle domains that are concentrically surrounded by variably thick, cracked rims that are equally homogenous but BSE-dull. In total 83 spots were analysed of which 52 presented acceptable data with minor cPb, the remaining having either significant cPb or representing poor analyses. Most analyses are close to 100% concordant but tend to fall slightly above the Concordia line. The uncorrected $^{207}\text{Pb}/^{206}\text{Pb}$ ages range from 1788 to 1828 Ma. Two U-Th groups might be subtly distinguished: a low-U group with U = 600-900 ppm and Th/U = 0.05, and a high-U group with U = 700-1900 ppm and Th/U = 0.02. The former group has overlapping $^{207}\text{Pb}/^{206}\text{Pb}$ ages of **1804 \pm 5 Ma** (MSWD = 5.5; n = 28) and **1802 \pm 5 Ma** (MSWD = 5.4; n = 24). A weighted average of all 52 data gives **1804.4 \pm 3.6 Ma** (MSWD = 8.4). The high MSWD indicates that the scatter of data points cannot be solely explained by analytical error but is likely to reflect partially open system behaviour over prolonged time period during cooling from peak metamorphic conditions.

588357: Zircon grains are generally anhedral, rounded to elongate varying in size from 100 to 200 μm long, but also include larger grains (up to 300 μm). Aspect ratios are 1:1 – 1:3, the smallest grains having semi-circular to oblate shapes. Most grains are homogenous BSE-bright, metamorphic appearance. Many grains are cracked and have BSE-dull altered domains, some are strongly metamict (particularly larger grains). In total 88 spots were analysed (avoiding altered domains) of which 63 presented acceptable data with minor cPb, the remaining having either significant cPb or being poor analyses. Most analyses are close to 100% concordant and cluster around the Concordia line. The uncorrected $^{207}\text{Pb}/^{206}\text{Pb}$ ages

define a continuous range from ca. 1840 to 1800 Ma (total range from 1857 to 1785 Ma). Uranium concentrations are mostly between 1000 and 2000 ppm and Th/U ratios below 0.1. Treating the entire group as one gives an age of **1819.2 ± 3.5 Ma** (MSWD = 9.7; n = 63), while an upper Concordia intersect yields a similar age of 1822.4 ± 5.2 Ma (MSWD = 9.2). The high calculated MSWD-values indicates an overdispersion of the data that likely reflects partially open system behaviour during prolonged cooling. The calculated age is therefore likely to represent a minimum age for the crystallisation of the garnet leucogranite.

In summary, the dated leucogranites yield ages between ca. 1800 and 1830 Ma, which broadly represent the timing of peak metamorphism and migmatitisation in the region. Only for sample 588317 it is possible to associate more specific ages within this wider range to distinct textural and U-Th specific zircon zones, namely 1829 ± 4 Ma and 1813 ± 8 Ma, both ages reflecting distinct episodes of metamorphic zircon recrystallisation. The ages obtained from samples 588350 (1803 ± 3 Ma) and 588357 (1820 ± 3 Ma) are associated with an overdispersion of data seen in high MSDW values. This is likely to reflect partially open system behaviour during cooling from peak metamorphic conditions; thus the calculated ages represent minimum dates for leucogranite formation.

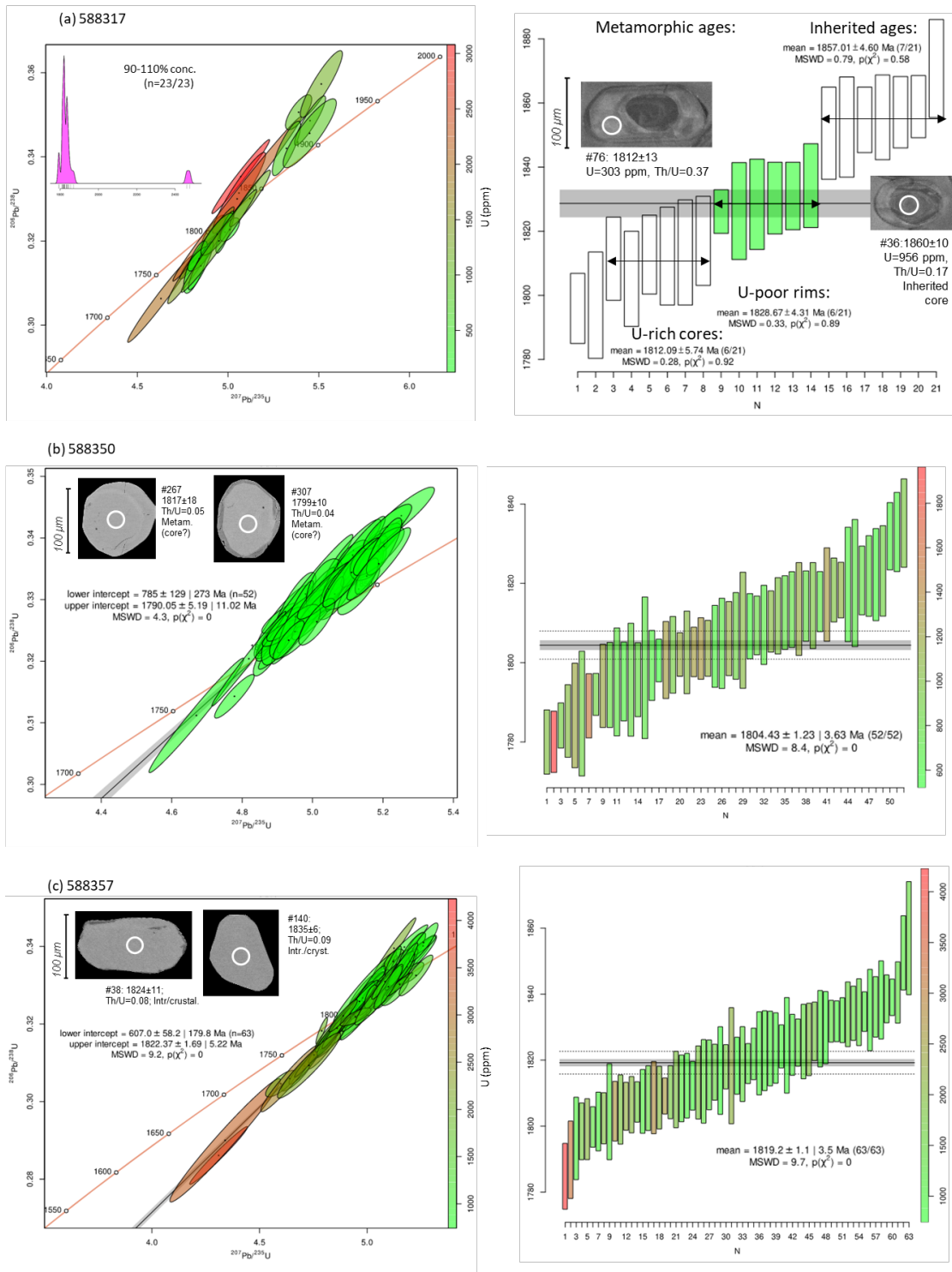


Figure 16. U-Pb data for leucogranites represented in Wetherill Concordia diagrams, calculated weighted average ^{207}Pb - ^{206}Pb ages and in Kernel Density Estimation (KDE) plots.

7.3.4 Migmatitic rocks of the Nûkavsak Formation

588334 (quartzite): Paleosome part of migmatite sampled as an inclusion within the PIC at the eastern side of Sullua fjord close to the contact to the surrounding metasedimentary rocks of the Karrat Group. Zircon grains are generally anhedral, rounded, and include mostly small (50-100µm) oval to elongate grains with low aspect ratios of 1:1 – 1:2. Many grains show faint oscillatory zoning in BSE-bright cores, often surrounded by a thin relatively BSE-dark metamorphic rim. In total 112 spots were analysed of which 76 presented acceptable data, the remaining having either significant cPb or being poor analyses. U-Pb concordancy ranges from 80 to 113%, but the far majority lie from 95 to 105%. The $^{207}\text{Pb}/^{206}\text{Pb}$ ages span widely from ca. 1660 to 3500 Ma with a main age peak at ca. 1950 Ma with smaller Paleoproterozoic peaks between ca. 1800 to 2100 Ma. Ages <1800 Ma have generally very high U contents (up to 8500 ppm) and are suspect of Pb-loss due to metamictisation. Fifteen Archean grains occur at 2500-2700 Ma, but also include a few older grains from 3100 to 3500 Ma.

588336 (paleosome quartzite): Paleosome part of migmatite sampled at the same locality as 588334 (see above). Zircons are generally sub- to anhedral, small (<100 µm), rounded to elongate with low aspect ratios of 1:1 – 1:2, occasionally higher. Most grains have uniform BSE-dull cores that sometimes are overgrown by BSE-brighter fractured rims, but also include examples of faint oscillatory-zoned grains. In total 148 spots were analysed of which 107 presented acceptable data with minor cPb, the remaining having either significant cPb or reflecting poor analyses. Most of the accepted data are close to being concordant, the oldest grains tending to be slightly more discordant. The detrital grains span a wide range of near concordant $^{207}\text{Pb}/^{206}\text{Pb}$ ages from ca. 1750 to 2900 Ma. Majority of ages fall in the range 1800-2000 Ma, with a distinct double peak at ca. 1930 and 1980 Ma and a similarly distinct peak at ca. 1850 Ma. In addition, a near continuum of smaller peaks and humps exist between 2150 and 2900 Ma.

588351 (paleosome quartzite): Paleosome part of migmatite sampled at Qoorsorfik at the southernmost tip of Qaarsorsuatsiaq. Zircons are generally sub- to anhedral, generally small (<100 µm), rounded to elongate with low aspect ratios of 1:1 – 1:2. A wide range of textural types occurs, including oscillatory-zoned grains and complex metamorphic grains with multi-stage growth zones. In total 159 spots were analysed of which 102 presented acceptable data with minor cPb, the remaining have significant cPb or represent bad analyses. Most of the accepted data plot close to Concordia. The detrital grains span a wide range of $^{207}\text{Pb}/^{206}\text{Pb}$ ages of ca. 1710 – 3200 Ma, with a majority of ages at 1800 – 2000 Ma, including a distinct peaks at ca. 1980, 1930 and 1880 Ma, and smaller peaks at ca. 1850 and 1830

Ma. In addition, a near continuum of smaller age peaks occur at ca. 2200, 2400, 2600-2700 and 2900-3200 Ma.

In summary, the age patterns described above are very similar to what has been found elsewhere in metasedimentary rocks of the Nukâvsak Formation (Guarnieri et al. 2023) supporting the view that the analysed wall rock lithologies belong to this formation of the Karrat Group.

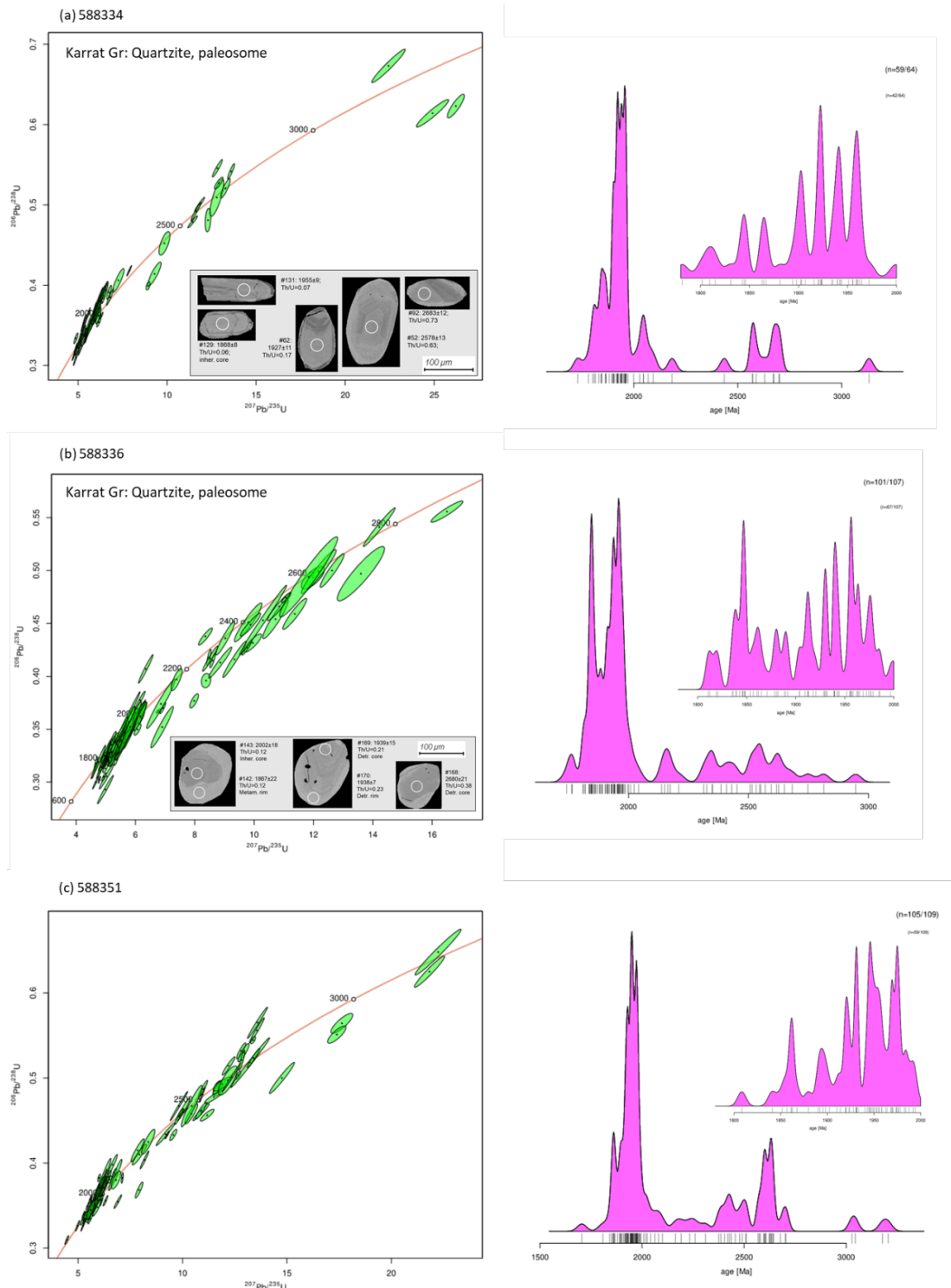


Figure 17. *U-Pb data for migmatitic rocks of the Nûkavsak Formation represented in Wetherill Concordia diagrams and in Kernel Density Estimation (KDE) plots.*

7.4 Summary of geochronology

Table 1 below summarises the geochronology results presented in sections 7.3.1 – 7.3.3.

Table 1. *Summary of geochronology results for 25 PIC samples*

Sample	Lat N	Long W	Map unit	Lithology unit	Chem group	Age (Ma)	2s error (+/- Ma)	n/N	MSWD	Age type	Comment
251806	72.3596	-54.7760	MPIC	Norite	mafic enclave	1874.0	3.0	53	3.02	Magmatic	Weighted average
						1837.2	3.5	14/15	2.2	Metamorphic	Weighted average
						1899.3	5.4	4/4	1.75	Inherited	Weighted average
251816	72.4760	-55.2858	LPIC	Charnockite	magnesian	1870.7	3.0	67/68	2.9	Magmatic	Weighted average
						1855.0	3.4	8/12	2.32	Metamorphic	Weighted average
						1897.9	3.2	22/25	3.98	Inherited	Weighted average
251820	72.3878	-55.4489	MPIC	Charnockite	magnesian	1875.6	3.0	47/47	3.33	Magmatic	Weighted average
						1848.8	3.2	16/18	5.29	Metamorphic	Weighted average
						1894.6	3.6	9/16	0.16	Inherited	Weighted average
251835	72.7017	-55.8721	MPIC	Charnockite	ferroan	1849.2	3.0	55/56	1.74	Magmatic	Weighted average
						1835.7	3.1	25/28	1.97	Metamorphic	Weighted average
						1873.0	4.3	5/6	0.83	Inherited	Weighted average
251847	72.4849	-54.5959	MPIC	Charnockite	magnesian	1878.8	3.0	32/41	2.21	Magmatic	Weighted average
						1853.4	3.4	7/9	0.5	Metamorphic	Weighted average
						1897.0	3.5	7/14	4	Inherited	Weighted average
251873	72.8329	-54.7787	MPIC	Charnockite	ferroan	1851.4	3.0	48/50	0.82	Magmatic	Weighted average
						1837.5	3.1	20/20	2.3	Metamorphic	Weighted average
						1865.8	3.3	13/13	1.68	Inherited	Weighted average
251890	72.7731	-55.4282	MPIC	Charnockite	ferroan	1850.1	3.1	64/65	0.63	Magmatic	Weighted average
						1839.0	10.0	7/8	0.75	Metamorphic	Weighted average
						1872.0	9.0	13	0.51	Inherited	Upper intercept
251915	72.9861	-55.1238	MPIC	Charnockite	ferroan	1853.6	3.0	62/65	2.64	Magmatic	Weighted average
						1832.2	3.3	11/11	3.6	Metamorphic	Weighted average
						1873.9	3.5	7/7	0.6	Inherited	Weighted average
251921	72.9257	-54.8588	MPIC	Charnockite	magnesian	1850.1	3.1	39	0.96	Magmatic	Upper intercept
						1838.6	3.5	26/27	0.77	Metamorphic	Weighted average
						1872.5	7.8	6	0.34	Inherited	Weighted average
483634	72.8462	-56.0156	LPIC	Charnockite	magnesian	1894.8	3.1	29/51	2.05	Magmatic	Weighted average
						1864.0	1.6	13/51	4.5	Metamorphic	Weighted average
						c. 1925-1980, 2200		5	4.5	Inherited	Two detrital groups
588301	72.6170	-54.9199	LPIC	Norite	mafic enclave	1851.4	3.3	11/24	0.75	Metamorphic	Weighted average
						1876.0	6.0	3		Magmatic	Weighted average
588310	72.6802	-55.1459	LPIC	Norite	mafic enclave	1866.4	5.6	13/34	4.4	Magmatic	Weighted average
						1848.3	4.8	8/34	2.3	Metamorphic	Weighted average
						2430		1		Inherited	Single grains
588311	72.6936	-55.0550	LPIC	Charnockite	magnesian	1870.6	3.5	12/32	1.5	Magmatic	Weighted average
						1891.0	5.2	5/32	4.5	Inherited	Weighted average
						c. 1931, 1950, 2085, 2505		5	4.5	Inherited	Single grains
588317	72.5946	-55.4390	LG	Leucogranite		1828.7	4.3	6/21	0.33	Magmatic	Weighted average
						1812.1	5.7	6/21	0.28	Metamorphic	Weighted average
						1857.0	4.6	7/21	0.79	Inherited	inherited cores
588321	72.6178	-55.4734	LPIC	Charnockite	magnesian	1867.3	4.4	14/46	2	Magmatic	Weighted average
						c. 1926, 2417, 2484		1		Inherited	Single grains
588322	72.6178	-55.4673	LPIC	Norite	mafic enclave	1872.3	2.0	38/71	0.76	Magmatic	Weighted average
						1852.0	2.6	15/71	1.1	Metamorphic	Weighted average
						1836.7	3.3	9/12	0.88	Metamorphic	Single grains
						ca. 1940 - 2180, 3480		5		Inherited	
588333	72.2454	-54.9178	MPIC	Charnockite	magnesian	1875.1	3.0	38/69	3.7	Magmatic	Weighted average
						c. 2550, 2651		1		Inherited	Single grains
588337	72.3046	-55.0022	MPIC	Charnockite	magnesian	1865.5	2.4	38/69	2.9	Magmatic	Weighted average
						c. 1950-2070		4		Inherited	4 grains
588340	72.4871	-54.5308	MPIC	Charnockite	magnesian	1870.6	2.0	32/71	0.61	Magmatic	Weighted average
						1852.5	2.4	21/71	1.2	Metamorphic	Weighted average
						c. 1887 - 1920		5	4.5	Inherited	4 grains
588345	72.9757	-56.4271	LPIC	Charnockite	magnesian	1854.7	3.6	18	1.8	Magmatic	Weighted average
						1823.2	2.9	30	2.6	Metamorphic	Weighted average
						c. 2118, 2171, 2718		5	4.5	Inherited	3 grains
588349	72.7175	-56.1702	LPIC	Charnockite	ferroan	1851.3	3.3	26/73	0.49	Magmatic	Weighted average
						1830.7	2.7	28/73	0.7	Metamorphic	Weighted average
						1868.0	4.0	16/73	0.52	Inherited	Weighted average
						1955		1		Inherited	Single grains
588350	72.6501	-56.0323	LG	Leucogranite		1804.4	3.6	52/52	8.4	Magmatic	Weighted average
588352	72.9716	-56.2652	LPIC	Charnockite	magnesian	1856.0	3.4	7/20	1.9	Magmatic	Weighted average
						c. 1875, 1910-1940, 2300-2320, 2460, 2660		10		Inherited	Ten grains
588355	72.9638	-54.9053	MPIC	Charnockite	ferroan	1845.7	3.3	12/37	1.4	Magmatic	Weighted average
						1829.8	2.3	17/37	1.3	Metamorphic	Weighted average
588357	72.8715	-55.4235	LG	Leucogranite		1819.2	3.5	63/63	9.7	Magmatic	Weighted average

Note: Numbers in bold indicate the largest zircon age population in the sample.

7.4.1 Magmatic ages

The magmatic ages summarised in Table 1 are based on zircon populations showing primary magmatic zonation, typically as oscillatory zoning or other primary textures, and usually associated with high Th/U ratios (> 0.1) and low to intermediate U concentrations (< 2000 ppm). Magmatic ages can in some cases also be established based on inherited populations, implying that a single sample in addition to its crystallisation age, also may yield an inherited magmatic crystallisation age. Thus, in addition to the 25 magmatic crystallisation ages, 12 inherited magmatic ages have been defined (Table 1), giving a total of 37 magmatic ages.

Figure 19 shows all 37 magmatic crystallisation ages in a combined histogram and probability density distribution (PDD) diagram. This indicates the existence of three distinct magmatic PIC age groups centred around the following three age maxima (from older to younger): (1) 1897 Ma, (2) 1872 Ma, and (3) 1851 Ma. Table 2 summarises the average ages for each magmatic age group, age intervals and the statistical uncertainty given as one standard deviation of the mean.

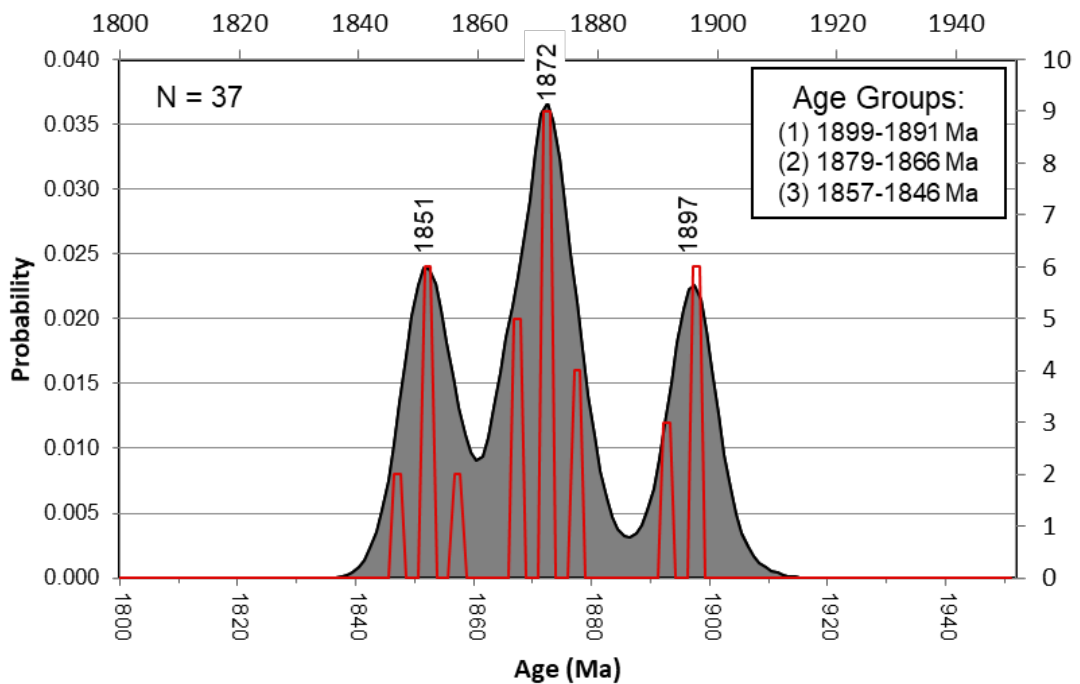


Figure 19. Combined histogram and probability density distribution (PDD) diagram plotting 37 magmatic PIC ages. Three well defined PIC age groups are identified: (1) an 1897 Ma age group, (2) an 1872 Ma age group, and (3) an 1851 Ma age group. Bin interval for histograms is 5 Myr.

Table 2. Magmatic PIC age groups

	#3	#2	#1
Age _{avg} (Ma)	1851.9	1871.6	1895.8
± 1 std. dev.	3.4	3.8	3.0
T _{min} (Ma)	1846	1866	1891
T _{max} (Ma)	1857	1879	1899
N	10	18	6

Magmatic age group 1 (Figure 20, purple) includes six zircon ages in the range 1899-1891 Ma; only one sample provides a primary crystallisation age (sample 483634), the remaining five represent minor inherited populations picked up by younger (mainly magnesian) PIC rocks belonging to age group 2.

Magmatic age group 2 (Figure 21, red) includes 18 zircon ages in the range 1879-1866 Ma; of these 12 represent primary crystallisation ages of the rock, while six represent inherited magmatic ages picked up by younger (mainly ferroan) PIC rocks belonging to age group 3.

Magmatic age group 3 (Figure 22, orange) includes ten zircon ages in the range 1857-1846 Ma; of which nine represent primary crystallisation ages of the rock, while one represents inheritance from a younger leucogranite (588317).

The geographical distribution of the three magmatic PIC age groups is shown separately in Figures 20-22 and in a single combined map in Figure 23. From this a systematic age distribution pattern is apparent:

- Magmatic age group 1 (1899-1891 Ma) occurs in a broadly NW-trending array in the central part of the intrusive complex from Karrat to the mainland east of Kangeq (Figure 20). The outer limit of this age domain is obviously very uncertain based on the highly restricted number of samples with this age, especially rocks with this as primary crystallisation age. Moreover, as the age group is based mostly on inherited zircons found in 'overprinting' Magmatic age group 2 rocks, the spatial extent (unsurprisingly) largely overlaps with the subsequent age group (Figure 23).
- Magmatic age group 2 (1879-1866 Ma) occupies large parts of the southern and central parts of the intrusive complex from Sullua in the SE to Nutaarmiut in the centre (Figure 21). Inherited ages of magmatic age group 2 extend further to the N and NW

where the host rocks belong to magmatic age group 3. To the east the geometry is uncertain due to lack of data.

- Magmatic age group 3 (1857-1846 Ma) occupies the northern and northwestern parts of the complex from Qaarsorsuatsiaq to the area around Upernavik Isfjord, and likely extends further to the north outside the study area (Figure 22). The eastern extent is likewise unconstrained due to lack of data.

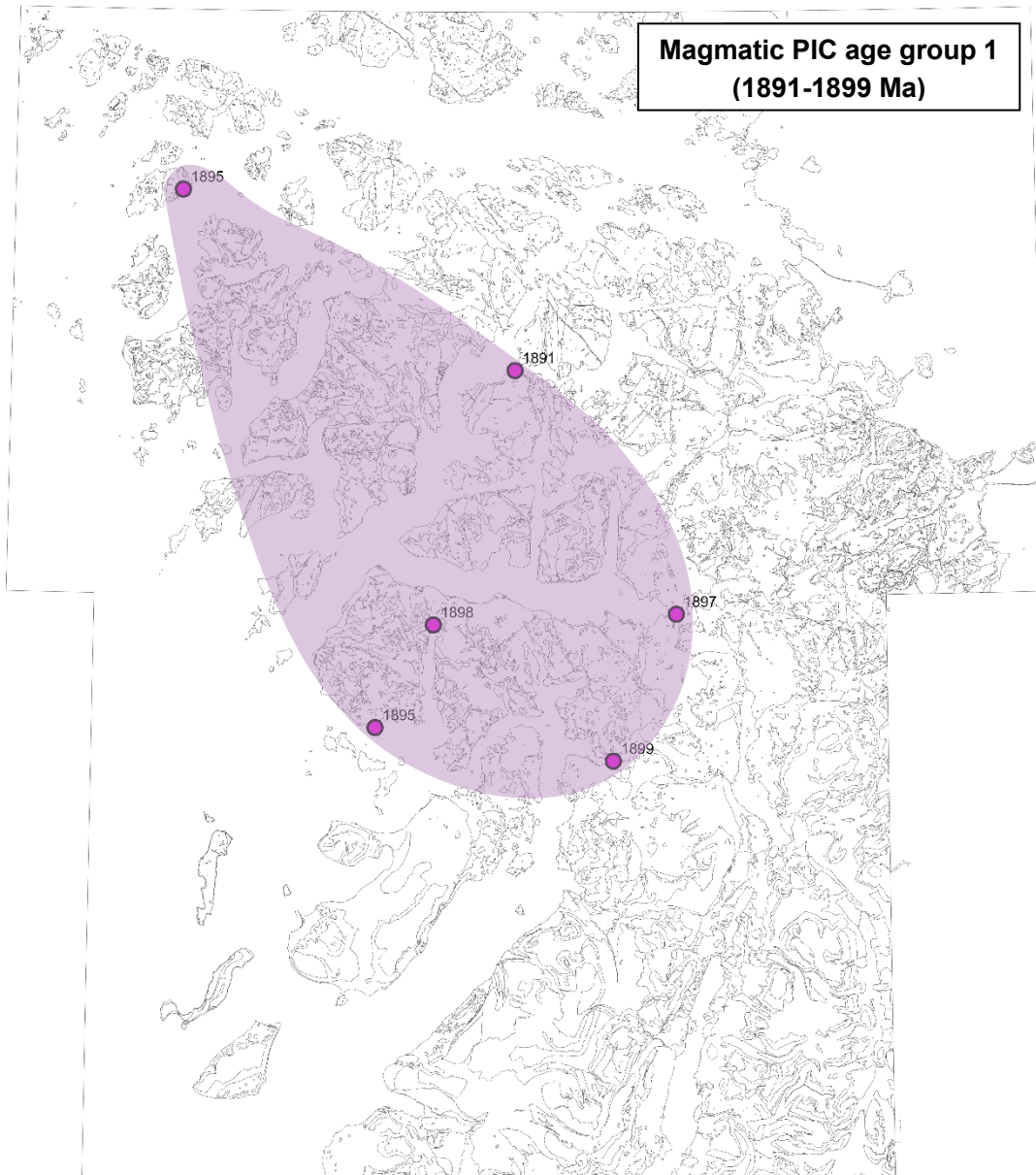


Figure 20. *Distribution map of Magmatic age group 1 (1899 - 1891 Ma), based on magmatic and inherited magmatic zircon ages.*

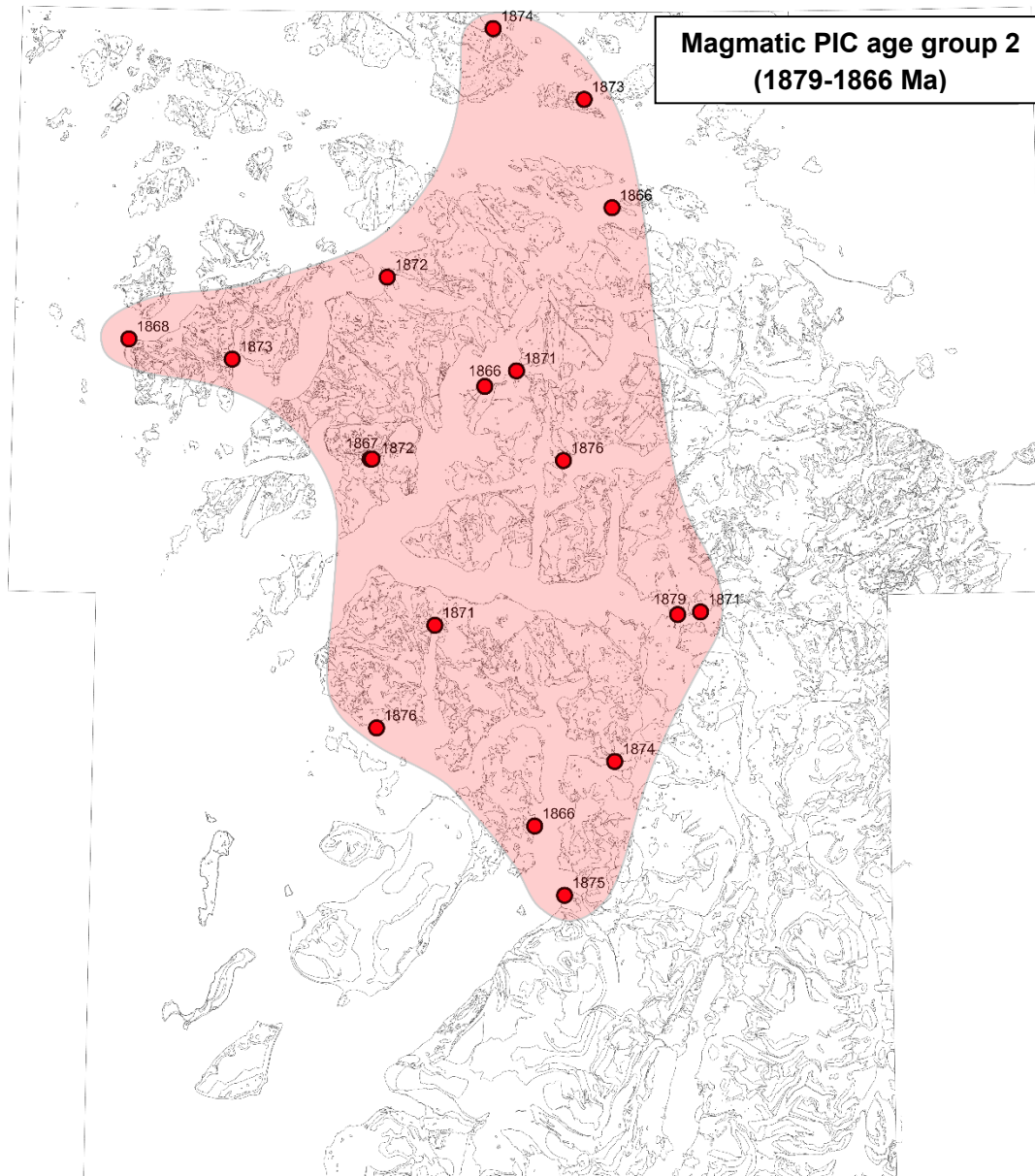


Figure 21. *Distribution map of Magmatic age group 2 (1879 - 1866 Ma), based on magmatic and inherited magmatic ages.*

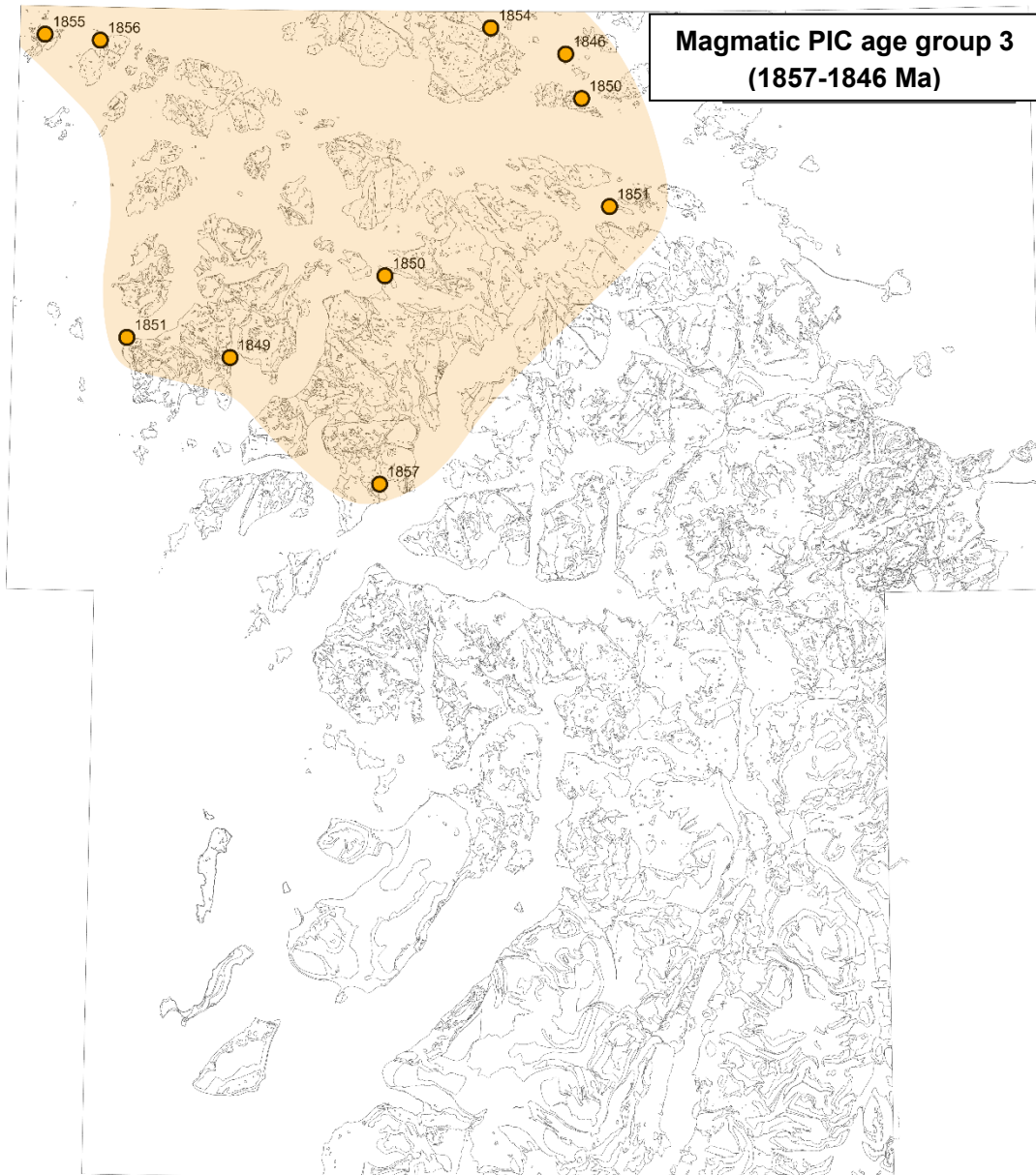


Figure 22. *Distribution map of Magmatic age group 3 (1857 - 1846 Ma), based on magmatic and inherited magmatic ages.*

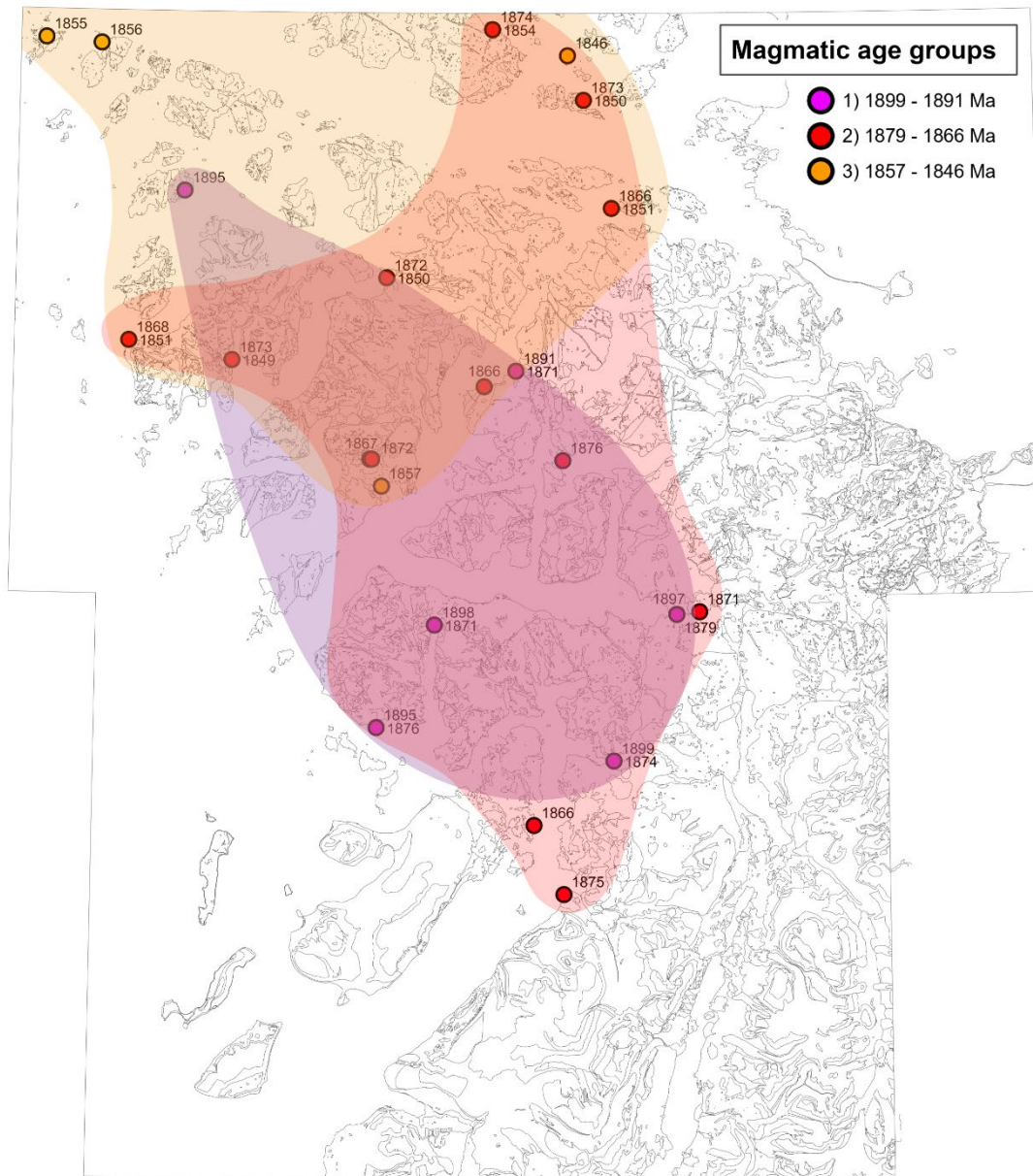


Figure 23. *Distribution map of Magmatic age group 1 - 3, based on magmatic and inherited magmatic ages.*

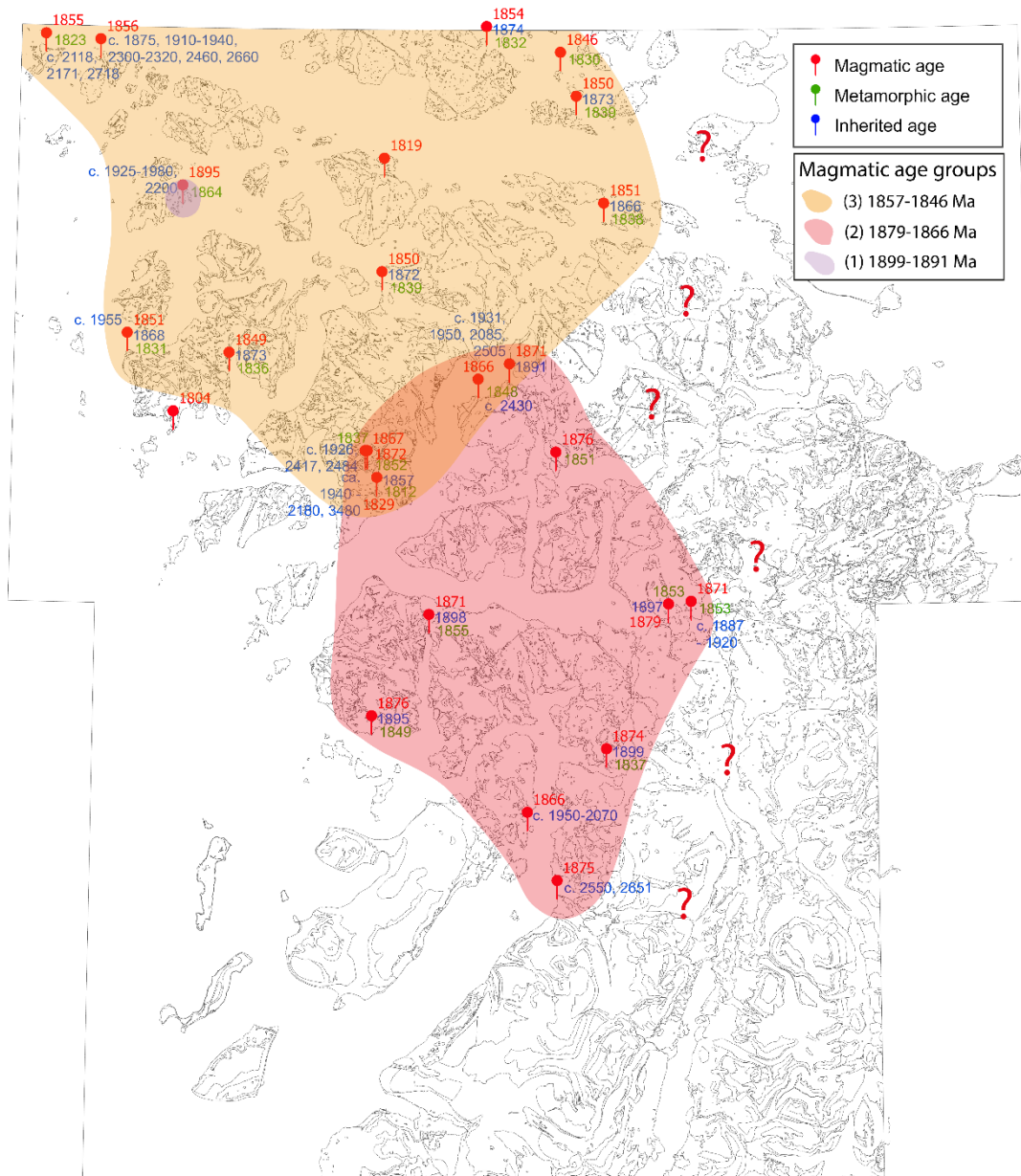


Figure 24. Distribution map of Magmatic age group 1 - 3, based on magmatic crystallisation ages only.

Figure 24 shows the extent of the magmatic age groups but unlike in Figures 20-22 here based solely on crystallisation ages of the host rocks (not considering inherited populations). By omitting the inherited magmatic ages, the geographical division between the ca. 1870 Ma and the ca. 1850 Ma magmatic events becomes clearer. It is however also evident that just as the ca. 1870 Ma magmatic event is traceable as an inherited signal all the way to the Upernavik Isfjord, where it is overprinted by the ca. 1850 Ma rocks, there is a distinct ca. 1850 Ma overprinting in the central and southern part as well, seen in metamorphic zircon growth at this age, as observed in rocks that crystallised at ca. 1870 Ma. Thus, the ca. 1870 Ma and the 1850 Ma magmatic events seem to have been equally widespread laterally but

with the younger magmatic event being displaced to the north relative to the ca. 1870 Ma event. The ca. 1850 Ma magmatic event resulted in metamorphic zircon growth to the south, whereas emplacement of new ferroan-type granitic magma only took place further to the north and northwest. In the framework of an arc setting, a NW-ward progression of magmatism could be explained by progressive roll-back of a SE-ward subducting slab.

7.4.2 Metamorphic ages

The metamorphic ages summarised in Table 1 are based on zircon populations showing typical metamorphic textural association, such as recrystallised rims and homogenous (overprinted) core domains, and usually have low Th/U ratios (< 0.1) and intermediate to high U concentrations (>1500 ppm). Metamorphic zircon ages have been retrieved from 22 samples and provide an age range of 1864-1804 Ma. We included the two crystallisation ages for leucogranite dykes into this category, because of the close association of migmatisation, intrusion of leucogranites and metamorphism.

When plotted in a PPD diagram (Figure 25) five approximate age peaks (statistical maxima values) can be distinguished variably successfully:

- (1) Ca. 1864 Ma; a small age peak based on a single sample on Karrat island (483634).
- (2) Ca. 1852 Ma; rather well defined, narrow age peak based on seven samples from the central part of the complex.
- (3) Ca. 1836 Ma; constituting a big broad peak, based on eight samples from mainly the northern part (plus a single sample in the far south).
- (4) Ca. 1823 Ma; a smaller age peak based on five samples, including two leucogranites with dated crystallisation ages of 1829 and 1819 Ma.
- (5) Ca. 1805 Ma; this age represents an emplacement age of a leucogranite dyke emplacement into paragneiss migmatites at Qaarsorsuatsiaq.

Overall, there is a general pattern of the oldest metamorphic ages at ca. 1850 Ma occurring in the south, whereas younger ages at ca. 1836 Ma are dominating in the north (Figure 26).

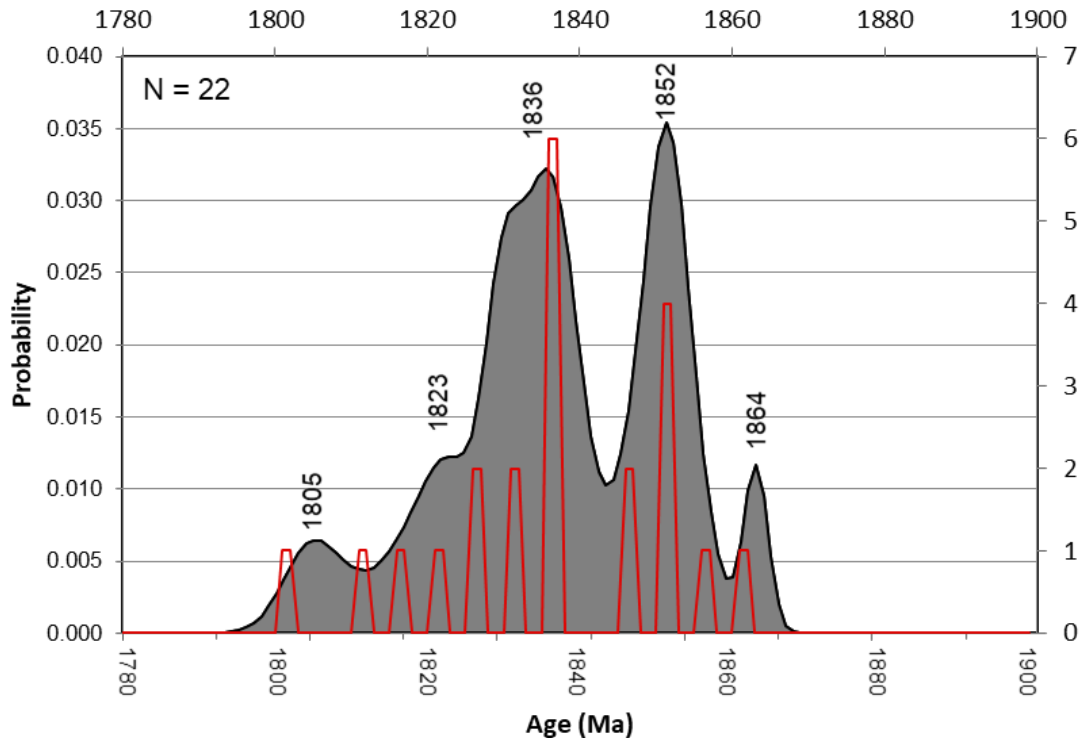


Figure 25. Combined histogram and probability density distribution (PDD) diagram plotting 22 metamorphic ages. Five maxima are identified, some of which are vaguely defined: (1) 1864 Ma, (2) 1852 Ma, (3) 1836 Ma, (4) 1823 Ma, and (5) 1805 Ma. Bin interval for histograms is 5 Myr.

7.4.3 Inherited ages

Inherited zircons occur in most analysed PIC rocks, usually as small age components (< 5-10% fractions). As described above, inherited zircons from older PIC intrusive phases are often seen in subsequent PIC rocks, i.e., ca. 1895 Ma grains are found in ca. 1870 Ma intrusive rocks and ca. 1875 Ma grains occur sporadically in ca. 1850 Ma PIC rocks.

Apart from the inherited magmatic PIC-related ages there are inherited populations of older age, namely older Paleoproterozoic and Archaean ages.

Archaean ages are found hosted in some PIC granites in the central part of the complex and include mainly Neoproterozoic ages (2500-2700 Ma), as well as a single Paleoproterozoic age (3480 Ma).

Paleoproterozoic ages are more widespread and include ages in the range of 1930-1980, and 2000-2200 Ma, which are typical for Nûkavsak metasediments as exemplified by samples of paleosome migmatites (samples 588334 and 588336).

8. Conclusions

Based on a new comprehensive dataset of whole rock geochemistry and geochronology data for charnockitic rocks of the PIC the following is concluded:

- The new dataset demonstrates a systematic spatial and temporal relationship within the PIC charnockitic rocks. Two older groups of magnesian charnockites at ca. 1895 and ca. 1870 Ma, respectively, are identified in the central and south-eastern part of the complex. The earliest group is largely obscured by the latter and is mainly identified based on sub-populations of inherited zircon. A younger and previously unidentified group at ca. 1850 Ma that mainly includes ferroan charnockites has been identified in the northern part of the complex (around Upernavik Isfjord).
- The two older PIC phases have rather similar chemistry, both showing an I-type geochemical character, i.e., are metaluminous to mildly peraluminous, magnesian and calc-alkalic compositions with moderate REE enrichment and relatively low Ti, Zr, Nb content and Ga/Al ratio.
- In contrast the ca. 1850 Ma PIC granites have elevated Ti, Zr, Nb and Ga/Al, a shared trace elemental features of some A-type granites, but without the typical alkalic character, and they plot outside the A-type fields in the Grebennikov-diagram.
- A distinction between the two groups is neither obvious in the field nor from mapping by photogrammetry and would require detailed sampling and geochemistry to establish in more detail.
- The finding of the earliest PIC phases being I-type (and not A-type) character is different from what was proposed previously by Thrane et al. (2005) and calls for a fundamental revision of the geotectonic model for the PIC.
- The shift in chemistry is tentatively explained by a change in source for the granitic melts; the first stages are consistent with the pre-collision stage of an arc (+ crustal contamination), while the latest magmatic phase has chemical resemblance to syn-collisional granites, possibly suggesting a prolonged collisional stage leading up to the peak-metamorphism starting some 20 Myr later and peaking at ca. 1830 Ma.
- The ca. 1850 Ma magmatic event is associated with widespread metamorphism in the central and southern part of the complex, as witnessed by growth of metamorphic textured zircons in ca. 1870 Ma old PIC charnockites.
- The intrusion of leucogranite sheets into the base of the PIC (LPIC unit) mark the high-grade metamorphism and migmatization of Nûkavsak Formation paragneisses; during this stage, the LPIC charnockites were strongly overprinted by migmatization. This

peak metamorphic event appears to be particularly pronounced in the northern and north-western parts of the complex.

9. References

- Bramm, L. (2021). Metamorphic evolution and tectonic significance of granulite facies rocks in and around the Prøven igneous complex, Rinkian Orogen, Central West Greenland. MSc Thesis at Ruhr Universität Bochum. 42 pp.
- Chappell, B. W. & White, A. J. R. (1974). Two contrasting granite types. *Pacific Geology*, 8, 173–174.
- Corrigan, D., Pehrsson, S., Wodicka, N. and de Kemp, E. 2009: The Palaeoproterozoic Trans-Hudson Orogen: a prototype of modern accretionary processes; in *Ancient Orogens and Modern Analogues*, J.B. Murphy, J.D. Keppie and A.J. Hynes (ed.), The Geological Society, London, Special Publications, v. 327, p. 457–479, doi:10.1144/SP327.19
- Dziggel, A., Diener, J. F. A., Kolb, J. & Kokfelt, T. F. (2014). Metamorphic record of accretionary processes during the Neoproterozoic: The Nuuk region, southern West Greenland. *Precambrian Research* 242, 22–38 (2014) <http://dx.doi.org/10.1016/j.precamres.2013.12.010>.
- Dziggel, A., Bramm, L., Kokfelt, T. F., Grocott, J. & Diener, J. F. A. (in prep.). Preservation of metamorphic and igneous charnockites in the Paleoproterozoic Prøven Igneous Complex, Rinkian Orogen, Central-West Greenland.
- Escher, A. & Pulvertaft, T.C.R. (1968). The Precambrian rocks of the Upernavik-Kraulshavn area (72° - 74°15' N), West Greenland. In: Report of activities, 1967: Grønlands Geol. Undersøgelse Rap. 15, 11–14.
- Escher, J. ca. & Stecher, O. (1978). Precambrian geology of the Upernavik–Red Head region (72°15'–75°15'N), northern West Greenland. *Rapport Grønlands Geologiske Undersøgelse*, 90, 23–26.
- Escher, A. & Pulvertaft, T. ca. R. (1976). Rinkian mobile belt of west Greenland. In: Escher, A., Watt, W.S. (Eds.), *Geology of Greenland*. Geological Survey of Greenland, Copenhagen, 105–119.
- Frost, R. B. & Frost, ca. D. (2008). On charnockites. *Gondwana Research* 13, 30–44.
- Frost, B. R., Barnes, ca. G., Collins, W. J., Arculus, R. J., Ellis, D. J. & Frost, ca. D. (2001). A geochemical classification for granitic rocks. *Journal of Petrology*, 42, 2033–2048, <https://doi.org/10.1093/petrology/42.11.2033>
- Frei, D. & Gerdes, A. (2009). Precise and accurate in situ U-Pb dating of zircon with high sample throughput by automated LA-SF-ICP-MS. *Chemical Geology*, 261(3-4), 261–270. <https://doi.org/10.1016/j.chemgeo.2008.07.025>
- Grocott, J., van den Eeckhout, B. & Vissers, R. L. M. (1987). Mantled gneiss antiforms and fold nappes in the Rinkian belt, West Greenland: diapiric structures or structures formed

- in a thrust system? *Journal of the Geological Society, London*, 144, 723–734, <https://doi.org/10.1144/gsjgs.144.5.0723>.
- Grocott, J. & Pulvertaft, T. ca. R. (1990). The Early Proterozoic Rinkian Belt of Central West Greenland. In: Lewry, J. F., Stauffer, M. R. (Eds.), *The Early Proterozoic Trans-Hudson Orogen of North America*. Geological Association of Canada Special Paper 37, 443–463.
- Grocott, J. & MacCaffrey, K. J. W. (2017). Basin evolution and destruction in an Early Proterozoic continental margin: the Rinkian fold–thrust belt of central West Greenland. *Journal of the Geological Society*. <https://doi.org/10.1144/jgs2016-109>.
- Grocott, J., Thrane, K., McCaffrey, K. J. W., Sleath, P. R., Dziggel, A. (2023). Andean-type, bivergent crustal shortening in the Rinkian orogen: New constraints on the tectonic evolution of Laurentia–West Greenland in the Paleoproterozoic. *Geosphere* 19 (5), 1231–1258. <https://doi.org/10.1130/GES02614.1>
- Guarnieri, P., Partin, ca. A. & Rosa, D. (2016). Palaeovalleys at the basal unconformity of the Palaeoproterozoic Karrat Group, West Greenland. *Geological Survey of Denmark and Greenland (GEUS) Bulletin* 35, 63–66
- Guarnieri, P., Rosa, D., Thrane, K., Kokfelt, T. F., Sørensen, E. V., De Wolfe, M. Y. & Baker, N. J. (2023). Tectonics of the Paleoproterozoic Rinkian orogen, central West Greenland. *GSA Bulletin*, <https://doi.org/10.1130/B36930.1>
- Hamilton, B. J. H. M. (2016). *Metamorphic Geology of Cumberland Peninsula, Baffin Island, Nunavut, Canada*. Hamilton, Brett John Hugh McAuley. University of Calgary (Canada) ProQuest Dissertations Publishing. <http://hdl.handle.net/11023/2869>
- Henderson, G. & Pulvertaft, T.C.R. (1967). The stratigraphy and structure of the Precambrian rocks of the Umanak area, West Greenland. *Meddelelser fra Dansk Geologisk Forening* 17, 1–22
- Henderson, G. & Pulvertaft, T. ca. R. (1987). The lithostratigraphy and structure of a Lower Proterozoic dome and nappe complex. Geological Survey of Greenland Descriptive text for Geological Map of Greenland 1:100 000-scale sheets Marmorilik 71V.2 Syd, Nûgât-siaq 71V.2 Nord, Pagnertôq 72V.2 Syd, Grønlands Geologiske Undersøgelse, Copenhagen.
- Hoffmann, A. W. (1988). Chemical differentiation of the Earth: the relationship between mantle, continental crust, and oceanic crust. *Earth and Planetary Science Letters*, 90, (3), 297–314. [https://doi.org/10.1016/0012-821X\(88\)90132-X](https://doi.org/10.1016/0012-821X(88)90132-X).
- Irvine, T. N. & Baragar, W. R. A. (1971). A Guide to the Chemical Classification of the Common Volcanic Rocks. *Canadian Journal of Earth Science*, 8, 523-548.
- Jackson, S., Pearson, N. J., Griffin, W. & Belousova, E. (2004). The Application of Laser Ablation-inductively Coupled Plasma-mass Spectrometry to in situ U-Pb Zircon Geochronology. *Chemical Geology*. 211. 47-69. [10.1016/j.chemgeo.2004.06.017](https://doi.org/10.1016/j.chemgeo.2004.06.017).

- Kokfelt, T. F. Sørensen, E. V., Grocott, J., Sleath, P. R., McCaffrey, K. W. & Rosa, D. (in prep. 2024a). Geological map of Greenland 1:100 000, Prøven 72 V. 1 Syd. <https://doi.org/10.22008/FK2/ATBJQD>, GEUS Dataverse.
- Kokfelt, T. F., Sleath, P. R., Grocott, J., Sørensen, E. V., McCaffrey, K. W. & Rosa, D. (in prep. 2024b). Geological map of Greenland 1:100 000, Upernavik 72 V. 1 Nord. <https://doi.org/10.22008/FK2/L9OA0J>, GEUS Dataverse.
- Kystol, J. & Larsen, L. M. (1999). Analytical procedures in the Rock Geochemical Laboratory of the Geological Survey of Denmark and Greenland. *Geology of Greenland Survey Bulletin*, 184, 59–62. <https://doi.org/10.34194/ggub.v184.5230>
- Larsen, J. G. & Larsen, L. M. (2022). Lithostratigraphy, geology and geochemistry of the Tertiary volcanic rocks on Svartenhuk Halvø and adjoining areas, West Greenland. *GEUS Bulletin*, 50. <https://doi.org/10.34194/geusb.v50.8295>
- Le Maitre, R.W. (1989). *A Classification of Igneous Rocks and Glossary of Terms*. Blackwell, Oxford.
- Le Maitre, R. W., Streckeisen, A., Zanettin, B., Le Bas, M. J., Bonin, B. & Bateman, P. (Eds.). (2005). *Igneous rocks: a classification and glossary of terms: recommendations of the International Union of Geological Sciences Subcommittee on the Systematics of Igneous Rocks*. Cambridge University Press.
- Middlemost, E. A. K. (1991). Towards a comprehensive classification of igneous rocks and magmas. *Earth-Science Reviews*, 31, 73–87, [https://doi.org/10.1016/0012-8252\(91\)90016-9](https://doi.org/10.1016/0012-8252(91)90016-9)
- Miyashiro, A. (1978). Nature of alkalic volcanic rock series. *Contributions to Mineralogy and Petrology*, 66, 91–104, <https://doi.org/10.1007/BF00376089>
- Ohta, T. & Arai, H. (2007). Statistical empirical index of chemical weathering in igneous rocks: A new tool for evaluating the degree of weathering. *Chemical Geology*, 240, 280–297.
- Paton, C., Hellstrom, J. C., Paul, P., Woodhead, J. D. & Hergt, J. M. (2011) Iolite: Freeware for the visualisation and processing of mass spectrometric data. *Journal of Analytical Atomic Spectrometry* 26, 2508–2518.
- Pearce, J. A. (1996). Sources and settings of granitic rocks. *Episodes* 19, 120–125.
- Pearce, J. A., Harris, N. B. W. & Tindle, A. G. (1984). Trace element discrimination diagrams for the tectonic interpretation of granitic rocks. *Journal of Petrology* 25, 956–983.
- Peccerillo, A., Taylor, S. R. (1976). Geochemistry of the Eocene calc-alkaline volcanic rocks from Kastamonu area, northern Turkey. *Contributions to Mineralogy and Petrology* 58, 63–81.
- Pehrsson, S. J., Berman, R. G., Eglington, B., & Rainbird, R. (2013). Two Neoproterozoic supercontinents revisited: The case for a Rae family of cratons. *Precambrian Research*, 232, 27–43.

- Petrus, J. A. & Kamber, B. S. (2012). VizualAge: A novel approach to laser ablation ICP-MS U-Pb geochronology data reduction. *Geostandards and Geoanalytical Research*, 36(3), 247–270.
- Pesonen, L. J., Elming, S. Å., Mertanen, S., Pisarevsky, S., D'Agrella-Filho, M. S., Meert, J. G., ... & Bylund, G. (2003). Palaeomagnetic configuration of continents during the Proterozoic. *Tectonophysics*, 375(1-4), 289–324.
- Rosa, D., Bernstein, S., DeWolfe, M., Dziggel, A., Grocott, J., Guarnieri, P., Kolb, J., Partin, ca. A., Sørensen, E. V. & Zimmermann, R. (2018). Architecture and mineral potential of the Paleoproterozoic Karrat Group, West Greenland: Results of the 2016 Season. *Geological Survey of Denmark and Greenland Report*, 2018/23. 102 p.
- Sanborn-Barrie, M., Thrane, K., Wodicka, N. & Rayner, N. (2017). The Laurentia-West Greenland connection at 1.9 Ga: new insights from the Rinkian belt. *Gondwana Research* 51, 289–309. doi.org/10.1016/j.gr.2017.07.002.
- Sawyer, E. W. (2008). Atlas of Migmatites. The Canadian Mineralogist, Special Publication 9. NRC Research press, Ottawa, Ontario, Canada. 371 p.
- Sláma, J., Košler, J., Condon, D. J., Crowley, J. L., Gerdes, A., Hanchar, J. M., ... & Whitehouse, M. J. (2008). Plešovice zircon—a new natural reference material for U–Pb and Hf isotopic microanalysis. *Chemical Geology*, 249(1-2), 1–35.
- Sleath, P. R. (2021). Tectonic Evolution of the Prøven Igneous Complex within the Rinkian Fold-Thrust Belt, West Greenland: Investigation using 3D Photogrammetry, Durham theses, Durham University. Available at Durham E-Theses Online: <http://etheses.dur.ac.uk/14088/>
- St-Onge, M. R., Van Gool, J. A., Garde, A. A., & Scott, D. J. (2009). Correlation of Archaean and Palaeoproterozoic units between northeastern Canada and western Greenland: constraining the pre-collisional upper plate accretionary history of the Trans-Hudson orogen. *Geological Society, London, Special Publications*, 318(1), 193–235.
- Thrane, K. (2021). The oldest part of the Rae craton identified in western Greenland. *Precambrian Research*, 357, 106139.
- Thrane, K., Baker, J., Connelly, J. & Nutman, A. (2005). Age, petrogenesis and metamorphism of the syn-collisional Prøven Igneous Complex, West Greenland. *Contributions to Mineralogy and Petrology*, 149 (5), 541–555.
- Vermeesch, P. (2018). IsoplotR: A free and open toolbox for geochronology. *Geoscience Frontiers* 9, 1479–1493.
- Whalen, J. B., Wodicka, N., Taylor, B. E., & Jackson, G. D. (2010). Cumberland batholith, Trans-Hudson Orogen, Canada: Petrogenesis and implications for Paleoproterozoic crustal and orogenic processes. *Lithos*, 117(1-4), 99–118.
- Whalen, J. B., Sanborn-Barrie, M. & Young, M. (2012). Geochemical data from Archean and Paleoproterozoic plutonic and volcanic rocks of Cumberland Peninsula, eastern Baffin

Island, Nunavut; Geological Survey of Canada, Open File 6933, 15 pages, <https://doi.org/10.4095/291453>.

Wiedenbeck, M. (1995). An example of reverse discordance during ion microprobe zircon dating: An artifact of enhanced ion yields from a radiogenic labile Pb. *Chemical Geology*, 125(3-4), 197–218.

Wiedenbeck, M., Hanchar, J. M., Peck, W. H., Sylvester, P., Valley, J., Whitehouse, M., ... & Zheng, Y. F. (2004). Further characterisation of the 91500 zircon crystal. *Geostandards and Geoanalytical Research*, 28(1), 9–39.

Wodicka, N., St-Onge, M.R., Corrigan, D.C., Scott, D.J., Whalen, J.B., 2014. Did a proto-ocean basin form along the southeastern Rae cratonic margin? Evidence from U-Pb geochronology, geochemistry (Sm-Nd and whole-rock) and stratigraphy of the Paleoproterozoic Piling Group, northern Canada. *Geological Society of America Bulletin* 126:1625–1653. <http://dx.doi.org/10.1130/B31028.1>.